REMARKS

Claim Amendments

Claims 1, 7, 15-35, and 39 are pending. Claims 1 and 7 are amended. Claim 39 has been added. Claims 15-32 stand withdrawn. Claims 8, 14, and 36-38 are canceled herein without prejudice or disclaimer to the subject matter therein. Applicants reserve the right to pursue cancelled subject matter in one or more divisional and/or continuation applications.

Support for the claim amendments may be found throughout the specification and in the claims as originally filed. *See e.g.*, ¶ [0085], Examples 4-5. Applicants respectfully request entry of the above amendments and submit that these amendments do not constitute new matter.

Claim Objections

Claims 1 and 7 are objected to for informalities. As per the Examiner's suggestion, Applicants have amended claims 1 and 7 to recite "an." Applicants request withdrawal of this objection.

Rejections under 35 U.S.C. § 112, First Paragraph — Enablement

Claims 1, 7, 8, 14, and 33-38 stand rejected under 35 U.S.C. § 112, first paragraph as allegedly failing to comply with the enablement requirement. Applicants respectfully disagree and traverse this rejection.

As an initial matter, Applicants point out that claim 1 has been amended to delete the hybridization language and the recitation of "or catheter based delivery." Claim 1 has also been amended to recite "a promoter operatively linked to the nucleic acid of the expression vector." Applicants believe these amendments address a substantial portion of the enablement rejection. Applicants also provide the following comments.

The Examiner states that the specification "enables a therapeutic method for heart disease that comprises delivery of an expression vector to heart cells of an individual." Office Action, page 10. The Examiner also acknowledges that the specification teaches an art accepted model for studying the effects of ischemia following treatment with an AOP-1 expression vector. *See id* at page 7. Furthermore, the Examiner agrees that the evidence of record suggests that both human and rat AOP-1 serve analogous functions in mitochondrial membrane activation. *Id.* at 16.

Nonetheless, the Examiner maintains the enablement rejection and asserts that the specification does not teach: (a) an association between decreased AOP-1 expression and chronic heart disease, ischemic heart failure, or ischemic heart disease; or (b) a therapeutic model for chronic heart disease, ischemic heart failure, or ischemic heart disease. *Id.* at page 10. The Examiner contends that the specification's ischemia model (Example 16) is a supraphysiological model that does not serve "as a model for all ischemic conditions of the heart, such as ischemic arrhythmia..." *Id.* at 7.

Applicants respectfully disagree and submit that the specification teaches an association between decreased AOP-1 expression and chronic heart disease, ischemic heart failure, and ischemic heart disease. *See, e.g.*, ¶ [0070]; *see also* Example 2 ("The results showed decreased expression of AOP-1 gene with the progress of the pathology of chronic heart failure in all the models."). Applicants also note that a recent article confirms that a decreased AOP-1 (Peroxiredoxin 3) expression is associated with human hear failure. *See* Brixius, *et al.* (2007) "Isoform-Specific Downregulation of Peroxiredoxin in Human Failing Myocardium." Life Science 81(10): 823-831, attached herewith as **Exhibit A**.

Applicants also disagree with the Examiner's comments regarding Example 16. Example 16 is a short-term ischemic reperfusion model. It is widely known that ischemia is caused by relative decrease in the number of capillaries in tissue during chronic heart failure. *See* Henquell, *et al.* (September 1977) "Intercapillary Distance and Capillary Reserve in Hypertrophied Rat Hearts Beating in Situ." Circulation Research 41(3): 400-408, attached herewith as **Exhibit B**. A significant decrease in myocardial ATP levels during chronic heart failure is also known in the art. *See e.g.*, Gourine, *et al.* (2004) "Interstitial purine metabolites in hearts with LV remodeling." Am J Physiol Heart Circ Physiol 286: H677-H684, attached herewith as **Exhibit C**. Thus, the model shown in Example 16 can be regarded as a model in which one of the exacerbating factors in chronic heart failure conditions is isolated and emphasized. Example 16 clearly demonstrates that this decrease in intracellular ATP levels during ischemia can be significantly prevented by activation of mitochondrial functions induced by AOP-1 gene transfer.

Moreover, in Examples 7 and 15 using *in vitro* experimental systems, complicated exacerbating factors in chronic heart failure were separated individually and analyzed for their effect on cell viability and pulsating function of cardiac myocytes; and the protective effect of

AOP-1 was also analyzed for each factor. These examples indicated that enhanced expression of AOP-1 prevented cell death of cardiac myoctes and reduction in their pulsating function in hypoxic and reoxygenation experiments which mimic ischemia and reperfusion, respectively. During chronic heart failure, cardiac myocytes are known to establish insulin resistance. *See* Paternostro, *et al.* (1999) "Insulin Resistance in Patients with Cardiac Hypertrophy." Cardiovascular Research 42(1): 246-253, attached herewith as **Exhibit D**. This insulin resistance will cause inhibition of glucose utilization, which in turn will lead to disadvantages in heart failure. A model which simplifies these processes is the experimental system of high-glucose exposure. *See e.g.*, Example 15. In this system, enhanced expression of AOP-1 was shown to prevent cell death of cardiac myocytes. These experimental data are sufficient to prove with considerable reliability that the examples in the specification support the usefulness and effectiveness of AOP-1 in chronic heart failure. Applicants also point out that they have published a paper demonstrating the effectiveness of AOP-1 gene transfer in a chronic heart failure model. *See* Matsushima, *et al.* (2006) "Overexpression of Mitochondrial Peroxiredoxin-3 Prevents Left Ventricular Remodeling and Failure after Myocardial Infraction in Mice." Circulation 113: 1779-1786, attached herewith as **Exhibit E**.

In view of the foregoing, Applicants respectfully request withdrawal of the enablement rejection.

CONCLUSION

Applicants respectfully submit that claims are in condition for allowance, and such disposition is earnestly solicited. Should the Examiner believe that any issues remain after consideration of this response, the Examiner encouraged to contact the Applicant's undersigned representative to discuss and resolve such issues.

It is believed that no additional fees are necessary for the submission of this response. However, should the USPTO determine that any additional fees are due in connection with this response, the Commissioner is hereby authorized to charge such fees to the undersigned's **Deposit Account No. 50-0206.**

Respectfully submitted,

HUNTON & WILLIAMS LLP

Date: July 28, 2008 By: _____

Robert M. Schulman
Registration No. 31,196

Christopher J. Nichols, Ph.D.
Registration No. 55,984

HUNTON & WILLIAMS LLP
Intellectual Property Development
1900 K Street, N.W., Suite 1200
Washington, D.C. 20006-1109
(202) 955-1500 (telephone)
(202) 778-2201 (facsimile)

Exhibit A

Brixius, *et al.* (2007)
"Isoform-Specific Downregulation of Peroxiredoxin in Human Failing Myocardium."
Life Science 81(10): 823-831

Available online at www.sciencedirect.com
ScienceDirect
Life Sciences 81 (2007) 823–831
Life Sciences
www.elsevier.com/locate/lifescie

Isoform-specific downregulation of peroxiredoxin in human failing myocardium

Klara Brixius [a], Robert H.G. Schwinger [b,c], Felix Hoyer [a], Andreas Napp [a,b], Robert Renner [a], Birgit Bölck [b], Angelika Kümin [c], Uwe Fischer [d], Uwe Mehlhorn [d], Sabine Werner [c], Wilhelm Bloch [a,e,*]

[a] Department of Molecular and Cellular Sport Medicine, Institute of Cardiology and Sport Medicine, German Sport University, Germany
[b] Laboratory of Muscle Research and Molecular Cardiology, Department of Internal Medicine III, University of Cologne, Cologne, Germany
[c] Medizinische Klinik II, Klinikum Weiden, Akademisches Lehrkrankenhaus der Universität Regensburg, Weiden, Germany
[d] Institute of Cell Biology, Department of Biology, ETH Zurich, Switzerland
[e] Clinic of Cardiothoracic Surgery, University of Cologne, Germany

Received 22 February 2007; accepted 4 July 2007

Abstract

Peroxiredoxins (Prx) are a family of antioxidant thioredoxin or glutathione dependent peroxidases. The major functions of Prx comprise modulation of signalling cascades that apply hydrogen peroxide (H_2O_2) and cellular protection against oxidative stress. Nothing is known about Prx isoforms in human myocardium. We investigated the protein expression of Prx isoforms 1–6 in human non-failing (NF, donor hearts, $n=6$, male, age: 53.3±2.1 years) and failing myocardium (DCM, orthotopic heart transplantation, dilated cardiomyopathy, $n=15$, male, 57.0±1.7 years). In addition, we performed immunohistochemical stainings and measured Prx 4 mRNA expression levels (RNAse protection assay). The protein expression of Prx 1–2 was similar in NF and DCM. The protein expression of Prx 3–6 and the mRNA-expression of Prx 4 were decreased in DCM. Immunohistochemical analyses provided evidence that all Prx isoforms are present in cardiomyocytes and endothelial cells. Whereas Prx 1–5 staining was more pronounced in endothelial cells, Prx6 staining was more evident in cardiomyocytes. This study provides evidence that Prx are differentially regulated in DCM. The selective downregulation of peroxiredoxin 3–6 isoforms may point towards a subcellular specific dysregulation of the antioxidative defence during the development of DCM.

Keywords: Heart failure; Signal transduction; Myocardium; Peroxiredoxin

Introduction

Peroxiredoxins are a new family of peroxidases that reduce H_2O_2 and various organic peroxides through the use of the reducing equivalents of thioredoxin or glutathione (Chae et al., 1994; Rhee et al., 2001). Since the molar efficiencies of peroxiredoxins are by orders of magnitude smaller than those of catalase and the selenium-containing glutathione peroxidases, they have been suggested as being predominantly required under stress conditions (Rhee et al., 2005). In addition, they may have distinct functions in metabolic regulation and cellular differentiation (reviewed by Hofmann et al., 2002). All peroxiredoxin enzymes contain a conserved cysteine residue (Cys) in the NH_2-terminal region (Cys47), which is the only redox-active residue and the primary site of oxidation by H_2O_2 (Rhee et al., 2001).

The six mammalian peroxiredoxin isoforms identified to date can be divided into three subgroups: the 2-Cys, atypical 2-Cys and 1-Cys subgroups (Kang et al., 1998; Rhee et al., 2001; Seo et al., 2000). The 2-Cys Prx proteins, which include peroxiredoxin 1–4, contain an additional conserved cysteine in the COOH-terminal region (Cys170). Peroxiredoxin 5, a member of

* Corresponding author. Department of Molecular and Cellular Sport Medicine, German Sport University Cologne, Carl-Diem-Weg 6, 50933 Cologne, Germany. Tel.: +49 221 4982 5380; fax: +49 221 4982 8370.
E-mail address: w.bloch@dshs-koeln.de (W. Bloch).

0024-3205/$ - see front matter © 2007 Elsevier Inc. All rights reserved.
doi:10.1016/j.lfs.2007.07.014

Table 1
Clinical characteristics of DCM-patients

No.	Age	EF	Ni	Diu	Further medication
1	55	10%		Furo, spironolactone	Amio, marc, allo
2	52		ISDN	Furo	ASS
3	60				Marc, KCL, Mg-oxide
4	56	17%		Furo	Marc, amio, allo
5	58		Glyceronitrate		Marc, met
6	57			Furo, xipamide	Marc, KCl, NaCl, simvastatin, carbamazepine, doxepin, amio
7	67		Molsidomin		Marc, amio, bezafibrate, levothyroxine, marc
8	65	10%	molsidomin		Marc, amio, levothyroxine, bezafibrate, met
9	63			Xipamide, furo, spironolactone	Marc, allo, car
10	40	30%	Molsidomin	Furo	Marc, omeprazole, metronidazole, car
11	55	12%		Furo, hydrochlorothiazide	Marc, amio, car
12	51	21%		Furo	Marc, amio, dytide, car

EF: ejection fraction (%), met: metoprolol, car: carvedilol, NI: nitrates, Diu: diuretics, marc: marcumar, furo: furosemide, amio: amiodarone, allo: allopurinol, ASS. ascorbic acid.
All patients were male and received an angiotensin converting enzyme-inhibitor and digitalis or digitoxin.

the atypical 2-Cys, contains an additional cysteine at another position and peroxiredoxin 6, which belongs to the 1-Cys subgroup, has no additional cysteine residue (Kang et al., 1998; Rhee et al., 2001; Seo et al., 2000). The extent of amino acid sequence identity among the three subgroups is low (<20%), whereas that among members of the 2-Cys subgroup is 60–80% (Seo et al., 2000). Among the 2-Cys peroxiredoxin isoforms, peroxiredoxin 1 and 2 are localized in the cytosol (Mizusawa et al., 2000; Oberley et al., 2001), whereas peroxiredoxin 3 is restricted to mitochondria (Oberley et al., 2001; Tyagi et al., 2005) and peroxiredoxin 4 is synthesized with an NH_2-terminal sequence for secretion and is present in the endoplasmatic reticulum as well as in the extracellular space (Rhee et al., 2001). Peroxiredoxin 5 is expressed in long and short forms, which are located in mitochondria and peroxisomes, respectively. Peroxiredoxin 5 has the widest intracellular localization among the peroxiredoxin family and is found in the cytosol, the mitochondria, peroxisomes and even the nucleus (Cha et al., 2003; Oberley et al., 2001; Seo et al., 2000). Peroxiredoxin 6 has been only found in the cytosol (Kang et al., 1998; Matsumoto et al., 1999).

There are indications that peroxiredoxins play a role in the prevention of cellular radical damage as antioxidative defenders. Recently, in a transgenic mouse model, it has been described that an over-expression of peroxiredoxin 3 inhibited left ventricular remodelling and failure after myocardial infarction (Matsushima et al., 2006). Although it has been well described that the generation of reactive oxygen species (ROS) is significantly increased in failing human myocardium (Giordano, 2005), only little is known about alterations in the cellular antioxidative defence mechanisms. Therefore, this study investigated the protein and mRNA expression, as well as the localization of peroxiredoxins 1–6, in human non-failing and failing myocardium.

Material and methods

Patients

Human left ventricular non-failing myocardium was obtained from 6 male donor hearts that could not be transplanted for technical reasons. The mean age of the donor group was 53.3± 2.1 years. No cardiac catheterization had been performed in the organ donor group, but none of the donors had a history of heart disease and all had normal left ventricular function as measured by echocardiography.

Failing left ventricular tissue was obtained during cardiac transplantation (n=12). Patients suffered from heart failure clinically classified as New York Heart Association class IV (AHA/ESC stadium D) on the basis of clinical symptoms and signs as judged by the attending cardiologist shortly before operation. All patients gave written informed consent before surgery. Only male patients were included in the study (mean age: 56.6± 2.1 years). Table 1 presents the clinical characteristics and medication of each patient as far as data were available. Drugs used for general anesthesia were flunitrazepam and pancuronium bromide with isoflurane. Cardiac surgery was performed on cardiopulmonary bypass patients with cardioplegic arrest during hypothermia. The cardioplegic solution (a modified Bretschneider solution) contained (in mmol/l) NaCl 15, KCl 9, $MgCl_2$ 4, histidine 180, tryptophan 2, mannitol 30, and potassium dihydrogen oxoglutarate 1.

Immediately after explantation, the myocardial tissues were placed in ice-cold aerated modified Bretschneider solution and delivered to the laboratory within 10 min. The study was approved by the local ethics committee and conforms with the Declaration of Helsinki.

Immunoblotting

After homogenization of ventricular tissue from human non-failing and failing myocardium, protein concentration was determined as described before (Bradford, 1976). For Western blot analysis, the proteins were separated electrophoretically in a continuous 4% stacking gel and a sodium dodecyl sulfate polyacrylamid (SDS)-12% gel (according to Laemmli, 1970) under constant current (70 mA [60 min] and 120 mA [180–240 min]) and transferred on to a polyvinyldienfluoride membrane (PVDF, Roche, Mannheim, Germany) (Towbin et al., 1979). Experiments were carried out as described previously (Schwinger et al., 1995).

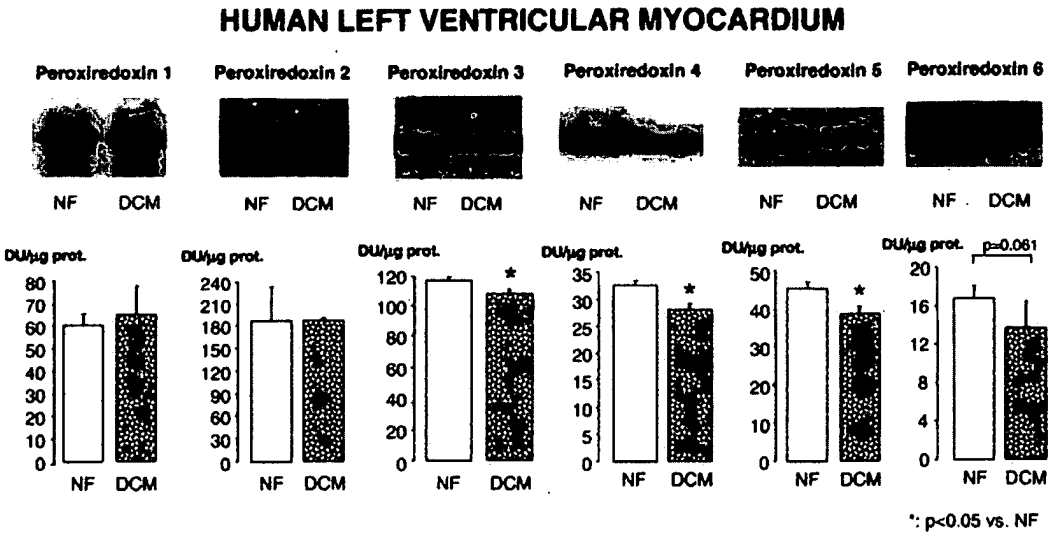

Fig. 1. Protein expression of peroxiredoxin isoforms 1–6 in human left ventricular non-failing ($n=6$) and failing ($n=12$) myocardium. No alterations were observed for the protein expression of peroxiredoxin 1–2 in human left ventricular myocardium. Isoform expression of peroxiredoxin 3–6 was downregulated in human left ventricular failing hearts compared to non-failing hearts. DCM: dilated cardiomyopathy, NF: non-failing, DU/µg prot.: densitometric units/mg protein.

RNA isolation and RNase protection assay

RNA isolation and RNase protection assay were carried out as previously described (Chomczynski and Sacchi, 1987; Werner et al., 1993). The cDNA template for a human peroxiredoxin 4 riboprobe (nt 556–794 of the cDNA (accession number BC016770)) was generated by RT-PCR and cloned into pBluescript KS+ (Stratagene, La Jolla, CA). For the RNase protection assay, samples of 10 µg total RNA were hybridized. As a loading control, a probe for the housekeeping gene glyceraldehyde-3-phosphate dehydrogenase (*gapdh*) was used (Braun et al., 2002).

Immunohistochemical studies

Immunocytochemistry

Prior to immunohistochemical examination, 10 µm slices of shock-frozen myocardial tissue were placed in a bathing solution of 3% H_2O_2 and 80% methanol for 30 min. We then permeabilized the specimens with 0.2% Triton-X 100 in

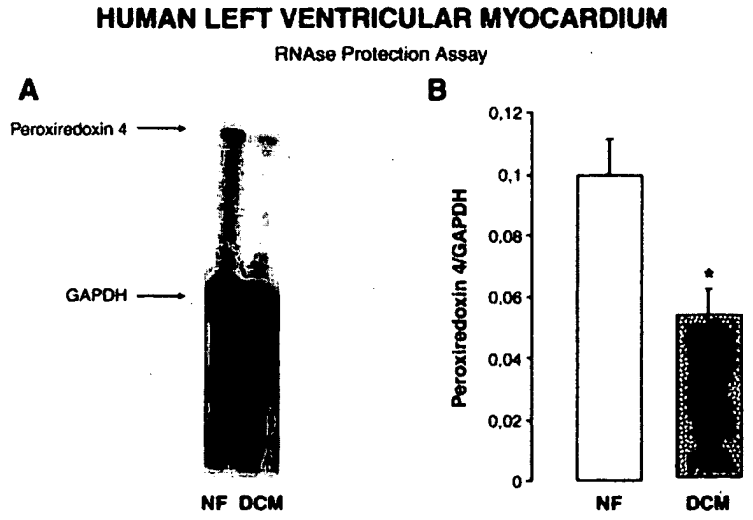

Fig. 2. RNAse protection assay of peroxiredoxin 4 and GAPDH A: original blot, B: summarized data. The mRNA expression of peroxiredoxin 4 was significantly downregulated in human left ventricular failing myocardium. DCM: dilated cardiomyopathy ($n=12$), NF: non-failing ($n=6$). *: $p<0.05$ vs. non-failing.

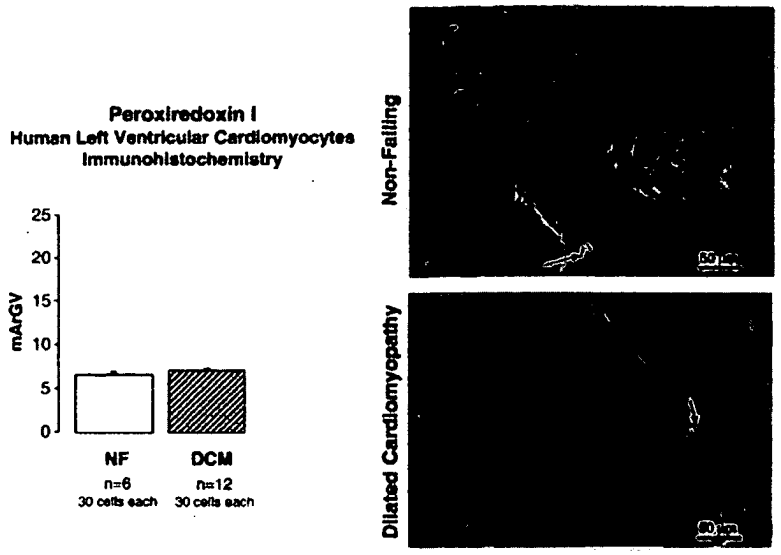

Fig. 3. Representative immunostainings and summarized data for peroxiredoxin I in human left ventricular non-failing ($n=6$) and failing ($n=12$) myocardium. The peroxiredoxin I staining is much more pronounced in the endothelial cells (arrows) than in the cardiomyocytes. DCM: dilated cardiomyopathy, NF: non-failing.

0.1 mol/l PBS. Thereafter, the specimens were treated with 5% bovine serum albumin (BSA) solution in PBS. Prior to each step, the sections were rinsed in PBS buffer at least three times. Incubation with the primary antibody was performed in a PBS-based solution of 0.8% BSA for 12 h at 4 °C. After rinsing with PBS, the sections were incubated with the corresponding secondary biotinylated goat anti-rabbit antibody for 1 h at room temperature. A streptavidin-horseradish peroxidase complex was then applied as a detection system (1:100 dilution) for 1 h. Finally, staining was performed for 3–15 min with 3,3-diaminobenzidine tetrahydrochloride (DAB) in 0.05 mol/l Tris–HCl buffer and 0.1% H_2O_2. Negative control sections were incubated without the primary antibody.

TV-densitometry

For intensity analysis of immunostaining in cardiomyocytes, we measured the gray values of 30 cardiomyocytes from 5 randomly selected areas of each slice. The intensity of

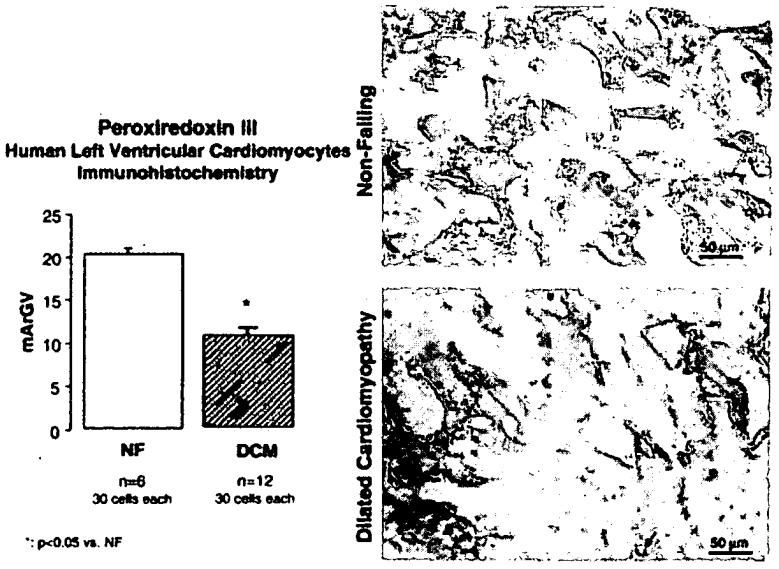

Fig. 4. Representative immunostainings and summarized data for peroxiredoxin 3 in human left ventricular non-failing ($n=6$) and failing ($n=12$) myocardium. The peroxiredoxin 3 staining is more pronounced in the endothelial cells (arrows) than in the cardiomyocytes. Peroxiredoxin 3 staining is reduced in human failing myocardium. DCM: dilated cardiomyopathy, NF: non-failing.

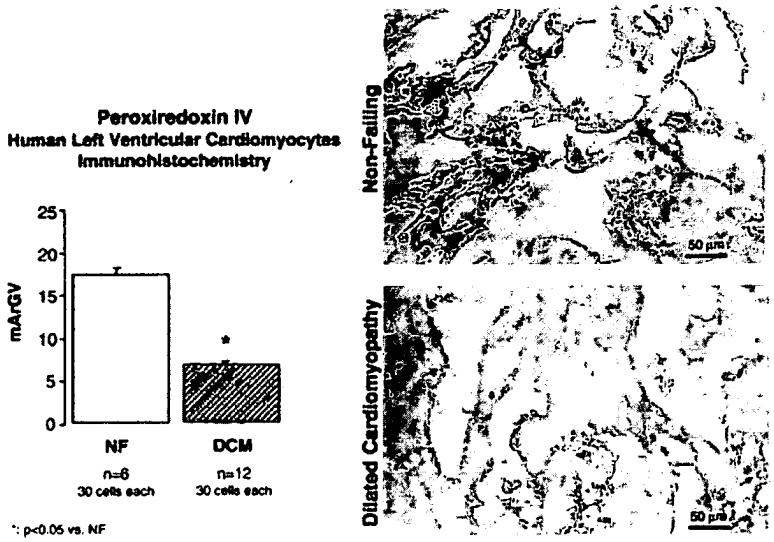

Fig. 5. Representative immunostainings and summarized data for peroxiredoxin 4 in human left ventricular non-failing ($n=6$) and failing ($n=12$) myocardium. The peroxiredoxin 4 staining is more pronounced in the endothelial cells (arrows) than in the cardiomyocytes. Peroxiredoxin 4 staining is reduced in human failing myocardium. DCM: dilated cardiomyopathy, NF: non-failing.

immunostaining was reported as percentage of the mean of measured cardiomyocyte gray value minus background gray value (%mArGV), where 0% was defined as totally white and 100% as totally black. The background gray value was measured in a cell-free area of the slice. For staining intensity detection, a Nikon microscope coupled to a black and white video camera connected to a frame grabber was used. The analysis was performed using the Optimas 6.01 image analysis program (WVU Dept. of Neurobiology and Anatomy, Morgantown, WV, USA). Staining and densitometry were performed as described previously.

Materials

The following primary antibodies were used for immunohistochemistry (IH) and Western blotting (WB): peroxiredoxin 1–5 antibody (all rabbit polyclonal IgG, WB: 1:2000, IH: 1:1000, Acris, Hiddenhausen, Germany). The peroxiredoxin 6 antibody,

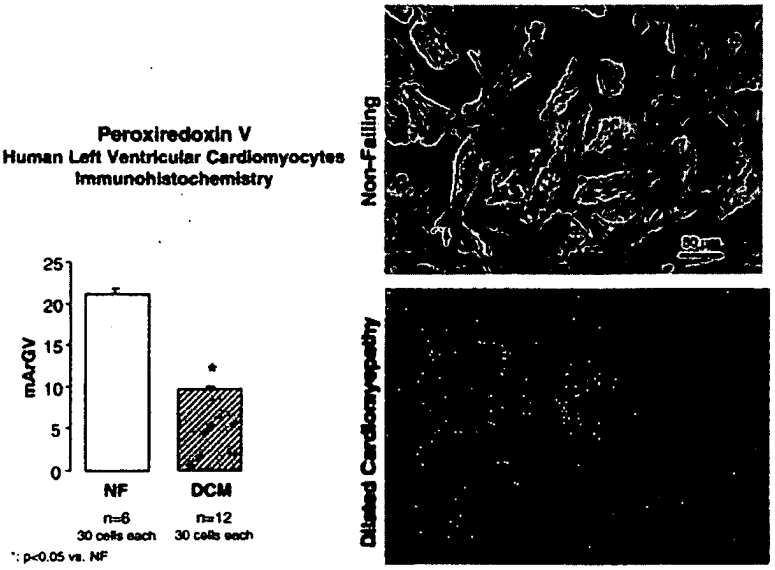

Fig. 6. Representative immunostainings and summarized data for peroxiredoxin 5 in human left ventricular non-failing ($n=6$) and failing ($n=12$) myocardium. The peroxiredoxin 5 staining is more pronounced in the endothelial cells (arrows) than in the cardiomyocytes. Peroxiredoxin 5 staining is reduced in human failing myocardium. DCM: dilated cardiomyopathy, NF: non-failing.

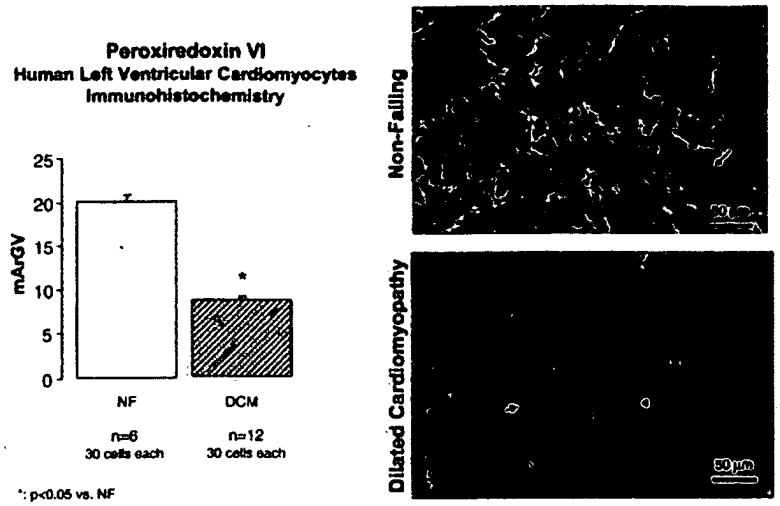

Fig. 7. Representative immunostainings and summarized data for peroxiredoxin 6 in human left ventricular non-failing ($n=6$) and failing ($n=12$) myocardium. The peroxiredoxin 6 staining is more pronounced in the cardiomyocytes than in the endothelial cells (arrows). Peroxiredoxin 6 staining is reduced in human failing myocardium. DCM: dilated cardiomyopathy, NF: non-failing.

which was used for Western blotting, was raised in rabbits against the C-terminal peptide NH_2-CELPSGKKYLRYTPQP-COOH coupled to BSA. The final bleed was directly used for Western blot analysis at a dilution of 1:2000–1:5000.

As secondary antibodies, a biotinylated goat anti-rabbit antibody was used for accentuation.

Statistical analysis

All data are presented as mean±SEM. Data were analyzed using Student's *t*-test for unpaired values under the assumption of similar variance. Additionally, a *t*-test of unconnected values with the assumption of non similar variances (Welch-correction) was performed. Significance was considered at p value <0.05.

Results

To investigate whether the expression of different peroxiredoxin isoforms may be altered in human end-stage heart failure, we performed Western blot experiments with homogenates from left ventricular myocardium of human non-failing and failing hearts. Fig. 1 summarizes the results. We did not observe alterations in the protein expression of peroxiredoxin 1 and 2 in human failing and non-failing myocardium. Peroxiredoxins 3–5 show a significant downregulation in end-stage heart failure. A trend was observed for a downregulation of peroxiredoxin 6.

To investigate whether the downregulation of peroxiredoxin 4 is due to transcriptional or post-transcriptional regulation, we performed RNase-protection assays with a peroxiredoxin 4-specific riboprobe using RNAs from human non-failing and failing myocardium. The results are presented in Fig. 2. A significant downregulation of peroxiredoxin 4 mRNA was observed in human failing myocardium.

Since the protein expression of peroxiredoxins 1–6 was measured in crude tissue homogenates, in which it is not possible to analyse the cellular location of the peroxiredoxin proteins, we performed immunohistochemical stainings in isolated trabeculae of human non-failing and failing myocardium. Figs. 3–7 show representative original immunostainings and summarize the results.

All peroxiredoxin isoforms were present in both endothelial cells and cardiomyocytes. The immunohistochemical stainings of peroxiredoxin 1 appeared to be stronger in the endothelium than in the cardiomyocytes (Fig. 3). No differences were observed for the peroxiredoxin 1-immunostaining between non-failing and failing myocardium.

Similar results were obtained for peroxiredoxin 2 (mArGV, non-failing vs. failing: 5.81±0.21 vs. 5.99±1.39).

As observed for peroxiredoxin 1 and 2, the staining of peroxiredoxins 3, 4 and 5 appeared to be stronger in endothelial than in cardiac cells, at least in non-failing human myocardium (Figs. 4–6). The staining for all three isoforms was decreased in failing human left ventricular myocardium.

Peroxiredoxin 6 was the only isoform for which the staining seemed to be more pronounced in the cardiomyocytes than in the endothelium (Fig. 7). We observed a prominent downregulation of this isoform in human failing left ventricular myocardium.

Discussion

In this study we investigated the protein expression and cellular distribution of peroxiredoxins 1–6 as well as the mRNA levels of peroxiredoxin 4 in human non-failing and failing myocardium. We showed for the first time that there are differences in the cellular distribution of the peroxiredoxin isoforms in human myocardium and that the peroxiredoxin isoforms are differentially regulated in end-stage heart failure.

Reactive oxygen species (ROS), in particular H_2O_2, can participate as benevolent molecules in cell signalling processes or they can induce irreversible cellular damage and death. The control of the elimination of H_2O_2, which results from dismutation of the superoxide anion, is likely to be of special importance, given that this molecule is readily converted to the destructive hydroxyl radical (Rhee, 1999). Enzymes that are capable of eliminating H_2O_2 include the conventional enzymes, catalase and seleno-glutatione peroxidases (Rhee, 1999). Whether these enzymes are altered in human heart failure is currently under discussion. Sam et al. (2005) reported an increased mRNA expression of catalase in patients with heart failure, Khaper et al. (2003) described a decrease in catalase activity, whereas glutathione peroxidase activity was not altered in patients with heart failure. In line with this, a decrease in catalase and glutathione peroxidase activity was also recently described in skeletal muscle of patients with heart failure (Adams et al., 2005).

In addition to catalase and the seleno-glutathione peroxidases, peroxiredoxins comprise a group of enzymes, which are most likely of major importance under stress conditions (reviewed by Hofmann et al., 2002; Rhee et al., 2005). Peroxiredoxins are a new family of peroxidases that reduce H_2O_2 and various organic peroxides with the use of the reducing equivalents of thioredoxin or glutathione (Chae et al., 1994; Rhee et al., 2001). Since the molar efficiencies of peroxiredoxins are by orders of magnitude smaller than those of catalase and the selenium-containing glutathione peroxidases, it has been suggested they are predominantly required under stress conditions (Rhee et al., 2005).

The results of our study suggest a differential regulation of the antioxidative defence mechanisms in human heart. The pure cytosolic isoforms of peroxiredoxin, i.e. isoforms 1 and 2 (which in addition have been found to be more prominent in the endothelial cells of the heart) seem to be unaffected by the enhanced ROS production that has been described in human heart failure (Ide et al., 1999). However, there is a selective downregulation of the mitochondrial peroxiredoxin isoforms 3 and 5, as well as that of the extracellular peroxiredoxin isoform 4 and that of peroxiredoxin 6, another cytosolic isoform.

Our study provides evidence that the downregulation of peroxiredoxin 4 is linked to a downregulation of its mRNA levels, indicating that the alterations in peroxiredoxin expression result from an altered gene expression rather than from alterations in post-transcriptional regulation.

Although the peroxiredoxin 6 isoform seems not to be present in mitochondria, it has been implicated in antioxidant defence, mainly by facilitating repair of damaged cell membranes via reduction of peroxidized phospholipids, especially in the lung (Manevich and Fisher, 2005; Tolle et al., 2005). In line with this, an increased content of peroxidized phospholipids has also been described in cardiomyocytes obtained from failing human hearts (Wolfram et al., 2005). In our study, peroxiredoxin 6 was the only isoform that was more present in the cardiomyocytes than the endothelial cells. The downregulation of the peroxiredoxin 6 isoform was the most prominent alteration we observed in the peroxiredoxin isoforms. Whether there is direct link between the increased content of peroxidized phospholipids and a downregulation of peroxiredoxin 6 has to be shown in further studies. A very recent study in peroxiredoxin knockout mice indicates a non-redundant role of peroxiredoxin 6 in ischemic reperfusion injury since catalase and gluthathione peroxidase could not make up for the deficiencies of peroxiredoxin 6 activities (Nagy et al., 2006).

In a very recent study, it was shown that an over-expression of peroxiredoxin 3 in murine myocardium may be beneficial in preventing cardiac failure (Matsushima et al., 2006). Over-expression of peroxiredoxin 3 inhibited left ventricular remodelling and failure after myocardial infarction (Matsushima et al., 2006). In contrast to our study, no downregulation of peroxiredoxin 3 was observed in wild-type mice with myocardial infarction. Hearts of the mice were excised 28 days after infarction. The different findings regarding peroxiredoxin 3 expression in murine and human heart failure may be due to species differences or may be due to the fact that the hearts of the infarcted mice were excised 28 days after infarct, a time that may be too short for a downregulation of the peroxiredoxins.

A downregulation of peroxiredoxin 3 and 6 has been described in various experimental models that are characterized by an increased cellular oxidative stress. Peroxiredoxin 3 is downregulated in the presence of mutant SOD1 in a cell-culture model and in the spinal cord mitochondria of mutant SOD1 transgenic mice, which are characterized by an increased neuronal oxidative stress. Using quantitative real-time PCR (Q-PCR), it was shown that Prx3 is also downregulated in spinal motor neurons from patients with both sporadic (sMND) and SOD1-related fMND (Wood-Allum et al., 2006). Similar to the findings for peroxiredoxin 3, a downregulation of peroxiredoxin 6 in response to oxidative stress has been described in the etiology of cataract (Pak et al., 2006). Thus, it may be concluded that an increase in cellular oxidative stress (a situation that has been described in human heart failure) seems to be paralleled by a downregulation of peroxiredoxin 3 and 6.

Less is known on the mechanisms underlying the peroxiredoxin downregulation. Interestingly, it has been described that NF-kappaB may suppress Prdx6-expression (Gallagher and Phelan, 2007). Additionally, it has been shown that serum samples from patients with heart failure induce a specific profile of pro- and anti-inflammatory mediators leading to an increase in nuclear factor (NF)-kappaB activation in human pulmonary artery endothelial cells (Hoare et al., 2006). However, whether this mechanism holds true in cardiomyocytes and whether it influences the protein expression of peroxiredoxins 3–5 must be investigated in further studies.

Limitations of the study

The left ventricular failing myocardium obtained for our study was, in some cases, taken from patients who were treated with the xanthine oxidase inhibitor allopurinol. However, we did not observe differences in the results when these patients were excluded. In line with previous studies (de Jong et al., 1990), these results may indicate that xanthine oxidase activity is of minor importance in end-stage heart failure or that ROS

generation by the xanthine oxidase does not affect the antioxidative defence by the peroxiredoxin system.

This study was focused on alterations of expression and cellular localization of the peroxiredoxin isoforms. However, it cannot be excluded that beside a downregulation of protein expression, the peroxiredoxin function may be impaired and/or disregulated by alterations in the phosphorylation of the protein (Chang et al., 2002) or by a hyperoxidation of the Cys-SH to Cys-SO_2H (Yang et al., 2002). This has to be evaluated in further studies.

Conclusions

This study provides evidence that peroxiredoxins are differentially regulated in dilated cardiomyopathy at the subcellular level. It may be speculated that the antioxidative defence, which is especially sensitive for a *high* ROS impact, is dysregulated at sites where an increased ROS-generation has been described in heart failure, i.e. the mitochondria (downregulation of peroxiredoxin 3 and 5). In addition, the "high ROS-specific antioxidative capacity" is downregulated at sites that are important for the maintenance of intracellular Ca^{2+}-homeostasis in end-stage heart failure, e.g. the sarcoplasmic reticulum (downregulation of peroxiredoxin 4). The latter is especially interesting when considering the L-type Ca-channel and the sarcoplasmic reticulum ryanodine receptor interaction. Thus, therapeutic interventions on proteins involved in the regulation of oxidative stress, especially peroxiredoxin isoforms, may be a future aim for the treatment of heart failure patients.

Acknowledgements

This work contains data from the doctoral thesis of F.H. This work was supported in part by the ETH Zurich (fellowship to A.K.) and the Swiss National Science Foundation (grant 3100A0-109340/1 to S.W.). In addition, the authors would like to thank Dr. H. Stützer from the Institute of Medical Statistics, Informatics and Epidemiology, University of Cologne.

References

Adams, V., Linke, A., Krankel, N., Erbs, S., Gielen, S., Mobius-Winkler, S., Gummert, J.F., Mohr, F.W., Schuler, G., Hambrecht, R., 2005. Impact of regular physical activity on the NAD(P)H oxidase and angiotensin receptor system in patients with coronary artery disease. Circulation 111, 555–562.

Bradford, M.M., 1976. A rapid and sensitive method for the quantitation of microgram quantities of protein utilizing the principle of protein-dye binding. Analytical Biochemistry 72, 248–254.

Braun, S., Hanselmann, C., Gassmann, M.G., auf dem Keller, U., Born-Berclaz, C., Chan, K., Kan, Y.W., Werner, S., 2002. Nrf2 transcription factor, a novel target of keratinocyte growth factor action which regulates gene expression and inflammation in the healing skin wound. Molecular and Cellular Biology 22, 5492–5505.

Cha, M.K., Choi, Y.S., Hong, S.K., Kim, W.C., No, K.T., Kim, I.H., 2003. Nuclear thiol peroxidase as a functional alkyl-hydroperoxide reductase necessary for stationary phase growth of Saccharomyces cerevisiae. Journal of Biological Chemistry 278, 24636–24643.

Chae, H.Z., Robison, K., Poole, L.B., Church, G., Storz, G., Rhee, S.G., 1994. Cloning and sequencing of thiol-specific antioxidant from mammalian brain: alkyl hydroperoxide reductase and thiol-specific antioxidant define a large family of antioxidant enzymes. Proceedings of the National Academy of Sciences USA 91, 1721–7017.

Chang, T.S., Jeong, W., Choi, S.Y., Yu, S., Kang, S.W., Rhee, S.G., 2002. Regulation of peroxiredoxin I activity by Cdc2-mediated phosphorylation. Journal of Biological Chemistry 277, 25370–25376.

Chomczynski, P., Sacchi, N., 1987. Single-step method of RNA isolation by acid guanidinium thiocyanate-phenol-chloroform extraction. Analytical Biochemistry 162, 156–159.

de Jong, J.W., van der Meer, P., Nieukoop, A.S., Huizer, T., Stroeve, R.J., Bos, E., 1990. Xanthine oxidoreductase activity in perfused hearts of various species, including humans. Circulation Research 67, 770–773.

Gallagher, B.M., Phelan, S.A., 2007. Investigating transcriptional regulation of Prdx6 in mouse liver cells. Free Radicals in Biology and Medicine 42, 1270–1277.

Giordano, F.J., 2005. Oxygen, oxidative stress, hypoxia, and heart failure. Journal of Clinical Investigation 115, 500–508.

Hoare, G.S., Birks, E.J., Bowles, C., Marczin, N., Yacoub, M.H., 2006. In vitro endothelial cell activation and inflammatory responses in end-stage heart failure. Journal of Applied Physiology 101, 1466–1473.

Hofmann, B., Hecht, H.J., Flohe, L., 2002. Peroxiredoxins. Biological Chemistry 383, 347–364.

Ide, T., Tsutsui, H., Kinugawa, S., Utsumi, H., Kang, D., Hattori, N., Uchida, K., Arimura, K., Egashira, K., Takeshita, A., 1999. Mitochondrial electron transport complex I is a potential source of oxygen free radicals in the failing myocardium. Circulation Research 85, 357–363.

Kang, S.W., Baines, I.C., Rhee, S.G., 1998. Characterization of a mammalian peroxiredoxin that contains one conserved cysteine. Journal of Biological Chemistry 273, 6303–6311.

Khaper, N., Kaur, K., Li, T., Farahmand, F., Singal, P.K., 2003. Antioxidant enzyme gene expression in congestive heart failure following myocardial infarction. Molecular and Cellular Biochemistry 251, 9–15.

Laemmli, U.K., 1970. Cleavage of structural proteins during the assembly of the head of bacteriophage T4. Nature 227, 680–685.

Manevich, Y., Fisher, A.B., 2005. Peroxiredoxin 6, a 1-Cys peroxiredoxin, functions in antioxidant defense and lung phospholipid metabolism. Free Radicals in Biology and Medicine 38, 1422–1432.

Matsumoto, A., Okado, A., Fujii, T., Fujii, J., Egashira, M., Niikawa, N., Taniguchi, N., 1999. Cloning of the peroxiredoxin gene family in rats and characterization of the fourth member. FEBS Letters 443, 50–246.

Matsushima, S., Ide, T., Yamato, M., Matsusaka, H., Hattori, F., Ikeuchi, M., Kubota, T., Sunagawa, K., Hasegawa, Y., Kurihara, T., Oikawa, S., Kinugawa, S., Tsutsui, H., 2006. Overexpression of mitochondrial peroxiredoxin-3 prevents left ventricular remodeling and failure after myocardial infarction in mice. Circulation 113, 1779–1786.

Mizusawa, H., Ishii, T., Bannai, S., 2000. Peroxiredoxin I (macrophage 23 kDa stress protein) is highly and widely expressed in the rat nervous system. Neuroscience Letters 283, 57–60.

Nagy, N., Malik, G., Fisher, A.B., Das, D.K., 2006. Targeted disruption of peroxiredoxin 6 gene renders the heart vulnerable to ischemia-reperfusion injury. American Journal of Physiology 291, H2636–H2640.

Oberley, T.D., Verwiebe, E., Zhong, W., Kang, S.W., Rhee, S.G., 2001. Localization of the thioredoxin system in normal rat kidney. Free Radicals in Biology and Medicine 30, 412–424.

Pak, J.H., Kim, T.I., Joon Kimm, M., Yong Kim, J., Choi, H.J., Kim, S.A., Tchah, H., 2006. Reduced expression of 1-cys peroxiredoxin in oxidative stress-induced cataracts. Experimental Eye Research 82, 899–906.

Rhee, S.G., 1999. Redox signaling: hydrogen peroxide as intracellular messenger. Experimental and Molecular Medicine 31, 53–59.

Rhee, S.G., Kang, S.W., Chang, T.S., Jeong, W., Kim, K., 2001. Peroxiredoxin, a novel family of peroxidases. IUBMB Life 52, 35–41.

Rhee, S.G., Chae, H.Z., Kim, K., 2005. Peroxiredoxins: a historical overview and speculative preview of novel mechanisms and emerging concepts in cell signaling. Free Radicals in Biology and Medicine 38, 1543–1552.

Sam, F., Kerstetter, D.L., Pimental, D.R., Mulukutla, S., Tabaee, A., Bristow, M.R., Colucci, W.S., Sawyer, D.B., 2005. Increased reactive oxygen species production and functional alterations in antioxidant enzymes in human failing myocardium. Journal of Cardiac Failure 11, 473–480.

Schwinger, R.H., Bohm, M., Schmidt, U., Karczewski, P., Bavendiek, U., Flesch, M., Krause, E.G., Erdmann, E., 1995. Unchanged protein levels of SERCA II and phospholamban but reduced Ca2+ uptake and Ca(2+)-ATPase activity of cardiac sarcoplasmic reticulum from dilated cardiomyopathy patients compared with patients with nonfailing hearts. Circulation 92, 3220–3228.

Seo, M.S., Kang, S.W., Kim, K., Baines, I.C., Lee, T.H., Rhee, S.G., 2000. Identification of a new type of mammalian peroxiredoxin that forms an intramolecular disulfide as a reaction intermediate. Journal of Biological Chemistry 275, 20346–20354.

Tolle, A., Schlame, M., Charlier, N., Guthmann, F., Rustow, B., 2005. Vitamin E differentially regulates the expression of peroxiredoxin-1 and -6 in alveolar type II cells. Free Radicals in Biology and Medicine 38, 1401–1408.

Towbin, H., Staehelin, T., Gordon, J., 1979. Electrophoretic transfer of proteins from polyacrylamide gels to nitrocellulose sheets: procedure and some applications. Proceedings of the National Academy of Sciences USA 76, 4350–4354.

Tyagi, N., Moshal, K.S., Ovechkin, A.V., Rodriguez, W., Steed, M., Henderson, B., Roberts, A.M., Joshua, I.G., Tyagi, S.C., 2005. Mitochondrial mechanism of oxidative stress and systemic hypertension in hyperhomocysteinemia. Journal of Cellular Biochemistry 96, 665–671.

Werner, S., Weinberg, W., Liao, X., Peters, K.G., Blessing, M., Yuspa, S.H., Weiner, R.L., Williams, L.T., 1993. Targeted expression of a dominant-negative FGF receptor mutant in the epidermis of transgenic mice reveals a role of FGF in keratinocyte organization and differentiation. Embo Journal 12, 2635–2643.

Wolfram, R., Oguogho, A., Palumbo, B., Sinzinger, H., 2005. Enhanced oxidative stress in coronary heart disease and chronic heart failure as indicated by an increased 8-epi-PGF(2alpha). European Journal of Heart Failure 7, 167–172.

Wood-Allum, C.A., Barber, S.C., Kirby, J., Heath, P., Holden, H., Mead, R., Higginbottom, A., Allen, S., Beaujeux, T., Alexson, S.E., Ince, P.G., Shaw, P. J., 2006. Impairment of mitochondrial anti-oxidant defence in SOD1-related motor neuron injury and amelioration by ebselen. Brain 129, 1693–1709.

Yang, K.S., Kang, S.W., Woo, H.A., Hwang, S.C., Chae, H.Z., Kim, K., Rhee, S.G., 2002. Inactivation of human peroxiredoxin I during catalysis as the result of the oxidation of the catalytic site cysteine to cysteine-sulfinic acid. Journal of Biological Chemistry 277, 3836–38029.

Exhibit B

Henquell, *et al.* (September 1977)
"Intercapillary Distance and Capillary Reserve in Hypertrophied Rat Hearts Beating in Situ."
Circulation Research 41(3): 400-408

Intercapillary Distance and Capillary Reserve in Hypertrophied Rat Hearts Beating in Situ

LOUIS HENQUELL, CHARLES L. ODOROFF, AND CARL R. HONIG

SUMMARY **Functional intercapillary distance (ICD) was measured in stop-motion photomicrographs of hypertrophied, normally compensated, well oxygenated rat hearts beating in situ. Left ventricular hypertrophy was produced by salt loading and unilateral nephrectomy. Minimum ICD (when all capillaries are open) also was measured. Ventricular weight increased by 30–40% within 8–9 weeks after nephrectomy. To compare the effect of normal and pathological growth, ICD was also measured in normal rats. In normal animals, minimum ICD and functional ICD increased linearly and proportionately with left ventricular weight. Consequently, the extent to which capillary recruitment could decrease ICD was the same in large and small normal hearts (about 2 μm). In the hypertrophied hearts, capillary recruitment could have maintained ICD within normal limits at rest for several weeks. After 8–9 weeks, however, the capillary reserve in hypertrophy was fully utilized at rest, and mean functional ICD was 1.5–2.0 μm greater than normal for the age of the animal. An analysis of O_2 transport indicates that anoxic foci would exist throughout the hypertrophied heart and particularly in subendocardium when the capillary reserve is exhausted. The calculated amount of anoxic tissue appears sufficient to account for the focal necrosis and fibrosis observed in hypertrophy and for the development of circulatory failure.**

WEARN et al.[1, 2] were the first to report that myocardial capillary circulation is compromised by the hypertrophy of disease. They concluded that neither the fibers nor the capillaries proliferate, and that the distance between capillaries increases because fiber diameter increases. This view has been challenged by recent studies based on different histological methods which purport to show that capillaries proliferate in pathological hypertrophy.[3–5] However, it seems likely that capillary growth is not proportional to hypertrophy of the muscle fibers.[1–3, 5, 6]

All such studies to date have been performed on dead hearts, and have been designed to determine the total number of capillaries present. Previous reports from this laboratory have shown that, in the rat, about 1/2 the capillaries in right ventricle[7–9] and 1/4 the capillaries in left ventricle[9, 10] are not perfused at rest. These unperfused capillaries constitute a functional reserve, available for adaptation to stress or disease. Consequently, diffusion distances could be maintained at or near the normal value at rest despite hypertrophy, as long as enough capillaries are available in the reserve. The study to be described was undertaken to: (1) evaluate the capillary reserve in hypertrophied hearts, (2) determine the effect of hypertrophy on the uniformity of diffusion distance, and (3) estimate the effect of altered capillary circulation on O_2 transport.

Methods

GENERAL

We studied female Sprague-Dawley rats. Eight pairs of littermates were fed a standard laboratory diet until they reached 160 g at about 45 days. One member of each pair then was subjected to unilateral nephrectomy. In addition, a 60-mg pellet of deoxycorticosterone was implanted under the skin of the back. One week later, 1% NaCl solution was added to the drinking water. Control rats were not nephrectomized, did not receive deoxycorticosterone, and drank only tap water. On the foregoing regimen, the increase in heart weight relative to control is maximal in about 8 weeks.[11] Cardiac failure appears at 10–12 weeks (J. Cohen, unpublished observations). Distances between perfused capillaries were measured at 8–9 weeks. Most experimental rats gained weight at the same rate as controls. If the rate of gain declined, food for the paired control littermate was restricted, so that body weight was the same for both members of the pair. In addition to the littermates described above, 17 female Sprague-Dawley rats weighing 130–580 g were studied to define the effect of normal growth.

To measure distances between capillaries, the rats were anesthetized with sodium pentobarbital, 5 mg/100 g body weight administered intraperitoneally. Cannulas were placed in the trachea, carotid artery, and jugular vein. Body temperature and the cardiac surface (see below) were maintained at 37°C. The rats were ventilated with an O_2-N_2 mixture saturated with water vapor by means of a Harvard rodent respirator at a rate which kept arterial pH (pH_a) within normal limits. Po_2 of inspired gas (PIo_2) was adjusted to maintain Pao_2 between 100 and 250 mm Hg. In this range, a change in Pao_2 has no significant effect on coronary ICD.[10] Phasic and mean arterial blood pressure, rate of change of pressure, and heart rate were monitored with an Electronics for Medicine polygraph.

The chest was opened through a midline incision. Donor blood (1 ml) was given to compensate for the effect of thoracotomy on venous return. The rat was fixed to a carrier fitted to a Leitz Ortholux microscope. By means of a pivot, the rat could be rotated on its long axis to expose the right or left ventricle. Blood gases and pH were mea-

From the University of Rochester, School of Medicine and Dentistry, Rochester, New York.

Supported by Grant HLB03290 from the U.S. Public Health Service and a Grant-in-Aid from the Genesee Valley Heart Association.

Dr. Henquell's present address is: Universite of Besancon, Faculte des Sciences et des Techniques, Laboratoire de Physiologie Animale, 25030 Besancon Cedex, France.

Received June 14, 1976; accepted for publication January 26, 1977.

sured with an Instrumentation Laboratories system before and after each ventricle was filmed. Optical and photographic techniques for stop-motion micrography of the beating heart have been described in detail in several previous reports.[7-10]

Diffusion distances are smallest when all capillaries present are open and perfused. To estimate this minimum distance, we forced precapillary sphincters to relax. To do this, we induced asphyxia by turning off the respirator.[10, 12] The heart stopped beating in 3-4 minutes, and the epicardium was filmed at 15 minutes.

At the end of each experiment, the heart was removed and the atria were trimmed away. The right ventricular free wall was excised and the left ventricle and septum were laid open. Both specimens were blotted and weighed to the nearest milligram on a Mettler analytical balance.

DATA ANALYSIS AND STATISTICS

Photomicrographs in which the capillaries were in sharp focus were projected to a final magnification of exactly 500×. Vessels up to 7 μm in diameter were regarded as capillaries. Center-to-center distances between capillaries in the projected images were 1-2 cm. Films were coded, randomized, and read "blind" by a single observer (L.H.). Cardiac capillaries are, for the most part, long parallel tubes.[7, 13] For each field, a single line was drawn perpendicular to the long axis of the capillaries. All measurements of ICD were made on this line. This measurement procedure is illustrated in Martini and Honig[7] and representative photomicrographs appear in Martini and Honig[7] and Henquell and Honig.[13] The method ensures that deviations from a parallel array do not bias our results and that each capillary is considered only once.

The distance measurements and other variables were entered into an IBM 360/65 computer data file. To check for possible error in the computations, results were analyzed with two types of least squares calculations,[14, 15] "robust" regression,[16] and analysis of variance,[14] with substantially the same result. Lack of sensitivity to choice of mathematical model is strong evidence that the analyses are valid descriptions of the data.

In previous reports, results were expressed as ICD, the distance from the wall of one capillary to the wall of the next. It represents the extra-capillary portion of the diffusion path. Mean capillary diameter with respect to time during the cardiac cycle is 4.4 μm in rat epicardium.[13] We therefore subtracted 4.4 μm from mean center-to-center distances to obtain the values of mean ICD reported in this paper.

Results

GENERAL CHARACTERISTICS OF CONTROL AND EXPERIMENTAL ANIMALS

No evidence of congestive heart failure was observed during life or at autopsy. Tolerance of control and experimental rats to surgery and filming was about the same; in both groups, a stable physiological state existed for 1-2 hours after thoracotomy. If either blood pressure or heart rate changed significantly and failed to respond to donor blood or change in body position, the experiment was terminated. Mean values for some salient parameters are shown in Table 1. Heart weight and left ventricular weight were about 1/3 larger in the experimental rats, even though body weight was the same as in littermate controls. Nevertheless, mean arterial pressure in the experimental rats before the chest was opened was within normal limits and was not significantly higher than in controls. Systolic pressure and pulse pressure, however, were much greater in the experimental rats, and the rate of change of pressure was also greater. Control and experimental rats were not significantly different with respect to heart rate and pH_a. *Mean arterial pressure, pH_a, and $Paco_2$ do not complicate interpretation of results in any event, because they have no significant effect on coronary ICD.*[12]

EXTENT OF HYPERTROPHY

The relations among age, body weight, and ventricular weight for normal rats are estimated by the regressions in Figure 1. The correlation coefficient indicates that 80% of the variability in right ventricular weight and more than 90% of the variability in left ventricular weight is explained by the regression. After adjusting for the difference in intercepts, the slope of the regression for left ventricle is about twice that of the right ($P < 0.001$). In 8 of 10 rats subjected to salt loading and nephrectomy, right ventricular weight fell within the confidence limits. In contrast, all 10 left ventricles were significantly larger than normal. Mean left ventricular weight in the experimental rats was 840 ± 18 (SEM) mg, and mean body weight was 279 ± 7 (SEM) g. The predicted mean left ventricular weight for a 279-g rat is 588 ± 35 mg. Thus the experimental interventions caused an average extra growth of 252 mg. This corresponds to 30% of the observed weight of the hypertrophic left ventricles and 43% of predicted normal left ventricular weight. Older (hence larger) normal rats have left ventricles substantially larger than the hypertrophied ones (see Fig. 1). The regression indicates that the mean left ventricular weight observed in hypertro-

TABLE 1 *General Characteristics of Experimental Rats and Littermate Controls*

	Control	Experimental	*P*
Body wt (g)	275 ± 21	279 ± 12	<0.4
Heart wt (g)	772 ± 53	1057 ± 76	<0.001
Right ventricular wt (g)	149 ± 36	159 ± 20	<0.5
Left ventricular wt (g) (wall and septum)	595 ± 39	840 ± 52	<0.001
Mean arterial pressure (mm Hg)	106 ± 31	118 ± 31	<0.25
Pulse pressure (mm Hg)	38 ± 6.4	52 ± 6.4	<0.02
Heart rate (beats/min)	378 ± 55	331 ± 59	<0.1
Arterial pH	7.43	7.47	<0.25

Results are given in mean ±SD.

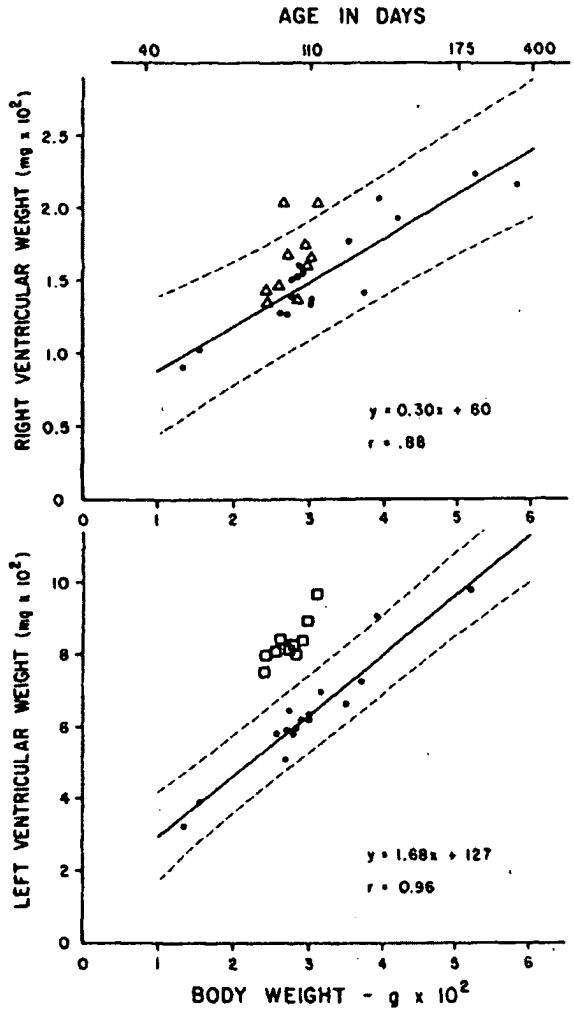

FIGURE 1 *Filled circles and corresponding regression lines indicate relation between ventricular weight and body weight for normal rats. Dashed lines indicate 95% confidence intervals for prediction of an individual value. Open triangles and squares represent values in hypertrophy.*

phy would have been expected had mean body weight been 155 g greater than observed. About 60 days would have been required to add 155 g through normal growth.

MINIMUM ICD

Mean values for ICD in experimental rats and paired littermate controls are shown in Table 2. Values at 0 Pao_2 indicate minimum ICD, provided: (1) asphyxia caused all precapillary sphincters to relax and (2) all capillaries contained enough erythrocytes to be recognized. For analysis of these assumptions, see Discussion. In each of 6 pairs, the apparent minimum diffusion distance was significantly greater in the hypertrophied heart. Mean minimum ICD was 12.89 μm in normal animals and 15.33 μm in hypertrophy. Analysis of histograms of ICD indicates that the higher mean minimum ICD in experimental rats is not attributable to a few very large values. Assuming a square capillary array, the apparent mean minimum ICD corresponds to about 3345 capillaries/mm² in the controls and 2570/mm² in hypertrophy.

MEAN ICD IN WORKING HEARTS (FUNCTIONAL ICD)

Results of nine comparisons in six pairs of rats are summarized in Table 2; see entries for which $Pao_2 > 0$. In eight of these comparisions, functional ICD was significantly greater, at the 2% level or higher, in the hypertrophied heart than in the paired control.

A parabolic relation exists between Pao_2 and ICD;[8, 10] ICD is short when Pao_2 is either less than 100 mm Hg or greater than 300 mm Hg. Intermediate values are associated with long ICD. Note in Table 2 that, in two comparisons, Pao_2 in the control and experimental animals differed by 10 mm Hg or less. In all other cases, the difference in Pao_2 is in the direction which would tend to decrease the observed difference in ICD. Mean functional ICD was 14.21 μm in controls and 15.97 μm in hypertrophy. These values correspond to about 2890 and 2410 capillaries/mm², respectively.

ANALYSIS OF MEAN DIFFERENCES IN ICD

The mean values cited above from data in Table 2 are not adequate for quantitative evaluation of differences in mean ICD in the population of rats. This is true because they are, in fact, means of mean ICD in individual rats. These latter are based on different numbers of observations in each experiment and, therefore, cannot be weighted equally. We therefore used the individual ICD measurements observed in each animal in a weighted, paired, two-way analysis of variance.[14] Littermates, or the same ventricle when normally oxygenated and anoxic, were paired. The weights were proportional to the number of observations.[15] Interactions were not statistically significant for any of the comparisons, indicating that the mathematical model is valid as applied to the data.

Results are summarized in Figure 2. In the normal rats,

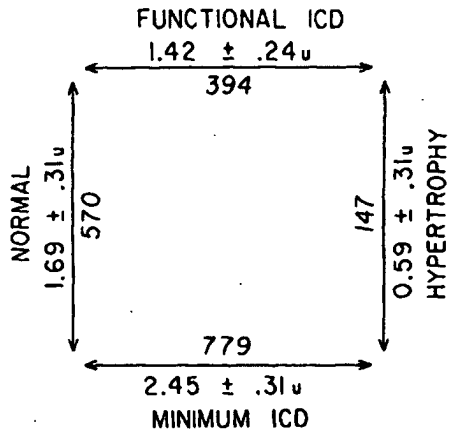

FIGURE 2 *Values outside the square are weighted mean differences in intercapillary distances (ICD) ± SE in microns. A 95% confidence interval for each difference is equal to the particular difference ±2 times its SE. Numbers inside the square indicate differences in calculated capillary densities. Differences are expressed as hypertrophy minus control (horizontal arrows), or functional ICD minus minimum ICD (vertical arrows).*

TABLE 2 *Mean Values of Minimum ICD (PaO_2 = 0) and Functional ICD (PaO_2 > 0)*

Identification no.	Pair no.	Control PaO_2 (mm Hg)	Control n	Control ICD (μm)	Control SD (μm)	Control CAP/mm²	Hypertrophy PaO_2 (mm Hg)	Hypertrophy n	Hypertrophy ICD (μm)	Hypertrophy SD (μm)	Hypertrophy CAP/mm²	P
31/32	1 a	60	92	13.65	3.37	3086	60	61	15.88	3.93	2429	<0.001
	1 b	180	46	14.70	4.25	2741	138	156	16.38	4.52	2316	<0.001
33/34	2 a	67	97	15.65	3.97	2488	55	126	18.29	4.30	1942	<0.001
	2 b	153	84	13.97	3.48	2963	140	95	16.56	5.39	2278	<0.001
36/37	3 a	155	102	13.53	3.48	3111	110	98	15.68	4.24	2480	<0.001
	3 b	240	56	12.60	3.36	3460	240	42	14.30	3.92	2860	<0.001
39/40	4	180	66	13.70	4.43	3052	130	58	13.96	4.00	2967	<0.35
57/58	5	190	62	15.77	4.53	2458	65	93	16.78	5.11	2229	<0.02
59/60	6	210	68	14.19	4.84	2894	130	118	15.92	4.14	2422	<0.001
	Mean			14.21					15.97			
31/32	1	0	81	13.38	4.61	3163	0	77	16.88	4.61	2210	<0.001
33/34	2	0	60	11.39	4.51	4011	0	46	15.21	4.88	2603	<0.001
36/37	3	0	209	12.29	3.43	3590	0	83	14.13	3.24	2912	<0.001
59/60	6	0	24	12.37	3.15	3556	0	66	15.45	4.07	2538	<0.001
63/64	7	0	207	15.38	4.48	2556	0	409	16.82	5.02	2223	<0.02
65/66	8	0	312	12.54	3.48	3485	0	373	13.41	4.11	3153	<0.05
	Mean			12.89					15.33			

n = number of observations; *P* based on paired *t*-test. Capillary densities are computed from ICD, assuming a square array.

functional ICD was 1.69 μm larger than minimum ICD, because about 570 capillaries/mm² were not perfused. These values are different from 0 ($P < 0.001$). In contrast, the mean difference between minimum and functional ICD in hypertrophied hearts was 0.59 μm, corresponding to a mean capillary reserve of 145 capillaries/mm². A 95% confidence interval for these values includes 0, indicating that, if a reserve of unperfused capillaries and of diffusion distance existed in the hypertrophied hearts, it was too small to be detected by our experiments.

Turning now to horizontal comparisons, both minimum ICD and functional ICD were significantly greater in hypertrophied hearts. Because the difference between normal and hypertrophy is significantly smaller for functional ICD than for minimum ICD ($P < 0.001$), recruitment did partly compensate for the effect of growth. This is, of course, expected, since the vertical comparisons indicate that virtually all capillaries in the hypertrophied hearts were being utilized.

COMPARISON OF MEAN ICD IN GROWTH AND HYPERTROPHY

The two regression lines in Figure 3 illustrate the effect of normal growth, as determined by a least-squares analysis performed on 3,483 individual observations of ICD in 30 rats. The normal rats in Table 2 were among those included in the analysis. The 10% difference in slopes of the two lines is not statistically significant, so the lines may be considered parallel. Thus, the maximum effect of capillary recruitment is the same at all ages and ventricular weights shown (about 2 μm). The fact that the open square lies precisely on the regression line indicates that the small sample of littermates used in our study of hypertrophy is representative.

The open triangle was positioned by adding the 1.69-μm difference between minimum and functional ICD obtained from Figure 2 to mean minimum ICD from Table 2. The dashed regression line falls within the 95% confidence interval computed for the 1.69-μm difference, indicating that functional ICD in the littermate controls was within the range expected for normal Sprague-Dawley rats.

The filled symbols in Figure 3 denoting values in hypertrophy were positioned by adding the appropriate differences from Figure 2 to the values represented by the open symbols in Figure 3. Note that minimum ICD in hypertrophy lies very close to the solid regression line. This means that the effect of hypertrophy on the total number of

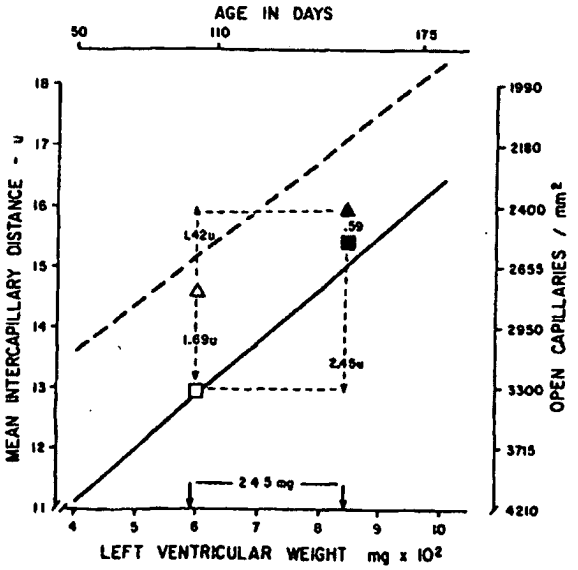

FIGURE 3 *Regressions of minimum ICD (solid line) and functional ICD (dashed line) on ventricular weight in normal rats. Capillary densities are calculated from ICD. Shaded area represents reserve of diffusion distance. Filled symbols represent mean ICD in hypertrophy; open symbols indicate mean ICD in littermate controls. Arrows and numerals are transposed from Figure 2 and have same significance. Upper ordinate (age) does not apply to filled symbols.*

capillaries is the same as if the ventricle had enlarged to the same weight more slowly through normal growth. Normal rats would be expected to have the same minimum ICD observed in hypertrophy only after growing for 2 additional months. At that time, their ventricular weight would have increased by about 45%, and mean minimum ICD would have increased by about 2.4 μm.

The filled triangle in Figure 3 lies well below the value of functional ICD predicted for a normal 840-mg ventricle. The discrepancy is highly significant; the dashed regression line lies outside a 99% confidence interval for functional ICD in hypertrophy. This means that the rats represented by the filled triangle do not belong to the population represented by the dashed regression line. The regression analysis therefore supports the conclusion from Figure 2 that the hypertrophied hearts utilized most or all of their capillary reserve, even under basal conditions. Despite this recruitment, functional ICD in hypertrophy is significantly longer than predicted for the age of the animal ($P < 0.01$); compare open and filled triangles. This is true because fiber diameter[17] and, hence, minimum ICD are larger than predicted for the age; compare open and filled squares.

FREQUENCY DISTRIBUTIONS

Frequency distributions of individual measurements of functional ICD from each of three rats are compared as ogives in Figure 4. They are representative of ogives in other animals, and are similar in shape to ogives for minimum ICD. Two of the 3 rats were normal. One of these weighed 135 g, and its left ventricle weighed 323 mg. The other weighed 520 g and had a 1020-mg ventricle. The shape of the ogives for these rats is similar; the only difference is location on the abscissa. The frequency distribution obtained for a 290-g rat whose ventricle had hypertrophied to 831 mg is also shown. It is nearly superimposable on the distribution for the large, normal rat. This means that the uniformity of capillary spacing with respect to the mean is not much affected by a 3-fold increase in ventricular mass regardless of whether the rate of growth is normal or is accelerated by hypertrophy.

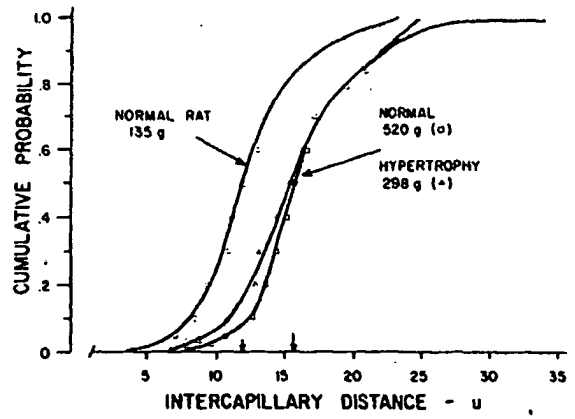

FIGURE 4 *Representative frequency distributions of individual values of ICD in a large and a small normal rat and in a rat with hypertrophy.*

For all 3 rats, the frequency distributions are kurtotic, with attenuated upper and lower "tails." Only about 20% of spacings exceed the median by more than 25%. This high degree of uniformity of spacing greatly facilitates O_2 transport.[8, 10]

Discussion

The unique contribution of the present study is the measurement of ICD in the beating, hypertrophied heart, in situ. This permits us to evaluate the effect of hypertrophy on the coronary capillary reserve. The principal findings are: (1) Recruitment can keep diffusion distances nearly normal at rest, despite a 30-40% increase in ventricular weight. (2) In the model we studied, the effect of hypertrophy on the number of available capillaries, and on the arrangement of capillaries, is the same as if the ventricle had attained the same weight through normal growth. (3) The capillary reserve is exhausted in the final stage of experimental hypertrophy. The following discussion interprets these results.

ROLE OF BLOOD PRESSURE

It is remarkable that ventricular weight should increase 30-40% without significant change in mean arterial pressure. However, peak systolic pressure and rate of change of pressure were greatly increased in every rat. Recent demographic evidence indicates that systolic hypertension is at least as important a determinant of hypertrophy as diastolic hypertension.[18] Our results provide experimental evidence consistent with this view.

CRITICISM AND LIMITATIONS OF EXPERIMENTS

We chose to measure ICD 1-2 weeks before congestive failure was expected. This permitted us to observe the largest possible change in the capillary circulation, but it resulted in the loss of four rats in which the disease progressed more rapidly than anticipated. Consequently, sample size was smaller and confidence intervals were larger than planned. This limits interpretation of our finding that the difference between minimum and functional ICD in hypertrophied hearts is indistinguishable from 0. In fact, a reserve of up to 0.6 μm could exist. However, our sample probably underestimates the effect of hypertrophy, because the reserve should have been smaller in those rats that died before measurements could be made.

The major measurement error in our experiments is in the estimation of minimum ICD. Although it is likely that all precapillary sphincters are relaxed by 15 minutes of asphyxia,[7, 8, 10, 12] capillaries are free to empty during this time. Since we could identify only those capillaries which contained erythrocytes, doubtless some capillaries were not recognized. To evaluate this error, in 2 experiments we identified capillaries by means of the optical properties of the endothelial cells.[13] Minimum ICD so determined was less than 10% shorter than minimum ICD measured in the usual way. The foregoing error does not apply to functional ICD, for, in this case, capillaries that do not contain erythrocytes should, in fact, be omitted from consideration.

Even if we could measure ICD with no error whatever, interpretation would be limited by the fact that we can

observe only the most superficial regions of the wall. In normal rats, mean ICD during diastole is shorter in subendocardium than in subepicardium.[19] This difference in ICD tends to minimize the transmural gradient in tissue Po_2.[20] In hypertrophy, however, the abundance of capillaries appears to be uniform across the wall.[21] The difference in ICD between normal and hypertrophied hearts should therefore be larger in subendocardium than subepicardium.

In considering the clinical relevance of our results, the reader should bear in mind that, in the rat, ventricular weight and ICD[22, 23] increase linearly throughout most of the rat's life, whereas, in normal human beings, ventricular growth virtually ceases after puberty, and minimum ICD remains nearly constant thereafter.[3] Furthermore, our results pertain only to pathological hypertrophy; physiological hypertrophy produces quite different changes in coronary capillary circulation.[24] Finally, the reserve of diffusion distance is much greater in large animals, such as dog and man, than it is in the rat.[8]

FREQUENCY DISTRIBUTIONS OF ICD AND FIBER DIAMETER

The frequency distribution of muscle-fiber diameter in our animal model[17] is remarkably similar to distributions in human hypertrophy secondary to chronic hypertension.[25] The curves have broad flanks, are skewed toward large diameters, and, in most cases, exhibit a long upper tail. In the absence of capillary growth, frequency distributions of minimum ICD in hypertrophy should exhibit similar characteristics. However, this is not the case. Distributions of ICD in hypertrophy have narrow flanks and very short upper tails. The sharp difference between frequency distributions of fiber diameter and ICD is the best evidence that capillaries proliferate in pathological as well as physiological hypertrophy. Capillary growth appears to be greatest where fiber diameter is largest. Nevertheless, growth is not proportional to growth of fibers, because mean minimum ICD is significantly increased.

MINIMUM ICD

According to Wearn and associates,[1, 2] fiber diameter increases and capillary density decreases in experimental hypertrophy in rodents[2] and in various forms of cardiac hypertrophy in man.[1] Wearn et al.[1, 2] claim that the fiber/capillary ratio remains constant, indicating that neither the fibers nor the capillaries multiply. However, the fiber/capillary ratio in their experiments ranged from 0.85–1.65, so partially compensatory growth of capillaries might not have been recognized. A small but statistically significant decrease in the fiber/capillary ratio has in fact been reported by Rakusan and Poupa.[6] They and others[3, 5] conclude, as do we, that capillary growth occurs, but is insufficient to prevent minimum diffusion distance from increasing.

The only investigator who dissents from the foregoing conclusion is Linzbach,[4] who believes that replication of capillaries in pathological hypertrophy maintains diffusion distances within normal limits. However, his histological data have been criticized on technical grounds.[3] Our data, based on a technique free of histological artifacts, indicate that minimum ICD is unmistakeably greater in hypertrophy. Since this has been observed in many forms of hypertrophy and in various species, including man,[1–3, 5, 6, 20] we conclude that a long diffusion path and small capillary reserve underlie the physiology of all forms of pathological hypertrophy.

FUNCTIONAL ICD AND THE CAPILLARY RESERVE

Our study provides the first measurements of functional ICD in hypertrophy. As shown in Figure 3, the rats could have maintained functional ICD within normal limits at rest for several weeks by drawing on the capillary reserve. This is a significant time, since 1 day in the life of a rat is roughly equivalent to 1 month of human life. The cost, of course, is capacity for adaptation to stress.

At the time we made our measurements, ICD was longer than predicted for age, even though virtually all capillaries were being utilized. Note in Figure 3 that minimum ICD in 100-day-old rats with hypertrophy was about the same as the functional ICD in normal littermates. If the experimental rats had not been killed, their functional ICD should have increased at the rate predicted by the solid rather than the dashed regression line. Calculations indicate that this uncompensated increase in diffusion path would have been accompanied by sufficient anoxia to account for cardiac failure.

Recent observations of T.H. Marsicano, R.W. Anderson, and W.N. Duran (personal communication) are in accord with our results. They measured the permeability-surface area product (Na^+) in dogs with experimental left ventricular hypertrophy. They interpret their data to mean that a large capillary reserve exists in normal myocardium and that this reserve is indeed exhausted in the final stage of hypertrophy.

If all capillaries are eventually utilized in hypertrophy, how do equally large normal hearts continue to function? Part of the explanation is that ventricular $\dot{V}o_2/g$ is lower in the normal heart. Normal growth in the rat is accompanied by decreased whole body $\dot{V}o_2$, heart rate, cardiac output, and cardiac work/g[10] all of which are significant determinants of cardiac $\dot{V}o_2/g$. In addition, multiple regression analysis indicates that cardiac $\dot{V}o_2$ decreases with age, per se.[26] During the 2 months which would be required for the ventricle to grow normally to the size observed in hypertrophy, all the foregoing factors would be expected to lower $\dot{V}o_2/g$ of ventricle by at least 25%. Consequently, tissue Po_2 can be maintained despite longer diffusion distances, and, hence, by a smaller fraction of the available capillaries than would be the case in hypertrophy.

EFFECT OF HYPERTROPHY ON O_2 TRANSPORT

In recent years, investigators have sought ultrastructural and biochemical explanations for ventricular dysfunction in hypertrophy and have suggested that diffusion distance is unlikely to be of major importance.[27] Apart from the influence of Linzbach,[4] the chief reason diffusion distance is deprecated is that its effect on O_2 transport in hypertrophy has not been quantified. In the following calculations based on the Krogh equation, we use measured values of capillary diameter, ICD, and the frequency distributions of these parameters, to illustrate the interaction of meta-

bolic and geometrical factors in the pathophysiology of hypertrophy.

Parameters were selected as follows. Mean functional ICD in hypertrophied hearts would have been about 17 μm had there been no compensation by recruitment. If all capillaries had been utilized, ICD would have been 15 μm. We therefore selected 17 and 15 μm for our calculations. Obviously, these values also represent functional and minimum ICD in normal ventricles of the same size.

Capillary diameter and its frequency distribution are not significantly affected by hypertrophy (unpublished observations). Mean capillary diameter over the entire cardiac cycle is 4.4 μm in subepicardium and about 3 μm within the wall.[13] The minimum diameter of a perfused capillary in subendocardium is 1.8 μm.[13]

Ventricular $\dot{V}O_2$ in a young adult (250-g) rat is about 6.5 $\times 10^{-3}$ ml/g per sec.[7, 8] We use this figure for both hypertrophied hearts and littermate controls.[28] Ventricular $\dot{V}O_2$/g is assumed to be 25% less in normal animals whose hearts have grown to the weight observed in hypertrophy.[10] O_2 extraction remains constant with normal growth, so mean capillary P_{O_2} should also be constant in normals.[10]

The only study of left-ventricular hypertrophy due to pressure overload in which coronary flow was measured by means of a flowmeter appears to be that of Malik et al.[28] They report that flow/g is reduced by 25% ($P < 0.05$), and that O_2 extraction is increased ($P < 0.01$). We therefore computed O_2 gradients for these conditions. Since their work lacks confirmation, gradients were also calculated assuming flow and extraction to be normal.

To obtain a "worst case" analysis, we set mean capillary P_{O_2} equal to venous P_{O_2}. One should recognize, however, that a frequency distribution of end-capillary P_{O_2} exists with many values less than half the mean.[29] Mean end-capillary P_{O_2} in the normal adult rat is 20–25 mm Hg,[7] and should be the same in hypertrophy if flow per gram is normal. If flow per gram is reduced by 25% in hypertrophy and $\dot{V}O_2$/g is constant,[28] end-capillary P_{O_2} would fall to about 15 mm Hg. In hypertrophy, the reduction in flow may be largely confined to the deep regions of the wall.[30] In this case, gradients computed for normal flow/g and normal extraction represent conditions in subepicardium, and gradients for reduced flow/g and increased extraction denote conditions in subendocardium.

Analysis of O_2 gradients for normal hearts even larger than the hypertrophied ones in this study indicates that almost no anoxic tissue is present.[10] Figure 5A illustrates the situation in hypertrophy if capillary recruitment did not or could not occur, and if mean ICD were 17 μm. Mitochondria can respire at maximum rate until intracellular P_{O_2} falls below 0.1 mm Hg.[31] Consequently the partial pressure of O_2 in the tissue (P_{TO_2}) should be adequate to support aerobic metabolism for mean ICD if O_2 tension in the capillary is 25 mm Hg (curves 1–3). If subendocardial flow in hypertrophy were restricted and mean end-capillary P_{O_2} were 15 mm Hg, up to $^2/_3$ of the tissue-cylinder cross-section would be anoxic around narrow capillaries (curves 5 and 6). Since mean capillary diameter over the entire cardiac cycle is about 3 μm in subendocardium,[13] anoxia there would be extensive, even for mean capillary spacing.

O_2 profiles around capillaries spaced 25% more widely than in Figure 5A are shown in Figure 5B. About 20% of capillaries are at least that far apart. Anoxia would be

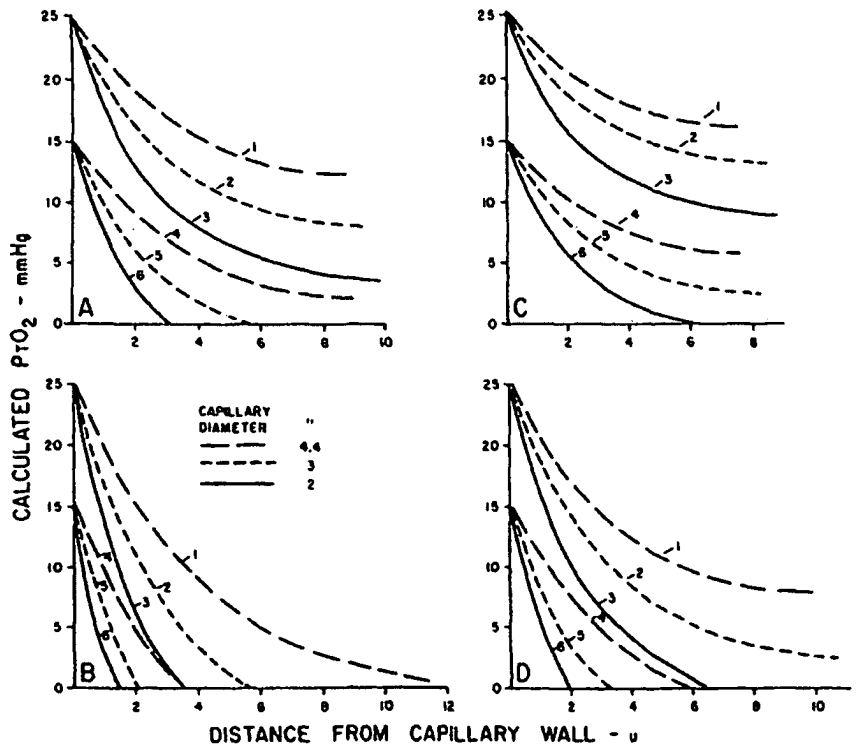

FIGURE 5 *Calculated O_2 gradients in hypertrophy if mean ICD is 17 μm (A and B) and 15 μm (C and D). For interpretation, see text.*

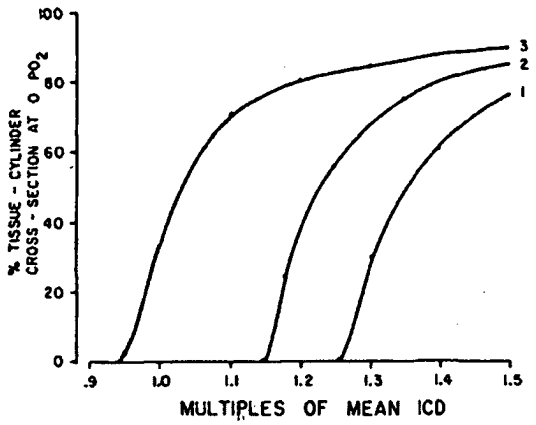

FIGURE 6 *Fraction of tissue-cylinder which is anoxic at venous end of 3 μm capillary for various multiples of 17 μm mean ICD. Curve 1 = normal rat, curves 2 and 3 = subepicardium and subendocardium, respectively, in hypertrophy.*

extensive around the venous ends of narrow capillaries even in the subepicardium (curves 2 and 3) and around all capillaries in the subendocardium (curves 4–6). The situation may be worse than shown, for we have ignored the frequency distribution end-capillary Po_2.

The effect of recruiting all capillaries is shown in Figure 5C. Though this reduces ICD by only 2 μm, it greatly improves O_2 transport. Even if ICD were 25% greater than the 15-μm mean, anoxia would exist only around the narrowest capillaries in subepicardium (see Fig. 5D, curves 1–3). The situation would be less favorable in the subendocardium (Fig. 5D, curves 4–6).

Had we waited until the 12th week, nephrectomized animals would have been in failure. Since the capillary reserve was fully utilized at about 9 weeks, ICD would have increased thereafter according to the solid line in Figure 3. At about 12 weeks, ICD would have reached 17 μm, and the gradients in Figure 5A and 5B would apply. Is the amount of anoxic tissue present under these conditions sufficient to explain the development of congestive failure? To answer this question we determined the fraction of tissue-cylinder cross-section which would be anoxic at the venous ends of 3 μm capillaries for multiples of the 17-μm mean spacing (see Fig. 6). In the normal heart, ICD must be 27% greater than the mean before any anoxia appears and 36% greater before half the tissue-cylinder is anoxic. Normally, less than 10% of capillary spacings exceed the mean by 36%. In contrast, in the subendocardium of the hypertrophied heart, anoxia appears when ICD is less than the mean, and 50% of the tissue-cylinder cross-section would be anoxic when ICD exceeds the mean by only 3%! About half the spacings are at least that long. We conclude that, when the capillary reserve is exhausted, focal anoxia is indeed sufficient to account for the development of cardiac failure. This anoxia also could underlie some of the biochemical and ultrastructural changes recently identified in hypertrophy.[26] Finally, focal anoxia provides the best explanation for patchy necrosis and fibrosis, especially in the subendocardium, in the terminal stage of hypertrophy in animals[5] and in man.[22]

Exercise hypertrophy differs from the hypertrophy of disease in that capillary growth maintains or even reduces minimum diffusion distances.[24] The stimulus is unknown. Quite recently, a humoral factor that promotes growth of capillaries has been isolated from tumors[33] and from ischemic kidneys.[34] Perhaps in pathological hypertrophy there is insufficient production, excessive destruction, or inability to respond to a similar humoral stimulus. If so, therapy designed to shorten diffusion distance may become possible. Our results and analysis strongly suggest that such therapy would eliminate a root cause of cardiac failure in pathological hypertrophy.

Acknowledgments

We are indebted to Dr. Jules Cohen, Professor of Medicine, University of Rochester, for stimulating discussions, and for generously sharing his supply of DOCA pellets. We thank Janet Gough for help with data processing and James L. Frierson for expert technical assistance.

References

1. Roberts JT, Wearn JT: Quantitative changes in the capillary-muscle relationship in human hearts during normal growth and hypertrophy. Am Heart J 21: 617–633, 1941
2. Shipley RA, Shipley LJ, Wearn JT: The capillary supply in normal and hypertrophied hearts of rabbits. J Exp Med 65: 29–42, 1937
3. Arai S, Machida A, and Nakamura T: Myocardial structure and vascularization of hypertrophied hearts. Tohoku J Exp Med 95: 35–54, 1968
4. Linzbach, AJ, Heart failure from the point of view of quantitative anatomy. Am. J. Cardiol. 5: 370–382, 1960
5. Ljungqvist A,Unge G: The finer intramyocardial vasculature in various forms of experimental cardiac hypertrophy. Acta Pathol Microbiol. Scand. [A] 80: 329–340, 1972
6. Rakusan K, Poupa O: Differences in capillary supply of hypertrophic and hyperplastic hearts. Cardiologia 49: 293–298, 1966
7. Martini J, Honig CR: Direct measurement of intercapillary distance in beating rat heart in situ under various conditions of O_2 supply. Microvasc. Res. 1: 244–256, 1969
8. Honig CR, Bourdeau-Martini J: Role of O_2 in control of the coronary capillary reserve. Adv Exp Med Biol 39: 55–71, 1973
9. Henquell L, Honig CR: Intercapillary distances and capillary reserve in right and left ventricles; significance for control of tissue Po_2. Microvasc Res 12: 35–41, 1976
10. Henquell L, Odorff CL, Honig CR: Coronary intercapillary distance during growth; relation to Pro_2 and aerobic capacity. Am. J. Physiol. 231: 1852–1859, 1976
11. Cohen J: Role of endocrine factors in the pathogenesis of cardiac hypertrophy. Circ. Res. 34 (suppl 2): 49–57, 1974
12. Bourdeau-Martini J, Honig CR: Control of intercapillary distance in rat heart; effect of arterial Pco_2 and pH. Microvasc. Res. 6: 286–296, 1973
13. Henquell L, Honig CR: Capillary diameter in rat heart in situ; relation to erythrocyte deformability, O_2 transport and transmural O_2 gradients. Microvasc. Res 12: 259–274, 1976
14. Snedecor GW, Cochran WG: Statistical Methods. Ames, Iowa, Iowa State University Press, 1967, pp 419–446
15. Kempthorne O: The Design and Analysis of Experiments. New York, Wiley, 1952, pp 47–49
16. Andrews DF: A robust method for multiple linear regression. Technometrics 16: 523–531, 1974
17. Chanutin A, Barksdale EE: Experimental renal insufficiency produced by partial nephrectomy. Arch. Intern Med. 52: 739–751, 1933
18. Kannel WB, Castelli WP, McNamara PM, McKee PA, Feinleib M: Role of blood pressure in the development of congestive circulatory failure. N Engl J. Med. 287: 781–787, 1972
19. Myers WW, Honig CR: Number and distribution of capillaries as determinants of myocardial oxygen tension. Am. J. Physiol, 207: 653–660, 1964
20. Kirk ES, Honig CR: Non-uniform distribution of blood flow and gradients of oxygen tension within the heart. Am. J. Physiol. 207: 661–668, 1964
21. Dowell RT: Left ventricular vascularity in the hypertrophied heart (abstr). Physiologist 18: 195 1975
22. Rakusan K, Poupa O: Capillaries and muscle fibers in the heart of old rats. Gerontology 9: 107–112, 1964
23. Rakusan K, Poupa O: Changes in the diffusion distance in the rat

heart muscle during development. Physiol Bohemoslov 12: 220-227, 1963
24. Tomanek RJ: Effects of age and exercise on the extent of the myocardial capillary bed. Anat. Rec. 167: 55-62, 1970
25. Lowe TE, Bate EW: The diameter of cardiac muscle fibers: A study of the diameter of muscle fibers in the left ventricle in normal hearts and in the left ventricular enlargement of simple hypertension. Med. J. Aust 1: 467-469, 1948
26. Cohn AE, Steele JM: The metabolism of the isolated heart of dogs related to age. J. Clin. Invest. 14: 915-922, 1935
27. Alpert NR (ed) Cardiac Hypertrophy. New York, Academic Press, 1971, pp 7 and 15
28. Malik AB, Abe T, O'Kane H, and Geha AS: Cardiac function, coronary flow, and oxygen consumption in stable left ventricular hypertrophy. Am. J. Physiol. 225: 186-191, 1973
29. Grunewald WA, Lübbers DW: Die Bestimmung der intracapillären HbO2-Sättigung mit einer kryomikrofotometrischen Methode angewandt ammyokard des kaninchens. Pfluegers Arch. 353: 255-273, 1975
30. Einzig S, Leonard JJ, Tripp MR, Burchell HB, Fox IJ: Regional myocardial blood flow in closed-chest dogs with left ventricular hypertrophy (abstr). Physiologist 18: 205, 1975
31. Chance B, Oshino N, Sugano T, Mayevsky A: Basic principles of tissue oxygen determination from mitochondrial signals. Adv. Exp Med. Biol. 37: 277-292, 1973
32. Büchner F: Pathologische Anatomie der Herzinsuffizienz. Verhandl. Deut Gesellschaft Kreislaufforsch. 16: 26-43, 1950
33. Folkman J, Merlen E, Abernathy C, Williams G: Isolation of a tumor factor responsible for angiogenesis. J. Exp Med. 133: 275-298, 1971
34. Cutteno JT Jr, Bartrum RJ, Jr, Hollenberg, NK and Abrams HL: Collateral vessel formation: Isolation of a transferable factor promoting a vascular response. Basic Res Cardiol. 70: 568-573, 1975

Circulation Research

JOURNAL OF THE AMERICAN HEART ASSOCIATION

American Heart Association.

Learn and Live℠

Intercapillary distance and capillary reserve in hypertrophied rat hearts beating in situ

L Henquell, CL Odoroff and CR Honig

Circ. Res. 1977;41;400-408

Circulation Research is published by the American Heart Association. 7272 Greenville Avenue, Dallas, TX 72514

 Print ISSN: 0009-7330. Online ISSN: 1524-4571

Exhibit C

Gourine, *et al.* (2004)
"Interstitial purine metabolites in hearts with LV remodeling."
Am J Physiol Heart Circ Physiol 286: H677-H684

Am J Physiol Heart Circ Physiol 286: H677–H684, 2004.
First published October 16, 2003; 10.1152/ajpheart.00305.2003.

Interstitial purine metabolites in hearts with LV remodeling

Andrey V. Gourine,[1] Qingsong Hu,[3] Paul R. Sander,[3] Aleksandr I. Kuzmin,[2]† Nadia Hanafy,[3] Svetlana A. Davydova,[2] Dmitry V. Zaretsky,[2] and Jianyi Zhang[3]

[1]Research Institute of Cardiology, Minsk 5172, Republic of Belarus; [2]National Cardiology Research Center, Moscow 7095, Russia; and [3]Department of Cardiology, University of Minnesota, Minneapolis, Minnesota 55455

Submitted 3 April 2003; accepted in final form 13 October 2003

Gourine, Andrey V., Qingsong Hu, Paul R. Sander, Aleksandr I. Kuzmin, Nadia Hanafy, Svetlana A. Davydova, Dmitry V. Zaretsky, and Jianyi Zhang. Interstitial purine metabolites in hearts with LV remodeling. *Am J Physiol Heart Circ Physiol* 286: H677–H684, 2004. First published October 16, 2003; 10.1152/ajpheart.00305.2003.—The myocardial ATP concentration is significantly decreased in failing hearts, which may be related to the progressive loss of the myocardial total adenine nucleotide pool. The total myocardial interstitial purine metabolites (IPM) in the dialysate of interstitial fluid could reflect the tissue ATP depletion. In rats, postmyocardial infarction (MI) left ventricular (LV) remodeling was induced by ligation of the coronary artery. Cardiac microdialysis was employed to assess changes of IPM in response to graded β-adrenergic stimulation with isoproterenol (Iso) in myocardium of hearts with post-MI LV remodeling (MI group) or hearts with sham operation (sham group). The dialysate samples were analyzed for adenosine, inosine, hypoxanthine, xanthine, and uric acid. LV volume was greater in the MI group (2.2 ± 0.2 ml/kg) compared with the sham group (1.3 ± 0.2 ml/kg, $P < 0.05$). Infarct size was 28 ± 4%. The baseline dialysate level of uric acid was higher in the MI group (18.9 ± 3.4 μmol) compared with the sham group (4.6 ± 0.7 μmol, $P < 0.01$). During and after Iso infusion, the dialysate levels of adenosine, xanthine, and uric acid were all significantly higher in the MI group. Thus the level of IPM is increased in hearts with postinfarction LV remodeling both at baseline and during Iso infusion. These results suggest that the decreased myocardial ATP level in hearts with post-MI LV remodeling may be caused by the chronic depletion of the total adenine nucleotide pool.

heart failure; ATP; β-adrenergic receptors; left ventricle

CONGESTIVE HEART FAILURE (CHF) is associated with abnormal myocardial energy metabolism (9, 12, 20, 31, 44). The mechanisms of this abnormality and the contribution to the evolution from compensated cardiac hypertrophy to CHF are not known (9, 12). The myocardial ATP concentration is significantly decreased in failing hearts (31) or in hearts with postmyocardial infarction (MI) left ventricular (LV) remodeling (44), which may be related to the progressive loss of the myocardial total adenine nucleotide (TAN) pool (31). The levels of interstitial purine metabolites (IPM) under catecholamine stimulation or during regional myocardial ischemia have been demonstrated as sensitive markers of tissue ATP depletion (7, 8, 36).

Previous studies have demonstrated that cardiac hypertrophy is accompanied by abnormal myocardial energetics with a decreased myocardial phosphocreatine (PCr)-to-ATP ratio (PCr/ATP) and increased myocardial free ADP level (17, 19, 27, 35, 39–44). The increase of myocardial free ADP initiates adenylate kinase (myokinase) activation, which catalyzes the transfer of a phosphoryl group between two ADP to form one AMP and one ATP (6, 11, 14, 30, 34). The increased AMP induces the conversion of AMP to adenosine (30). Adenosine can cross the cell membrane and get into the interstitial space, where it is further degraded to inosine and hypoxanthine and leaves the heart with myocardial perfusion (16). The resulting loss of TAN from adenosine diffusion leads to a high demand of the de novo synthesis pathway. This loss of TAN results in the reduction of ATP concentration because the de novo synthesis of the adenine nucleotide is a slow and energy costly process, where inosine monophosphate (IMP) is produced from ribose-5-phosphate, which utilizes six high-energy phosphate bonds (16). In the postischemic myocardium of the dog heart, it was found that the recovery process of the TAN pool takes a few days to complete (11, 32, 34). In dogs with rapid pacing-induced CHF, Shen et al. (31) found that the decreased myocardial ATP concentration is related to the reduction of myocardial TAN (31). The underlying mechanisms of this progressive depletion of the TAN pool during the development of CHF are not known. We hypothesized that if the reduction of myocardial ATP concentration of the remodeling ventricle is caused by a reduction of the TAN pool, then the levels of interstitial purine metabolites (IPM) in the interstitial fluid should be significantly increased in these hearts. Using a rat model of post-MI LV remodeling and the cardiac microdialysis method, we found that the level of IPM was significantly increased in myocardium remote from the LV infarction both at baseline and during isoproterenol (Iso) infusion. These results provide direct evidence to support the hypothesis that the depletion of the TAN pool is significantly greater in hearts with post-MI LV remodeling, which could cause the reduction of the steady-state myocardial ATP concentration in the dysfunctional LV (19, 31, 38, 40, 41, 44). These changes may contribute to the progression of cardiac hypertrophy to chronic heart failure.

METHODS

Animal Model

The experiments were carried out in accordance with the National Institutes of Health *Guide for the Care and Use of Laboratory Animals* and by the regional ethical committee for laboratory animal experiments.

Male Wistar rats ($n = 53$), weighing 250–280 g, underwent either left coronary artery ligation (MI group, $n = 40$) or sham operation (sham group, $n = 13$). MI was produced by left coronary artery

†Deceased 26 April 2000.

Address for reprint requests and other correspondence: J. Zhang, Univ. of Minnesota Health Science Center, Cardiovascular Div., Mayo Mail Code 508, 420 Delaware St. SE, Minneapolis, MN 55455 (E-mail: zhang047@umn.edu).

The costs of publication of this article were defrayed in part by the payment of page charges. The article must therefore be hereby marked "*advertisement*" in accordance with 18 U.S.C. Section 1734 solely to indicate this fact.

ligation by a method described previously (24). Briefly, animals were anesthetized with ketamine hydrochloride (20 mg/kg ip), intubated, and mechanically ventilated with room air. A left thoracotomy through the fourth intercostal space was performed, and the pericardium was removed. The heart was exteriorized by putting pressure on the right hemithorax, and the left coronary artery was occluded with a 6.0-silk suture 1 to 2 mm below the left atrial appendage. Successful occlusion was confirmed by pallor of the anterior wall of the LV and ST segment elevation on ECG. The sham group underwent an identical procedure without coronary artery ligation. All surviving rats between 21 and 24 days after surgery were included in the study. The rats were anesthetized with pentobarbital sodium (50 mg/kg ip). Endotracheal tubes were placed, and the lungs were ventilated with room air (1.2 ml/100 g body wt, 50–60 strokes/min). The right jugular vein and femoral artery were cannulated for drug administration and monitoring of blood pressure (BP), respectively. The chest was opened, and a 2.5-mm electromagnetic flow probe (Transonic Systems; Ithaca, NY) was placed around the ascending aorta. Hemodynamic measurements, including heart rate (HR), mean arterial BP, and cardiac output (CO), were continuously recorded.

To examine whether a significant LV contractile dysfunction occurred in hearts with LV remodeling, LV pressure were measured in a separate group of eight animals with post-MI LV remodeling with a pressure transducer placed in the LV, and results were compared with five sham-operated normal animals.

Cardiac Microdialysis Techniques and Experimental Protocol

A microdialysis probe was implanted into the LV myocardium remote from the LV scar in the MI group and into a nearly similar area of the myocardium in the sham group. Microdialysis probes were constructed with a single dialysis fiber (Cordis Dow; Brussels, Belgium; 0.25 mm outer diameter, molecular weight cutoff 5,000). Each end of the fiber was inserted into outflow and inflow silicon tubes and sealed in place with cyanoacrylic glue. The dialysis fiber length was 6–8 mm and varied depending on the size of infarction. The inflow silicon tube was connected to a glass syringe of a perfusion pump (CMA 100, Carnegie Medicine). After implantation, the microdialysis probe was perfused with Ringer solution [containing (in mM) 147 NaCl, 4.0 KCl, and 2.3 $CaCl_2$] at a rate of 3.0 μl/min. Dialysate sample collection was started 60 min after the probe implantation. The starting infusion rate of Iso was 0.28 $\mu g \cdot kg^{-1} \cdot min^{-1}$ iv. The rate of infusion increased 10-fold every 15 min during the following 1 h. Dialysate samples were collected every 15 min at 30 min before, 60 min during, and 30 min after the end of Iso infusion.

LV Infarct Size and LV Volume

At the end of the hemodynamic experiments and the sample collection, the hearts were arrested by infusion of ice-cold saturated KCl through the jugular vein, excised, and placed in ice-cold KCl to achieve uniform diastolic arrest. The right ventricle was excised, the LV was weighed, and 10% phosphate-buffered formalin was infused continuously into the LV cavity through a double lumen catheter for 24 h. The catheter resulted in a fixation pressure of 7.5 mmHg and was constant for all hearts. After fixation, the LV volume was measured and the base of the heart was excised at the level of the atrioventricular groove. The LV cavity was blotted dry and then filled to volume with saline solution by a 1-ml syringe. Three measurements were averaged for each heart and were corrected for body weight. The hearts were weighed and transversely cut from the apex to base into four uniform slices. Each slice was weighed and scanned on both sides of each slice. The infarct size was measured using Windows-based computer planimetry. The lengths of the scar and noninfarcted muscle for the endocardial and epicardial surfaces were calculated. The ratio of the length of the scar and surface circumferences defined the infarct size for endo- and epicardial surfaces, respectively. Infarct size was determined as the average of endo- and epicardial surfaces and is given as a percentage.

Dialysate Analytic Procedures

The dialysate samples were analysed for adenosine, inosine, hypoxanthine, xanthine, and uric acid (UA) by HPLC with an ultraviolet detection at 254 nm on a 80 × 4.6-mm inner diameter HR-80 column packed with C-18 3-μm particles (ESA). The concentration of adenosine was determined with a mobile phase of 50 mM KH_2PO_4, 2.1 mM sodium octane sulfonate, 2.4 mM sodium hexane sulfonate, and 15% (vol) methanol (pH 4.40) at a flow rate 1 ml/min. The concentrations of inosine, hypoxanthine, xanthine, and UA were determined with a mobile phase of the same content but without methanol (pH 2.35). The absolute detection limit (signal-to-noise ration 3:1) was calculated as 1 pmol/injection for adenosine and as 1.5–2.5 pmol/injection for its metabolites.

Statistical Analysis

All values are presented as means ± SE. Data were analyzed with one-way ANOVA for repeated measurements. The unpaired *t*-test was used for the comparison of data between groups. A value of $P < 0.05$ was required for significance.

RESULTS

Mortality and Exclusions From the Study

Twenty-six of the initially included fifty-three rats died before the experiments (23 in the MI group and 3 in the sham group). Thirteen deaths occurred within the first day after the coronary artery ligation, and another ten animals died after 24 h. All other deaths were between 15 and 23 days after surgery. Autopsy revealed extensive MI and signs of CHF. Three animals died within the first 24 h in the sham group. Four rats were excluded because the infarct size was <15% of the LV. Two animals in the MI group died during the Iso infusion. Two animals in the MI group were excluded from the study due to a large infarct size (>45% of the LV) and wrong position of the microdialysis flow probe. The remaining 19 rats, 9 in the MI group and 10 in the sham group, were included in the cardiac microdialysis study (Table 1). To examine whether a significant LV contractile dysfunction occurred in hearts with LV remodeling, LV pressure was measured in a separate group of eight animals with post-MI LV remodeling (3 of which died within the first 24 h), and the results were compared with five sham-operated normal animals (Table 2).

Body Weight, LV Weight, and Infarct Size

No significant changes in body weight were observed in the MI group compared with the sham group (286 ± 11 vs. 294 ± 14 g, $P > 0.05$). LV mass in the MI group was not significantly higher than that in the sham group (data not shown). LV volume in the MI group was larger (2.2 ± 0.2 ml/kg) compared with the corresponding value in the sham group (1.3 ± 0.2 ml/kg, $P < 0.01$). Mean infarct size was 28 ± 4%.

Baseline Hemodynamic Data and Steady-State IPM Concentrations

The baseline hemodynamic data and steady-state IPM concentrations are summarized in Table 1. Under basal conditions, the HR, CO, and mean arterial BP were not significant different between the two groups (Table 1; P = not significant). In hearts with post-MI LV remodeling, the steady-state concentrations of adenosine, xanthine, and UA were increased significantly (each $P < 0.05$; Table 1).

Table 1. *Hemodynamic and steady-state interstitial purine metabolite concentration*

Groups	n	Heart Rate, beats/min	Cardiac Output, ml/min	Mean Arterial Pressure, mmHg	Steady-State Interstitial Purine Metabolites, μM													
					Adenosine			Inosine			Hypoxanthine			Xanthine			Uric Acid		
					BL	Iso	Recovery	BL	Iso	Recovery	BL	Iso	Recovery	BL	Iso	Recovery	BL	Iso	Recovery
Sham operation	10	297 ±5	53 ±4	118 ±5	0.12 ±0.04	0.19 ±0.08	0.10 ±0.06	0.22 ±0.05	0.56 ±0.06	0.38 ±0.02	0.06 ±0.02	0.29 ±0.13	0.21 ±0.15	0.26 ±0.04	0.56 ±0.17	0.51 ±0.11	5 ±1	13 ±3	19 ±3
LV remodeling	9	292 ±12	45 ±5	109 ±5	0.16 ±0.06	0.24* ±0.07	0.18 ±0.08	0.12 ±0.03	0.46 ±0.07	0.27 ±0.04	0.05 ±0.02	0.23 ±0.06	0.19 ±0.06	0.34* ±0.08	0.75* ±0.12	0.79* ±0.21	19* ±3	55* ±7	70* ±16

Values are means ± SE; *n*, no. of animals. BL, baseline [before isoproterenol (Iso) infusion], Iso, end of Iso infusion; Recovery, end of recovery period after Iso infusion; LV, left ventricular. *$P < 0.05$ vs. sham operation group.

LV Contractile Function

LV contractile function of a separate group of five animals with MI versus five sham-operated normal animals are summarized in Table 2. The LV end-diastolic pressure was significantly increased in hearts with MI ($P < 0.05$), which was accompanied by a significant decrease of the first derivative of LV pressure ($P < 0.05$). These data demonstrate a significant decreased LV contractile performance in the post-MI LV remodeling group.

Time-Course Hemodynamic Data

Figure 1 illustrates the HR, CO, and mean aortic BP before, during, and after the Iso infusion. There were no significant differences between the two groups in hemodynamics before the onset of the Iso infusion. HR did not significantly change in the both groups during the Iso infusion, and there were no other differences between the groups at any time point (Fig. 1*A*). At the highest dose of the Iso infusion and 30 min after the cessation of infusion, higher levels of the rate-pressure product (RPP) were observed in the sham group compared with the MI group (data not shown). Iso induced an increase CO in the sham group only at the lowest rate of infusion but had no effect at higher infusion rates. CO in the MI group did not change throughout the experiment (Fig. 1*C*). Iso in increasing doses in both groups induced a decrease of BP, which persisted until the end of the experiment. At the highest dose of the Iso infusion and 30 min after the cessation of the infusion, higher levels of BP ($P < 0.05$) were observed in the sham group compared with the MI group (Fig. 1*B*).

Time-Course Myocardial Dialysate Purine Metabolite Levels

The temporal profile of dialysate adenosine levels are shown in Fig. 2*A*. The baseline adenosine levels were not different between the two groups. During Iso infusion, adenosine levels increased significantly in the both groups ($P < 0.05$), which was significantly greater in the MI group (Table 1 and Fig. 2*A*).

Table 2. *LV contractile function of animals with postinfarction LV remodeling compared with sham-operated normal animals*

Groups	n	LV dP/dt, mmHg/s	LV End-Diastolic Pressure, mmHg	Infarct Size, %
Sham operation	5	7.6±1.2	6±3	
LV remodeling	5	4.1±1.4*	18±5*	31±4*

Values are means ± SE; *n*, no. of animals. LV dP/dt, first derivative of LV pressure. *$P < 0.05$ vs. sham operation group.

Adenosine levels returned to near-baseline levels in both groups after 30 min after the cessation of the Iso infusion. The sum of dialysate adenosine levels during the Iso infusion was significantly higher ($P < 0.05$) in the MI group than in the sham group (Fig. 2*B*). The temporal profiles of dialysate inosine and hypoxanthine levels are shown in Fig. 3, *A* and *B*. These metabolites increased significantly ($P < 0.05$) in both groups of animals during the Iso infusion and remained elevated after the cessation of the Iso infusion.

The temporal profile of the dialysate xanthine level is shown in Fig. 4*A*. The xanthine level increased significantly during the Iso infusion in both groups ($P < 0.05$) and tended to be higher in the MI group ($P < 0.05$; Table 1). The total sum of dialysate xanthine levels was significantly higher ($P < 0.05$) in the MI group compared with the sham group during and after the cessation of the Iso infusion (Fig. 4*B*). Figure 5 illustrates the temporal profile of dialysate UA level changes. The baseline UA level was fourfold greater in the MI group (18.9 ± 3.4 μM/l) compared with the sham group (4.6 ± 0.7 μM/l, $P < 0.01$). During Iso infusion, the UA levels increased significantly in both groups and tended to increase more in the MI group (Fig. 5; $P < 0.01$). Compared with baseline, the UA levels were increased roughly 400% (Fig. 5) and remained elevated after the discontinuation of Iso infusion.

During the first 30 min of the Iso infusion, the most rapid increase levels of IPM except UA were noted. After this time, the levels were relatively stable through the end of the experiment.

DISCUSSION

The major findings of the present study are that the levels of IPM in myocardium remote from the LV scar both at baseline and during Iso administration were significantly higher in the MI group than in the sham group. These results provide support to the hypothesis that the loss of the TAN pool is significantly greater in hearts with cardiac hypertrophy. These changes may contribute to the decreased myocardial ATP concentration in hypertrophied and failing hearts.

Animal Model

The severity of LV hypertrophy and the rate of development of CHF are proportional to the infarct size (23). Our data showing an increase in LV geometry and decreases of cardiac function are in accordance with previously published data (22, 25, 26, 37).

Cardiac Microdialysis

Van Wylen et al. (36) established cardiac microdialysis as a reliable method to directly measure the purine metabolites

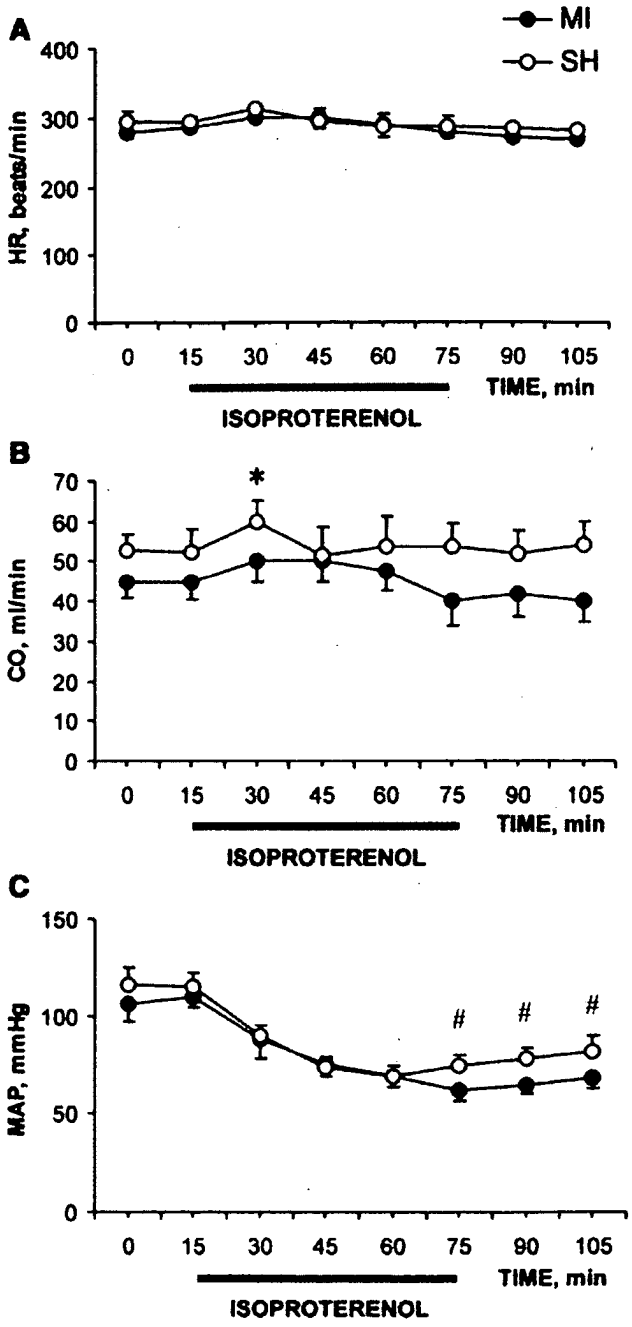

Fig. 1. Time course of changes in heart rate (HR; *A*), mean arterial pressure (MAP; *B*), and cardiac output (CO; *C*) before, during, and after graded β-adrenergic receptor stimulation induced by isoproterenol (Iso) at different rates of infusion in postmyocardial infarction (MI, $n = 10$) or sham-operated (SH, $n = 9$) animals. The starting infusion rate was 0.28 $\mu g \cdot kg^{-1} \cdot min^{-1}$, which was subsequently increased 10-fold every 15 min during the following hour. Data are presented as means ± SE. Significant differences from preinfusion values ($^*P < 0.05$) and the sham group ($\#P < 0.05$) are shown.

during myocardial ischemia or in response to catecholamine stimulation. Headrick (7), using a rat model, demonstrated that the basal dialysate adenosine level was 0.10 ± 0.01 μM and with epinephrine infusion was 3.2 and 8.0 $\mu g \cdot kg^{-1} \cdot min^{-1}$ iv, causing increases in the RPP by 72% and 157%, respectively. This RPP increase was associated with an increase of dialysate adenosine levels to 0.26 ± 0.04 and 0.65 ± 0.11 μM (7), therefore supporting the idea that cardiac interstitial adenosine levels increase in response to catecholamine stimulation dose dependently. A further study by Headrick et al. (8) using a similar infusion rate of epinephrine also demonstrated that the increased myocardial free ADP level (as indicated by the decrease of PCr/ATP) was accompanied by an increased in the dialysate adenosine level. This earlier work is further supported by the present study, as a graded Iso infusion resulted in significant higher dialysate adenosine levels in the MI group ($P < 0.05$; Fig. 2*B*) as a result of the loss in the TAN store.

Myocardial High-Energy Phosphate Metabolism During Catecholamine Stimulation

In the normal heart, the myocardial oxidative phosphorylation (OXHPOS) regulation remains constant over moderate increases of workload (RPP up to ~35,000 $mmHg \cdot beats \cdot min^{-1}$) (1, 13, 40). At higher cardiac workloads (RPP > 45,000 $mmHg \cdot beats \cdot min^{-1}$), several investigators observed that myocar-

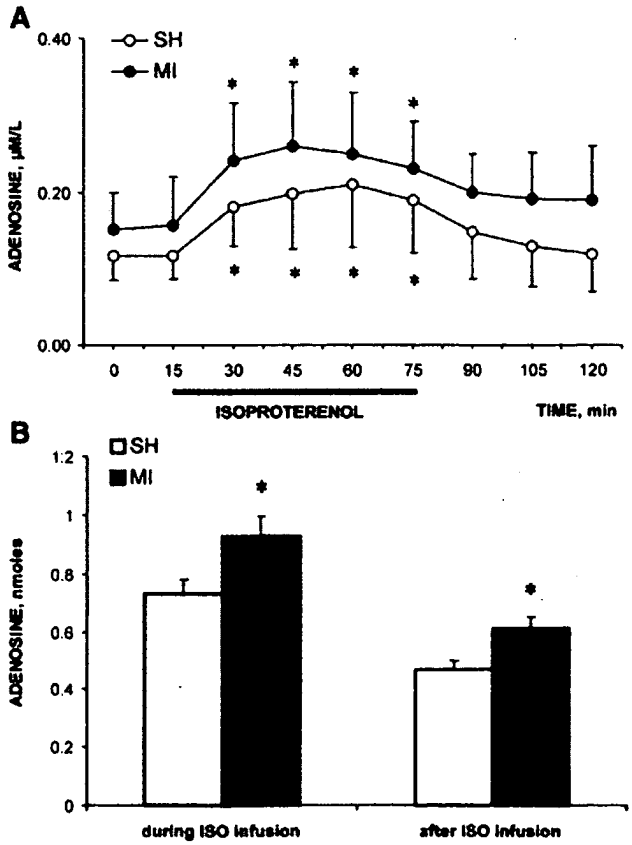

Fig. 2. Time course of changes in dialysate adenosine (*A*) and total dialysate adenosine levels (*B*) during and after graded β-adrenergic receptor stimulation induced by Iso at different rates of infusion in post-MI ($n = 10$) or sham-operated ($n = 9$) animals. The starting infusion rate was 0.28 $\mu g \cdot kg^{-1} \cdot min^{-1}$, which was subsequently increased 10-fold every 15 min during the following hour. Data are presented as means ± SE. Significant differences from preinfusion values ($^*P < 0.05$) and the sham group ($\#P < 0.05$) are shown.

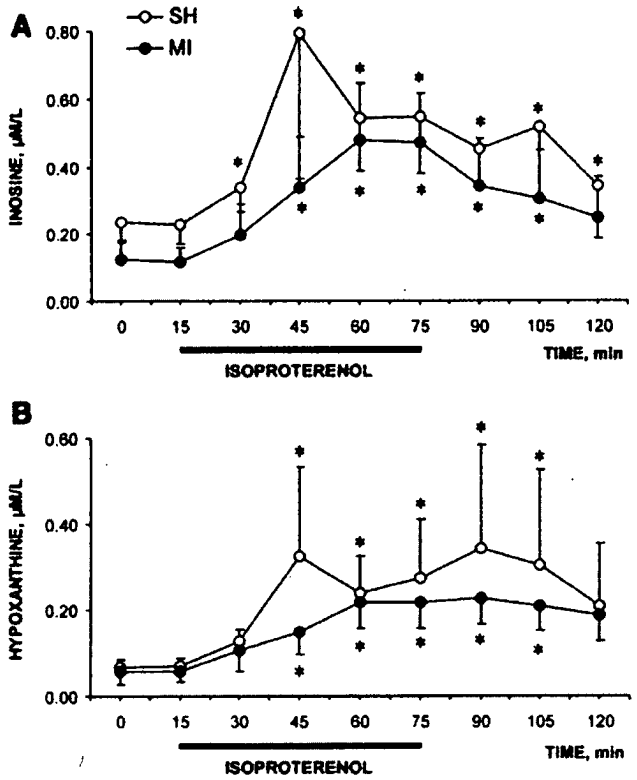

Fig. 3. Time course of changes in dialysate inosine (*A*) and hypoxanthine (*B*) before, during, and after graded β-adrenergic receptor stimulation induced by Iso at different rates of infusion in post-MI (n = 10) or sham-operated (n = 9) animals. The starting infusion rate was 0.28 $\mu g \cdot kg^{-1} \cdot min^{-1}$, which was subsequently increased 10-fold every 15 min during the following hour. Data are presented as means ± SE. Significant differences from preinfusion values ($^*P < 0.05$) are shown.

dial PCr levels fell and calculated ADP levels rose. These changes were associated with the appearance of P_i and some loss of ATP (17, 39). With the recent use of ^1H magnetic resonance spectroscopy to examine the myoglobin oxygen saturation, it was found that these myocardial high-energy phosphate changes that occurred during high-dose catecholamine stimulation were independent from myocardial ischemia (43). Using an experimental system in which the oxygen supply was a strictly controlled variable, Stumpe et al. (33) found that the critical P_{O_2} was 3 mmHg based on the ATP decrease and adenosine increase. In the rat heart in situ, Headrick et al. (8) demonstrated that epinephrine infusion (0.9 $\mu g \cdot kg^{-1} \cdot min^{-1}$ iv) induced an increase of RPP by twofold that was accompanied by a significant decrease of PCr/ATP and a threefold increase of myocardial free ADP. The increase of epinephrine infusion to 2.8 $\mu g \cdot kg^{-1} \cdot min^{-1}$ iv further increased the RPP to 2.7-fold and elevated ADP more than 4-fold (8). These data suggest that in the in vivo heart at high cardiac work states, the myocardial free ADP level is significantly increased, which is accompanied by increased adenosine release. This increase of the myocardial free ADP level is independent from myocardial ischemia but may reflect a different metabolic setpoint of mitochondrial OXPHOS compared with basal cardiac work states.

Increase of Myocardial Free ADP and Reduction of ATP Concentrations

ATP concentration is significantly decreased in large animal models of end-stage CHF with clinical evidence of water retention (ascites) (31, 44). However, decreases in myocardial ATP concentration were not reported in some studies using small animal models of CHF. This discrepancy is most likely due to the fact that the experiments were done at different phases of CHF. The phase of clinical end-stage CHF is very rapid, and it is sometimes difficult to examine the animals at this time point of CHF. In a pig model of CHF, we examined animals at the clinical end stage of CHF. Once cyanosis or an increase of respiration rate occurred, the animals were terminally examined immediately, regardless of the time of the day. This timing may not be possible at other institutions or with other animal models of CHF.

The reasons for the depressed level of ATP in remodeled hearts are not known. Repetitive episodes of ischemia can cause a persistent depression of ATP levels, and this could apply to the subendocardium of CHF hearts in which the coronary reserve is impaired (41). However, no such abnormality was observed (19). An alternative possibility is that the

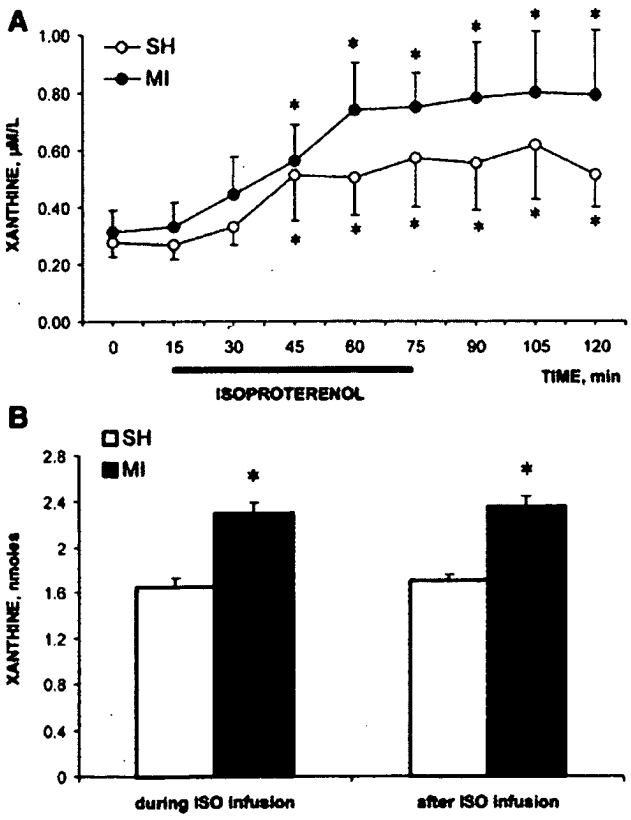

Fig. 4. Time course of changes in dialysate xanthine (*A*) and total dialysate xanthine levels (*B*) during and after graded β-adrenergic receptor stimulation induced by Iso at different rates of infusion in post-MI (n = 10) or sham-operated (n = 9) animals. The starting infusion rate was 0.28 $\mu g \cdot kg^{-1} \cdot min^{-1}$, which was subsequently increased 10-fold every 15 min during the following hour. Data are presented as means ± SE. Significant differences from preinfusion values ($^*P < 0.05$) and the sham group ($^\#P < 0.05$) are shown.

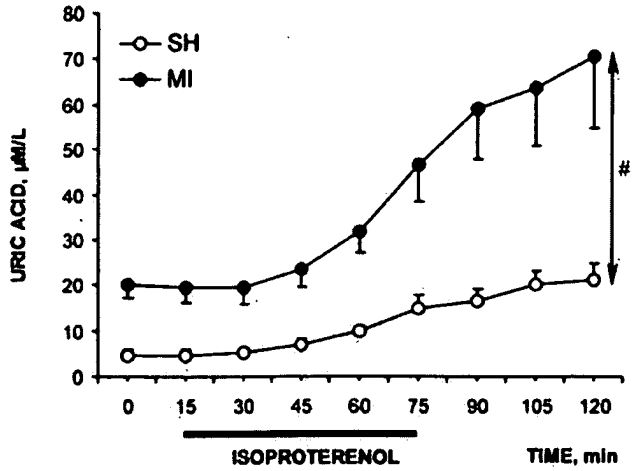

Fig. 5. Time course of changes in dialysate uric acid levels changes before, during, and after graded β-adrenergic receptor stimulation induced by Iso at different rates of infusion in post-MI (n = 10) or sham-operated (n = 9) animals. The starting infusion rate was 0.28 $\mu g \cdot kg^{-1} \cdot min^{-1}$, which was subsequently increased 10-fold every 15 min during the following hour. Data are presented as means ± SE. Significant differences from preinfusion values ($^*P < 0.05$) and the sham group ($\#P < 0.05$) are shown.

higher ADP levels in the remodeled hearts enhanced ATP catabolism via myokinase (7) and subsequent degradative reactions (31). In the myocyte, the mechanism that controls the set point of steady-state ATP levels is unclear, but it must reflect a balance between adenine nucleotide synthesis and degradation. If degradative reaction rates are even slightly enhanced in the absence of a compensatory increase in nucleotide synthetic rates, the net result could be a lower equilibrium for steady-state ATP levels. In principle, the ATP production rate should contribute to the steady-state myocardial ATP concentration. However, in the in vivo heart, this equation is complicated by the high reserve capacity of mitochondrial ATPase and the multiple regulations of the cascade ATP production pathway.

Reduced ATP production. In the heart, the contractile chemical energy ATP is mainly produced in mitochondria. Mitochondrial ATP synthase (mtATPase), which is embedded in the mitochondrial inner membrane, drives ATP synthesis using energy generated from the electrochemical proton gradient across the inner mitochondrial membrane (5, 15). The protein levels of mtATPase F_1F_0 subunits were all lower in failing versus normal hearts, and the decreases were significantly related to the degree of reduction of the myocardial steady-state high-energy phosphate levels: PCr and ATP (15, 38). This implies that reductions of ATPase protein expression are associated with the degree of reduced ATP concentration (15, 38). A decrease of the β-F_1-ATPase activity or an increase of its apparent K_m value with respect to ADP could require an increase of cytosolic ADP and P_i levels to maintain a given rate of ATP synthesis. In the in vivo heart, because of the presence of endogenous inhibitors, including inhibition factor 1, ATP synthetic activity cannot be directly equated with the myocardial F_1-ATPase content. Because of the presence of baseline inhibition, the protein content cannot be directly equated with in vivo enzyme activity. However, the decreased protein expression could limit the maximum ATP synthesis rates achievable during state of an maximum increased ATP demand/utilization, which could result in a reduction of ATP concentration.

Decrease of ATP transfer. Mitochondrial creatine kinase (CK) and the β-subunit of F_1-ATPase, respectively, facilitate ADP/ATP exchange across the inner mitochondrial membrane and catalyze the phosphorylation of ADP to form ATP. The specific intracellular localization of CK isoforms serves to maintain low cytosolic ADP levels in the normal heart. In post-MI LV remodeled hearts and in failing hearts, a fetal shift of myocardial CK expression has been reported, with a decrease in the MM isoform and increases in the MB and BB isoforms (9, 19, 38). Similar findings were observed in a canine model of LV hypertrophy produced by ascending aortic banding. Although the mechanism and functional consequences of these CK isoform shifts in the hypertrophied and failing heart are unclear, previous studies have demonstrated that decreases of CK activity have the potential to affect myocardial ATP concentration and performance. Mitochondrial CK is located in association with adenine nucleotide translocase, where it catalyzes the transfer of a phosphoryl from ATP to creatine, forming PCr. In this fashion, mitochondrial CK can maintain high local levels of ADP for ATP synthase but low mean cytosolic ADP values. Conversely, CK-MM, located adjacent to myosin ATPase, can catalyze phosphoryl transfer from PCr to ADP formed during contraction, thereby maintaining high ATP levels to drive contraction and also acting to maintain low mean cytosolic levels of ADP. The reexpression of the fetal gene program with increased CK-B and decreased CK-M and mitochondrial CK in the post-MI heart is associated with higher cytosolic levels of ADP for any rate of ATP synthesis. Therefore, it is possible that alterations of CK isoform expression could have contributed to the decreased myocardial ATP level in failing hearts.

Increased ATP utilization. One primary indicator of heart failure is a significantly increased LV volume/end-diastolic pressure (Table 2). A dilated ventricle by necessity requires significantly more ATP to support itself in accordance with Laplace's Law.

Reduction of the TAN pool. During the steady state of metabolic activity of normal myocardium, the balance of the continual loss of myocardial purine nucleotides is mainly via the salvage pathways by which one enzyme convert a purine nucleotide or base to another nucleotide (16). However, in postischemic myocardium, the reestablish of the normal TAN pool is thought to occur via a de novo pathway by which purine nucleotides are synthesized from nonpurine precursors (11, 16, 32, 34). In diseased myocardium, the increase of myocardial free ADP initiates adenylate kinase (myokinase) activation, which catalyzes the transfer of a phosphoryl group between two ADP to form one AMP and one ATP (8, 16). The resulting increased AMP would favor the conversion of AMP to adenosine (33), finally leading to myocyte adenosine deaminase degradation of adenosine to inosine (2, 32). Unlike adenine nucleotides, which do not cross the sarcolemma, adenosine and inosine can cross the cell membrane to the interstitial space, where they are degraded to hypoxanthine, xanthine, and UA (16, 18, 31) and subsequently eliminated from the heart via myocardial blood flow. This depletion of the TAN pool results in a reduction of ATP as the resynthesis of adenine nucleotide is a slow and energy costly process. The resynthesis of adenine

nucleotide is through de novo synthesis, where inosine monophosphate is produced from ribose-5-phosphate, which uses six high-energy phosphate bonds (16). It has been reported that in the stunned myocardium the loss of ATP during acute myocardial ischemia as a consequence of the reduction of TAN requires several days to recover (16, 34). In the present study, we found that the myocardial IPM level was significantly increased in hearts with post-MI LV remodeling. This change may be caused by a significant increase of the myocardial free ADP level that was repeatedly observed in hearts with cardiac hypertrophy of different animal models (21, 22, 29, 30, 43). The depletion of TAN, as indicated by the increased IPM levels in cardiac microdialysis, could result in a significant decrease of myocardial ATP concentration in failing hearts (31, 41).

Increased IPM and Increased Reactive Oxygen Species

The last purine metabolite, UA, is formed by the enzyme xanthine oxidase (XO) (10). Data from the present study indicate that dialysate xanthine and UA in hearts with post-MI LV remodeling were significantly increased, which indicates that XO activity may also be increased. Ekelund et al. (4) found that XO activity was fourfold increased in failing hearts compared with controls. It is interesting to note that XO forms superoxide radical in the terminal step of the purine metabolism that has been proposed as a pathogenic factor in the development of CHF (5). More recently, data from both experimental animal models as well as clinical observations indicate that the XO inhibitor allopurinol decreases the myocardial energy demands and at the same time increases cardiac contractility in failing hearts but not in normal hearts (3, 4). This observation supports the hypothesis that superoxide radical is increased in myocardium of failing hearts, which may be caused by the abnormal protein expression of the enzymes of mitochondrial oxidative phosphorylation regulation (OXPHOS) (15, 38).

In conclusion, failing hearts are associated with an increased level of myocardial total interstitial purine metabolites both at baseline and during Iso infusion, which may be triggered by the alterations in the mitochondrial OXPHOS set point with a manifestation of increased cytosolic free ADP. This abnormality may contribute to the reduction of myocardial ATP concentration in failing hearts, which, in turn, could contribute to the progression of cardiac hypertrophy to chronic heart failure.

GRANTS

This study was supported by National Heart, Lung, and Blood Institute Grants HL-50470, HL-61353, HL-67828, and HL-71970 and an Established Investigator Award from the American Heart Association.

REFERENCES

1. **Balaban RS, Kantor HL, Katz LA, and Briggs RW.** Relation between work and phosphate metabolite in the in vivo paced mammalian heart. *Science* 232: 1121–1123, 1986.
2. **Bowditch J, Brown AK, and Dow JW.** Accumulation and salvage of adenosine and inosine by isolated mature cardiac myocytes. *Biochim Biophys Acta* 844: 119–128, 1985.
3. **Cappola TP, Kass DA, Nelson GS, Berger RD, Rosas GO, Kobeissi ZA, Marban E, and Hare JM.** Allopurinol improves myocardial efficiency in patients with idiopathic dilated cardiomyopathy. *Circulation* 104: 2407–2411, 2001.
4. **Ekelund UE, Harrison RW, Shokek O, Thakkar RN, Tunin RS, Senzaki H, Kass DA, Marban E, and Hare JM.** Intravenous allopurinol decreases myocardial oxygen consumption and increases mechanical efficiency in dogs with pacing-induced heart failure. *Circ Res* 85: 437–445, 1999.
5. **Ghatak A, Brar MJ, Agarwal A, Goel N, Rastogi AK, Valsh AK, Sircar AR, and Chandra M.** Oxy free radical system in heart failure and therapeutic role of oral vitamin E. *Int J Cardiol* 57: 119–127, 1996.
6. **Gustafson LA and Kroll K.** Downregulation of 5′-nucleotidase in rabbit heart during coronary underperfusion. *Am J Physiol Heart Circ Physiol* 274: H529–H538, 1998.
7. **Headrick JP.** Interstitial adenosine and function in rat heart in vivo: effects of adrenaline and 8-cyclopentyl-1,3-dimethylxanthine. *Clin Exp Pharmacol Physiol* 23: 386–394, 1996.
8. **Headrick JP, Dobson GP, Williams JP, McKirdy JC, Jordan L, and Willis RJ.** Bioenergetics and control of oxygen consumption in the in situ rat heart. *Am J Physiol Heart Circ Physiol* 267: H1074–H1084, 1994.
9. **Ingwall JS.** Is cardiac failure a consequence of decreased energy reserve? *Circulation* 87, *Suppl* VII: VII-58–VII-62, 1993.
10. **Jarasch ED, Bruder G, and Heid HW.** Significance of xanthine oxidase in capillary endothelial cells. *Acta Physiol Scand Suppl* 548: 39–46, 1986.
11. **Jennings RB, Riemer KA, Hill ML.** Total ischemia in dog hearts. *Circ Res* 49: 901–911, 1981.
12. **Katz AM.** Cardiomyopathy of overload. A major determinant of prognosis in congestive heart failure. *N Engl J Med* 322: 100–110, 1989.
13. **Katz LA, Swain JA, Portman MA, and Balaban RS.** Relation between phosphate metabolites and oxygen consumption of heart in vivo. *Am J Physiol Heart Circ Physiol* 256: H265–H274, 1989.
14. **Kroll K, Kinzie DJ, and Gustafson LA.** Open-system kinetics of myocardial phosphoenergetics during coronary underperfusion. *Am J Physiol Heart Circ Physiol* 272: H2563–H2567, 1997.
15. **Liu J, Wang C, Murakami Y, Gong G, Ishibashi Y, Prody C, Ochiai K, Bache RJ, Godinot C, and Zhang J.** Mitochondrial ATPase and high energy phosphates in failing heart. *Am J Physiol Heart Circ Physiol* 281: H1319–H1326, 2001.
16. **Manfredi JP and Holmes EW.** Purine salvage pathways in myocardium. *Annu Rev Physiol* 47: 691–705, 1985.
17. **Massie BM, Schwartz GG, Garcia J, Wisneski JA, Weiner MW, and Twyman O.** Myocardial metabolism during increased work states in the porcine left ventricle in vivo. *Circ Res* 74: 64–73, 1994.
18. **Moriwaki Y, Yamamoto T, and Higashino K.** Enzymes involved in purine metabolism–a review of histochemical localization and functional implications. *Histol Histopathol* 14: 1321–1340, 1999.
19. **Murakami Y, Zhang Y, Cho YK, Mansoor AM, Chung JK, Chu C, Francis G, Ugurbil K, Bache RJ, From AH, Jerosch-Herold M, Wilke N, and Zhang J.** Myocardial oxygenation during high work states in hearts with postinfarction remodeling. *Circulation* 99: 942–948, 1999.
20. **Neubauer S, Horn M, Cramer M, Harre K, Newell JB, Peters W, Pabst T, Ertl G, Hahn D, Ingwall JS, and Kochsiek K.** Myocardial phosphocreatine-to-ATP ratio is a predictor of mortality in patients with dilated cardiomyopathy. *Circulation* 96: 2190–2196, 1997.
21. **Neubauer S, Horn M, Naumann A, Tian R, Hu K, Laser M, Friedrich J, Gaudron P, Schnackerz K, and Ingwall JS.** Impairment of energy metabolism in intact residual myocardium of rat hearts with chronic myocardial infarction. *J Clin Invest* 95: 1092–1100, 1995.
22. **Omerovic E, Bollano E, Basetti M, Kujacic V, Waagstein L, Hjalmarson A, Waagstein F, and Soussi B.** Bioenergetic, functional and morphological consequences of postinfarct cardiac remodeling in the rat. *J Mol Cell Cardiol* 31: 1685–1695, 1999.
23. **Pfeffer MA and Braunwald E.** Ventricular remodeling after myocardial infarction. Experimental observations and clinical implications. *Circulation* 81: 1161–1172, 1990.
24. **Pfeffer MA, Pfeffer JM, Fishbein MC, Fletcher PJ, Spadaro J, Kloner RA, and Braunwald E.** Myocardial infarct size and ventricular function in rats. *Circ Res* 44: 503–512, 1979.
25. **Pfeffer JM, Pfeffer MA, Fletcher PJ, and Braunwald E.** Progressive ventricular remodeling in rat with myocardial infarction. *Am J Physiol Heart Circ Physiol* 260: H1406–H1414, 1991.
26. **Pfeffer MA, Pfeffer JM, Steinberg C, and Finn P.** Survival after an experimental myocardial infarction: beneficial effects of long-term therapy with captopril. *Circulation* 72: 406–412, 1985.
27. **Saupe KW, Spindler M, Tian R, and Ingwall JS.** Impaired cardiac energetics in mice lacking muscle-specific isoenzymes of creatine kinase. *Circ Res* 82: 898–907, 1998.
28. **Schoutsen B and de Jong JW.** Age-dependent increase in xanthine oxidoreductase differs in various heart cell types. *Circ Res* 61: 604–607, 1987.

29. **Schutz W, Schrader J, and Gerlach E.** Different sites of adenosine formation in the heart. *Am J Physiol Heart Circ Physiol* 240: H963–H970, 1981.
30. **Skladanowski AC and Newby AC.** Partial purification and properties of an AMP-specific soluble 5′-nucleotidase from pigeon heart. *Biochem J* 268: 117–122, 1990.
31. **Shen W, Asai K, Uechi M, Mathier MA, Shannon RP, Vatner SF, and Ingwall JS.** Progressive loss of myocardial ATP due to a loss of total purines during the development of heart failure in dogs: a compensatory role for the parallel loss of creatine. *Circulation* 100: 2113–2118, 1999.
32. **St Cyr JA, Bianco RW, Schneider JR, Mahoney JR Jr, Tveter K, Einzig S, Foker JE.** Enhanced high energy phosphate recovery with ribose infusion after global myocardial ischemia in a canine model. *J Surg Res* 46: 157–162, 1989.
33. **Stumpe T and Schrader J.** Phosphorylation potential, adenosine formation, and critical P_{O_2} in stimulated rat cardiomyocytes. *Am J Physiol Heart Circ Physiol* 273: H756–H766, 1997.
34. **Swain JL, Sabina RL, McHale PA, Greenfield JC Jr, and Holmes EW.** Prolonged myocardial nucleotide depletion after brief ischemia in the open-chest dog. *Am J Physiol Heart Circ Physiol* 242: H818–H826, 1982.
35. **Tian R, Musi N, D'Agostino J, Hirshman MF, and Goodyear LJ.** Increased adenosine monophosphate-activated protein kinase activity in rat hearts with pressure-overload hypertrophy. *Circulation* 104: 1664–1669, 2001.
36. **Van Wylen DG, Willis J, Sodhi J, Weiss RJ, Lasley RD, and Mentzer RM Jr.** Cardiac microdialysis to estimate interstitial adenosine and coronary blood flow. *Am J Physiol Heart Circ Physiol* 258: H1642–H1649, 1990.
37. **Waller C, Hiller KH, Kahler E, Hu K, Nahrendorf M, Voll S, Haase A, Ertl G, and Bauer WR.** Serial magnetic resonance imaging of microvascular remodeling in the infarcted rat heart. *Circulation* 103: 1564–1569, 2001.
38. **Ye Y, Gong G, Ochiai K, Liu J, and Zhang J.** High-energy phosphate metabolism and creatine kinase in failing hearts. *Circulation* 103: 1570–1576, 2001.
39. **Zhang J, Duncker DJ, Xu Y, Zhang Y, Path G, Merkle H, Hendrich K, From AHL, Bache RJ, and Ugurbil K.** Bioenergetic responses of normal myocardium at very high workstates: an in vivo transmural ^{31}P NMR study. *Am J Physiol Heart Circ Physiol* 268: H1891–H1905, 1995.
40. **Zhang J and McDonald K.** Bioenergetic consequence of left ventricular remodeling secondary to discrete myocardial infarction. *Circulation* 92: 1011–1019, 1995.
41. **Zhang J, Merkle H, Hendrich K, Garwood M, From AH, Ugurbil K, and Bache RJ.** Bioenergetic abnormalities associated with severe left ventricular hypertrophy. *J Clin Invest* 92: 993–1003, 1993.
42. **Zhang J, Tober C, Zhang Y, Ugurbil K, Bache RJ, and Homans D.** Bioenergetic consequences of volume overloaded hypertrophy. *Circulation* 96: 334–343, 1997.
43. **Zhang J, Murakami Y, Zhang Y, Cho YK, Ye Y, Gong G, Bache RJ, Ugurbil K, and From AHL.** Oxygen delivery does not limit cardiac performance during high work states. *Am J Physiol Heart Circ Physiol* 276: H50–H57, 1999.
44. **Zhang J, Wilke N, Wang Y, Zhang Y, Wang C, Eijgelshoven MH, Cho YK, Murakami Y, Ugurbil K, Bache RJ, and From AH.** Functional and bioenergetic consequences of postinfarction left ventricular remodeling in a new porcine model. MRI and ^{31}P-MRS study. *Circulation* 94: 1089–1100, 1996.

(2)

Exhibit D

Paternostro, *et al.* (1999)
"Insulin Resistance in Patients with Cardiac Hypertrophy."
Cardiovascular Research 42(1): 246-253

ELSEVIER

Cardiovascular Research 42 (1999) 246–253

Cardiovascular Research

Insulin resistance in patients with cardiac hypertrophy[1]

Giovanni Paternostro[a], Domenico Pagano[b], Tomaso Gnecchi-Ruscone[a], Robert S. Bonser[b], Paolo G. Camici[a,*]

[a]MRC Cyclotron Unit, Imperial College School of Medicine, Hammersmith Hospital, Du Cane Road, London W12 0NN, UK
[b]Queen Elizabeth Hospital, Birmingham, UK

Received 28 May 1998; accepted 14 July 1998

Abstract

Objective: Animal studies suggest that left ventricular hypertrophy might be associated with insulin resistance and alterations in glucose transporters. We have previously demonstrated myocardial insulin resistance in patients with post-ischemic heart failure. The aim was to investigate whether myocardial insulin resistance could be demonstrated in human cardiac hypertrophy in the absence of hypertension, diabetes and coronary artery disease. **Methods:** Eleven normotensive nondiabetic patients with cardiac hypertrophy due to aortic stenosis and angiographically normal coronary arteries were compared to 11 normal volunteers. Myocardial glucose uptake (MGU) was measured with positron emission tomography and [^{18}F]2-fluoro-2-deoxy-D-glucose during fasting (low insulinemia) or during euglycemic–hyperinsulinemic clamp (physiologic hyperinsulinemia). Myocardial biopsies were obtained in order to investigate changes in insulin-independent (GLUT-1) and insulin-dependent (GLUT-4) glucose transporters. **Results:** During fasting, plasma insulin (7±1 vs. 6±1 mU/l) and MGU (0.12±0.05 vs. 0.11±0.04 μmol/min/g) were comparable in patients and controls. By contrast, during clamp, MGU was markedly reduced in patients (0.48±0.02 vs. 0.70±0.03 μmol/min/g, $p<0.01$) despite similar plasma insulin levels (95±6 vs. 79±6 mU/l). A decreased GLUT-4/GLUT-1 ratio was shown by Western blot analysis in patients. **Conclusions:** Insulin resistance seems to be a feature of the hypertrophied heart even in the absence of hypertension, coronary artery disease and diabetes and may be explained, at least in part, by abnormalities in glucose transporters.

Keywords: Glycolysis; Heart failure; Hyertrophy; Membrane transport; Valve (disease); Positron emission tomography

1. Introduction

Whole body insulin resistance, mainly due to a decreased responsiveness to insulin of skeletal muscle [1], has been demonstrated to be associated with systemic conditions such as diabetes (both type 1 and type 2), hypertension and coronary artery disease [1]. More recently, the non-invasive measurement of myocardial uptake of the glucose analogue [^{18}F]2-fluoro-2-deoxy-D-glucose (FDG) by positron emission tomography (PET), has made it possible to assess the presence of cardiac insulin resistance in humans. We have previously reported that insulin resistance is present in the non-infarcted myocardium of patients with previous myocardial infarction and heart failure [2]. These myocardial regions, remote from the infarct, are likely to undergo compensatory hypertrophy [3]. On the other hand, in patients with type 1 diabetes, peripheral (skeletal muscle) insulin resistance is not accompanied by a reduced cardiac FDG uptake [4,5]. Likewise, in young subjects with mild hypertension and no cardiac hypertrophy, Nuutila et al. [6] could show skeletal but not cardiac insulin resistance.

Insulin promotes glucose uptake and decreases the utilisation of free fatty acids by the human heart [7–9]. Glucose is a particularly important substrate for the heart. It is more efficient than other substrates in terms of oxygen consumption (more ATP is synthesized per mole of oxygen consumed) and its uptake is increased in myocardial ischemia [10,11]. In addition, glucose seems to be important for the production of ATP for ion channels and pumps [12,13] and has an anaplerotic role, i.e. it provides

*Corresponding author. Tel.: +44-181-383-3186; fax: +44-181-383-3742.
E-mail address: paolo@cu.rpms.ac.uk (P.G. Camici)

[1]See pages 12–14.

Time for primary review 19 days.

0008-6363/99/$ – see front matter
PII: S0008-6363(98)00233-8

oxaloacetate, thus replenishing Krebs cycle intermediates [14].

Glucose enters the cell using specific transporters [15]. There are five facilitative glucose transporters, named GLUT-1 to GLUT-5. Of these, only GLUT-1 and GLUT-4 are present in the heart. Immunofluorescence has demonstrated the presence of both on cardiac myocytes [16]. The GLUT-1 isoform, located mainly in the sarcolemmal membrane, is thought to be involved in glucose transport in the basal metabolic state. Under such conditions, less than 1% of GLUT-4 (the insulin-responsive isoform) is located in the sarcolemma [17]. After insulin stimulation, however, glucose transport is accelerated by translocating GLUT-4 from an intracellular pool to the T-tubule and sarcolemmal membrane [17,18]. GLUT-4 levels are decreased in adipose tissue in diabetic patients [19,20], but probably not in skeletal muscle [18]. However, it has been reported that GLUT-4 translocation is diminished in the skeletal muscle of diabetic patients [21]. Much less is known about GLUT-4 in the insulin-resistant heart. We have previously shown that a decreased expression of cardiac GLUT-4 mRNA accompanies insulin resistance in the hypertrophied heart of the spontaneously hypertensive rat [22]. In this model, increased basal deoxyglucose uptake and a reduced response to insulin could be demonstrated [22]. In a different model of cardiac hypertrophy in the rat (aortic banding), a decreased ratio of GLUT-4 to GLUT-1 mRNA expression has been reported [23].

The purpose of the present study was to establish if myocardial insulin resistance is a feature of cardiac hypertrophy in the absence of systemic conditions that are known to be associated with a reduced response to this hormone (diabetes, hypertension, coronary artery disease). Myocardial glucose uptake was estimated using PET in patients with pure aortic stenosis. Furthermore, alterations in the expression of glucose transporters, as a possible molecular basis for insulin resistance, were investigated in cardiac biopsies.

2. Methods

2.1. Study protocol

PET was used to measure myocardial blood flow and FDG uptake at two different levels of plasma insulin: a very low one corresponding to fasting conditions and a level >ten times higher during hyperinsulinemic euglycemic clamp. Five patients and five controls were studied during fasting; six patients and six controls were studied during hyperinsulinemic euglycemic clamp. The expression of the glucose transporters GLUT-1 and GLUT-4 was measured by Western blot analysis in cardiac biopsies from the patients with aortic stenosis. Additional biopsies were obtained from failing and donor hearts at the time of cardiac transplantation. The investigation conforms with the principles outlined in the Declaration of Helsinki.

2.2. Study population

2.2.1. PET

2.2.1.1. Patients The patient population consisted of 11 normotensive, nondiabetic patients (ten men, aged 63±2 years) with pure aortic stenosis and with normal or non-significantly diseased coronary arteries, who were on the waiting list for valve replacement. All patients were in NYHA class II and no attempt was made to standardize medical therapy. Three patients were on diuretics, one was on ACE inhibitors, one was on digitalis, one was on calcium antagonists and one was on nitrates. Before the PET scan, all patients were studied by echocardiography, according to the guidelines of the American Society of Echocardiography (Esaote Biomedica SIM 7000 CFM echograph). The posterior and septal wall thickness were measured in M-mode in the left parasternal projection (at end diastole). Since these measurements never differed by more than 1 mm, thus excluding asymmetric hypertrophy, only their average thickness is reported in Section 3.

2.2.1.2. Controls The results of the PET studies in patients were compared with those obtained in 11 healthy male volunteers (aged 47±2 years, $p<0.05$ vs. patients) matched for body mass index. All had a negative history for coronary artery disease, normal physical examination, resting 12 lead electrocardiogram and echocardiogram and a treadmill exercise test (Bruce protocol) negative for myocardial ischemia at high workload.

2.3. Cardiac biopsies

2.3.1. Patients

Cardiac biopsies were obtained from four of the aortic stenosis patients (all males, age 57±1 years) studied by PET, at the time of aortic valve replacement. In a separate experiment, biopsies were also obtained from five explanted hearts of patients with end stage heart failure (all males, age 45±1 years). Three of these explanted hearts were from patients with non-ischemic cardiomyopathy and two were from patients with severe coronary artery disease.

2.3.2. Controls

Cardiac biopsies were obtained from four donor hearts, at the time of heart transplant. The donors were also all males and aged 32±4 years ($p<0.05$ vs. patients).

2.4. Hyperinsulinemic euglycemic clamp

Before the PET scan, a 20-G polyethylene cannula was inserted in a superficial forearm vein for infusion of

glucose and insulin, as described by DeFronzo et al. [24], in order to obtain a near-steady state at physiological concentration of glucose and at plasma insulin values similar to those of the post-prandial state. A second cannula was threaded retrogradely into a superficial vein of the wrist or hand that had been arterialized using a heating pad set at 50°C. At time zero, a primed-constant insulin infusion (40 mU min^{-1} m^2 of body surface area) was started. The body surface area was calculated from the formula of Du Bois and Du Bois [25]. The prime consisted of four times the final constant rate for the first 4 min, followed by two times the constant rate for 3 min. Four min into the insulin infusion, an exogenous D-glucose infusion was started at an initial rate of 1.5 mg min^{-1} per kg of body weight. The plasma glucose concentration in arterialized blood was measured at baseline and then every 5 min during the clamp. The glucose infusion rate was adjusted according to the change in plasma glucose during the preceding 5 min. Samples for insulin assay were taken from the arterialized vein at 20, 40 and 60 min during the clamp.

Glucose was measured with an automatic analyser (2300Stat, Yellow Spring, USA) which required around 30 s per measurement (this is essential during the clamp because the rate of infusion has to be adjusted as quickly as possible). Insulin was measured in the Endocrinology Laboratory of Hammersmith Hospital using an immunoradiometric assay.

Under the near-steady-state conditions of euglycemic hyperinsulinemia prevailing during the second hour of an insulin clamp, the exogenous glucose infusion rate equals the total amount of glucose metabolized by all tissues and, therefore, is an index of whole-body insulin sensitivity (expressed in μmol min^{-1} per kg of body weight).

2.5. PET scanning and data analysis

PET scanning was carried out in all subjects, as previously reported [2]. Briefly, the optimal imaging position was determined using a 5-min rectilinear scan and a 20-min transmission scan was then performed. The blood pool was imaged by inhalation of tracer amounts of ^{15}O-labelled carbon monoxide ($C^{15}O$). Myocardial blood flow (MBF) was measured using inhaled ^{15}O-labelled carbon dioxide ($C^{15}O_2$), which is rapidly converted to ^{15}O-labelled water ($H_2^{15}O$) by carbonic anhydrase in the lungs [26]. Myocardial glucose uptake was measured with the glucose analogue FDG. Image manipulation and kinetic analyses were performed using the ANALYZE (Version 3.0, Biodynamics Research Unit, Mayo foundation, Rochester, MN, USA) and the MATLAB (The MathWorks Inc., Natick, MA, USA) software packages, respectively. Cardiac images were resliced in the short axis view. Tissue FDG time-activity curves were analysed by using the linearized approach proposed by Patlak et al. [27] for irreversible processes. Myocardial glucose uptake (MGU) was then obtained by multiplying regional influx rates by the plasma concentration of cold glucose, assuming a lumped constant of one, and by dividing the product by the corresponding tissue fraction. This last step was performed in order to correct for partial volume effect. A conversion for millilitres to grams of perfusable tissue was made by dividing the flow and metabolic data by the tissue density (1.04 g/ml). Thus, MGU is expressed as μmol min^{-1} per g of water perfusable tissue.

2.6. Western blots

All cardiac biopsies were transmural, taken from the left ventricle in an area with no macroscopic signs of fibrosis. The biopsies from the explanted hearts were cut with a scalpel. The biopsies from the donor hearts and patients undergoing valve replacement were taken using a Tru-cut (Baxter) biopsy needle and were of smaller dimensions (around 30 mg). The tissue was immediately frozen in liquid nitrogen and then stored at −70°C. At the time of analysis, the samples were pulverized on dry ice with a mortar and pestle, then 100 μl of sample buffer were added to the pulverized tissue. The sample buffer contained 62.5 mM Tris, 10% glycerol, 2% sodium dodecyl sulfate (SDS), 2 mM EDTA (all from Sigma) plus the following protease inhibitors: 1 mg/ml AEBSF, 10 mg/ml E64, 1 mg/ml pepstatin (all from Boehringer Mannheim). After the addition, the tubes were quickly frozen in liquid nitrogen, then boiled and vortex-mixed repeatedly until the tissue appeared to be completely solubilized. After 5 min centrifugation at the maximum speed on an Eppendorf bench top centrifuge, the supernatant was isolated, 10 μl were used for the protein assay and the rest was frozen in liquid nitrogen and kept at −70°C. The protein content was measured using the assay of Lowry et al. [28]. For electrophoresis, β-mercaptoethanol (3% final) was added to a volume of sample equivalent to 30 μg of protein and then volumes were equalized with sample buffer containing bromophenol blue. Western blotting was performed according to standard procedures [29]. The same filter was then probed with two antibodies: anti-GLUT-4 (rabbit polyclonal, a kind gift from Dr Gwyn Gould) [30], anti-GLUT-1 (rabbit polyclonal, from Charles River Laboratories, Wilmington, MA, USA) [31] using dilutions of 1:1300 for GLUT-4 and 1:2000 for GLUT-1. Ponceau S staining of filters was used to assess total protein. Preliminary experiments were performed with control filters in order to show that the expected band (at 50 kilodaltons) was absent if the primary antibody was omitted. Immunodetection was performed with the ECL system (Amersham). After each immunodetection, the filter was stripped using a 30-min incubation in stripping buffer (100 mM β-mercaptoethanol, 2% SDS, 62.5 mM Tris, pH 6.7) and two washing in phosphate-buffered saline (PBS)–Tween at room temperature. The efficiency of stripping was checked by reprobing in the absence of primary antibody. The

intensity of the bands on the autoradiography film were quantified using the image analysis program, ANALYZE.

2.7. Statistical analysis

All results are expressed as mean±standard error of the mean. The Mann-Whitney U test was used to compare mean group values, whereas paired comparisons were performed by the Wilcoxon signed-rank test. Comparisons of more than two groups were performed using the Kruskall-Wallis test. We have used these non-parametric tests because the number of subjects is limited and the assumptions on which parametric tests are based cannot be easily verified [32]. Regression analysis was performed according to standard techniques. A value of $p<0.05$ was considered to be statistically significant.

3. Results

3.1. Characteristics of the study population

The body mass index (weight/height [2]) was 25±1 kg/m^2 in controls and 27±1 kg/m^2 in patients (p=NS). The left ventricular wall thickness was 10±0.3 mm in controls and 16±0.8 mm in patients ($p<0.01$). There was no difference in left ventricular wall thickness between patients studied during fasting and during clamp (16±1 mm in the fasting state and 17±1.4 mm in the clamped state, p=NS). There were no significant differences between patients and controls in systolic blood pressure (126±3 mmHg in controls vs. 126±4 mmHg in patients), diastolic blood pressure (75±3 mmHg in controls vs. 74±2 mmHg in patients) and heart rate (64±2 bpm in controls vs. 71±4 bpm in patients). The baseline plasma glucose concentration was 5.0±0.2 mM in controls, and 4.6±0.2 mM in patients (p=NS). During clamp, plasma glucose levels were 6.0±0.4 and 5.5±0.2 mM (p=NS) in controls and patients, respectively. Plasma insulin was 7±1 and 6±1 mU/l (p=NS) during fasting and 79±6 and 95±6 mU/l (p=NS) during clamp, in controls and patients, respectively. The glucose metabolized by the whole body during the last 60 min of the clamp study was 37±4 μmol min^{-1} kg^{-1} in controls and 19±2 μmol min^{-1} kg^{-1} in patients ($p<0.01$).

3.2. Myocardial blood flow and glucose uptake (Table 1)

There was no difference amongst the four groups in terms of myocardial blood flow rates. There was also no difference in glucose uptake between patients and controls during fasting. By contrast, myocardial glucose uptake during clamp was 31% lower in patients. Thus, a 13-fold increase in plasma insulin could increase glucose uptake by 6.4-fold in controls but only four-fold in patients (Fig. 1). During clamp, cardiac glucose uptake was linearly related to whole-body glucose utilization (r=0.70, $p<0.01$).

Table 1
Myocardial blood flow and glucose uptake rates during fasting and during euglycemic hyperinsulinemia (clamp) in patients and controls

	Controls	Patients	p
Myocardial blood flow during fasting (n=5) (ml min^{-1} g^{-1})	1.04±0.06	1.10±0.08	NS
Myocardial blood flow during clamp (n=6) (ml min^{-1} g^{-1})	1.09±0.06	1.22±0.08	NS
Myocardial glucose uptake during fasting (n=5) (μmol min^{-1} g^{-1})	0.11±0.04	0.12±0.05	NS
Myocardial glucose uptake during clamp (n=6) (μmol min^{-1} g^{-1})	0.70±0.03	0.48±0.02	p=0.0001

Myocardial glucose uptake was decreased in patients with aortic stenosis during clamp but not during fasting, while there was no difference in myocardial blood flow in either condition.
Comparing fasting to clamp, there were significant ($p<0.01$) differences in myocardial glucose uptake but not in blood flow.

3.3. Glucose transporters

In the patients with cardiac hypertrophy and aortic stenosis, the GLUT-4/GLUT-1 ratio was decreased compared to controls (1.2±0.2 vs. 2.3±0.2, p=0.009). The GLUT-4/GLUT-1 ratio was equally decreased in the explanted hearts of the patients with heart failure (1.2±0.1) compared to controls (2.6±0.3; p=0.002) (Fig. 2). When GLUT-1 and GLUT-4 were expressed as a ratio to total protein (in arbitrary density units), the changes were not significant. In patients with aortic stenosis, GLUT-4 was 1.6±0.3 vs. 2.3±0.7 in controls and GLUT-1 was 1.3±0.3 vs. 1.0±0.4 in controls. In the explanted hearts of patients with heart failure, GLUT-4 was 1.9±0.3 vs. 2.6±0.4 in controls and GLUT-1 was 1.5±0.4 vs. 1.0±0.4 in controls. The cause of heart failure did not seem to influence the GLUT-4/GLUT-1 ratio, which was 1.3±0.1 in the three patients with heart failure due to non-ischemic cardiomyopathy and 1±0.1 in the two patients with heart failure due to coronary heart disease.

4. Discussion

The results obtained in patients with aortic stenosis are similar to those we have previously reported in the non-infarcted myocardium of patients with post-ischemic heart failure [2] and suggest that insulin resistance accompanies cardiac hypertrophy per se, even in the absence of coronary artery disease, diabetes and/or hypertension.

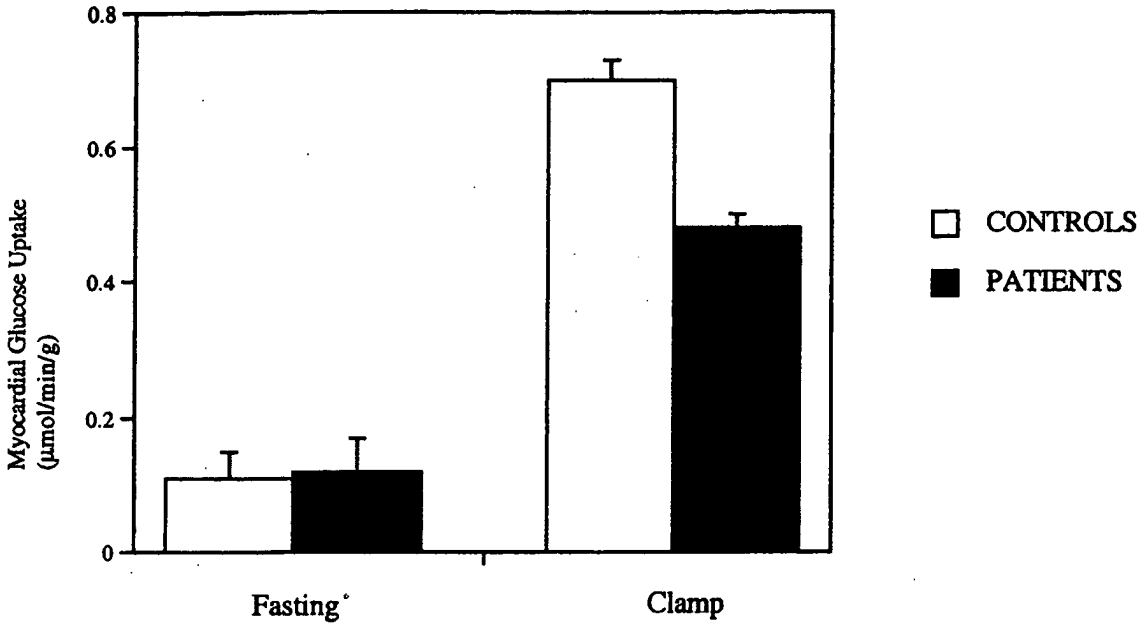

Fig. 1. Myocardial rates of glucose uptake are shown during fasting and during euglycemic hyperinsulinemic glucose clamp in patients with aortic stenosis and normal controls. Only during the clamp is there a significant difference between patients and normal controls. (See also Table 1).

4.1. Glucose transporters

We found a reduced GLUT-4/GLUT-1 protein ratio in hearts from patients with end-stage heart failure and in those with aortic stenosis and we hypothesize that this is a possible molecular basis for the cardiac insulin resistance shown by PET. This is also consistent with previous reports of lowered GLUT-4/GLUT-1 mRNA ratio in animal models of cardiac hypertrophy [22,23]. Interestingly, transgenic mice lacking GLUT-4 expression have cardiac hypertrophy and a decreased life span [33], raising the possibility that alterations of glucose metabolism might contribute to and not simply be a consequence of cardiac disease. Furthermore, Sun et al. [34] have shown that myocardial ischemia causes translocation of GLUT-4 to the plasma membrane of cardiac myocytes, leading to increased glucose uptake. GLUT-4 depletion could therefore limit glucose availability under conditions of hypoxia and contribute to myocardial dysfunction. On the other hand, it is well known that cardiac hypertrophy is associated with the reappearance of a pattern of gene expression that is present in the fetal and newborn heart [35]. The fetal rat heart has less GLUT-4 and more GLUT-1 than the adult [36,37] and our results are in line with the concept of re-expression of fetal genes in cardiac hypertrophy. Our finding that comparable reductions in the GLUT-4/GLUT-1 ratio could be demonstrated in biopsies from patients with cardiac diseases of different severity and etiology suggests that this might be part of a general response of the myocardium to insult. Similar cardiac isoform switches have been reported for several other proteins, including myosin heavy chain [38], Na–K-ATPase [39] and creatine kinase [40].

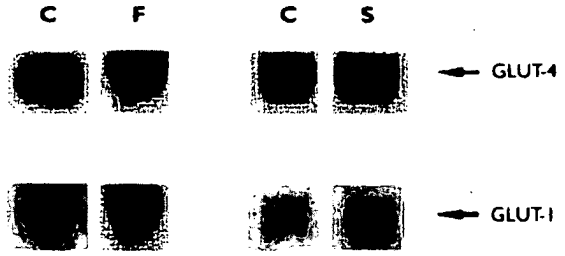

Fig. 2. Representative Western blots from biopsies obtained from failing explanted hearts (F) and controls (C) on the left and from hearts of aortic stenosis patients (S) and respective controls (C) on the right. The filters were probed with anti-GLUT-1 and anti-GLUT-4 antibodies. The GLUT-4/GLUT-1 ratio is reduced in both groups of patients.

4.2. Myocardial blood flow and glucose uptake

Changes in blood flow could affect glucose uptake [41], but our PET measurements do not show any significant effect of insulin on myocardial blood flow during hyperinsulinemic euglycemic clamp. While there is growing evidence that insulin can act as a vasodilator in human skeletal muscle [42], several studies have shown that hyperinsulinemia has no effect on coronary blood flow in

man [8,43] or in dogs when physiological doses of insulin were applied [44].

The FDG–PET results obtained during fasting, with low plasma insulin, are different from those reported by several in vitro animal studies, both by us and by others (e.g. [22,45]), where deoxyglucose uptake in the absence of insulin was shown to be higher in hypertrophied hearts compared to controls. No other human studies of myocardial glucose uptake in global cardiac hypertrophy have been published. An in vivo NMR animal study [46] has also reported an increase in deoxyglucose-6-phosphate accumulation in hypertrophied hearts, in the presence of low circulating insulin values. A dog model of hypertrophy secondary to aortic constriction was employed. A possible reason for the different results obtained in man is the presence of generalized metabolic alterations that occur in patients with heart failure [47], especially an increase in circulating free fatty acids, since substrate competition regulates cardiac glucose uptake [48,49]. Alterations in fatty acid levels were however not present in the experiment of Zhang et al. [46] and this might explain why their results differed from those we report in man.

The results of our study are consistent with those of Maki et al. [50] in patients with coronary artery disease and demonstrate that, in the human heart in vivo, the increase of glucose uptake in response to insulin is much higher than that in isolated perfused hearts [45,51–53]. A possible explanation for this difference could be that in vivo insulin-stimulated myocardial glucose uptake is not only due to stimulation of GLUT-4 translocation, but also to a decrease in circulating fatty acids [8,54]. Furthermore, the possible limitations [55] inherent with the use of FDG for the quantitation of myocardial glucose uptake, which are discussed below, are more serious when different metabolic states are compared.

Several medications are known to affect whole body insulin resistance. ACE-inhibitors are known to improve insulin sensitivity, while other drugs (e.g. diuretics) might worsen it [56]. It might be an objective for future studies to elucidate the effects of ACE-inhibitors on cardiac insulin resistance.

4.3. Possible limitations

Heart failure and hypertrophy are accompanied by an increase in extracellular collagen deposition [57,58]. Therefore, normalizing the Western blot results by total protein might be inappropriate. The choice of an internal control is also difficult, since it implies that the control protein is known not to be altered. Although the GLUT-4/GLUT-1 ratio provides a relative measurement, this has a clear physiological meaning and has the additional advantage of correcting for possible variations in the handling of the samples or in the efficiency of protein transfer during the blotting procedure. Any change in this ratio will influence glucose responsiveness to insulin (that is, the difference in glucose uptake between high and low insulin concentrations), but could be due to a decrease in GLUT4, an increase in GLUT1 or to both. Changes in GLUT1 and GLUT4 expressed as a ratio to total protein were not significant, but, as mentioned above, these measurements can be considered less reliable than the ratio of the two transporters. In fact, Western blots from cardiac biopsies are often quantified as a ratio of two proteins [59–62]. For ethical reasons, we could obtain only very limited amounts of tissue from donor hearts and from the hearts of patients undergoing valve replacement, therefore, we were unable to investigate this point further. However, several authors have quantified their glucose transporter measurements as a ratio of the two transporters [23,63,64].

It must also be noted that our control group was composed of younger individuals compared to the patient group. Indeed, in human biopsies studies using donor hearts as a control group, an age difference is difficult to avoid. However, although insulin resistance does increase with age, the age-related changes are very gradual and are only minimal between the age groups that we have studied [65].

PET allows for attenuation correction of annihilation photons, thus enabling the accurate measurement of absolute radioactivity concentration in tissues [66]. In the case of FDG measurements, however, there are some assumptions that we have discussed in detail previously [2]. Briefly, in order to account for differences in affinity between FDG and glucose, both for glucose transporters and hexokinase, the estimate of glucose uptake obtained from FDG–PET is normally divided by the so-called lumped constant [67–69]. However, studies in isolated rat hearts have shown that the lumped constant might vary under different experimental conditions [55]. Therefore, it has been recommended that PET studies of FDG uptake in the heart should be performed under controlled metabolic conditions [55,70], as those employed in the present study. It is worth noting that the difference in myocardial glucose uptake between fasting and euglycemic clamp estimated with FDG–PET is very similar to that measured in humans during simultaneous arterial and great cardiac vein catheterization [8].

5. Conclusions

The response of glucose uptake to insulin in the hypertrophied human heart is reduced and this reduction is independent of myocardial blood flow and predisposing conditions (hypertension, coronary artery disease, diabetes). A lower GLUT-4/GLUT-1 ratio is a possible molecular basis for this decreased responsiveness. It remains to be seen if interventions that are known to improve whole body insulin resistance might have an effect on cardiac insulin resistance and the progression to heart failure.

Acknowledgements

The authors wish to thank the Medical Research Council (U.K.) for financial support.

References

[1] Ferrannini E, Natali A. Essential hypertension, metabolic disorders, and insulin resistance. Am Heart J 1991;121:1274–1282.
[2] Paternostro G, Camici PG, Lammerstma AA, et al. Cardiac and skeletal muscle insulin resistance in patients with coronary heart disease. A study with positron emission tomography. J Clin Invest 1996;98:2094–2099.
[3] Liedtke AJ, Nellis SH, Whitesell LF. Effects of regional ischemia on metabolic function in adjacent aerobic myocardium. J Mol Cell Cardiol 1982;14:195–205.
[4] Nuutila P, Knuuti J, Ruotsalainen U, et al. Insulin resistance is localized to skeletal but not heart muscle in type 1 diabetes. Am J Physiol 1993;264:E756–E762.
[5] vom Dahl J, Herman WH, Hicks RJ, et al. Myocardial glucose uptake in patients with insulin-dependent diabetes mellitus assessed quantitatively by dynamic positron emission tomography. Circulation 1993;88:395–404.
[6] Nuutila P, Maki M, Laine H, et al. Insulin action on heart and skeletal muscle glucose uptake in essential hypertension. J Clin Invest 1995;96:1003–1009.
[7] Camici P, Ferrannini E, Opie LH. Myocardial metabolism in ischemic heart disease: basic principles and application to imaging by positron emission tomography. Prog Cardiovasc Dis 1989;32:217–238.
[8] Ferrannini E, Santoro D, Bonadonna R, et al. Metabolic and hemodynamic effects of insulin on human hearts. Am J Physiol 1993;264:E308–E315.
[9] Rogers WJ, Russell Jr. RO, McDaniel HG, Rackley CE. Acute effects of glucose–insulin–potassium infusion on myocardial substrates, coronary blood flow and oxygen consumption in man. Am J Cardiol 1977;40:421–428.
[10] Oliver MF, Opie LH. Effects of glucose and fatty acids on myocardial ischaemia and arrhythmias. Lancet 1994;343:155–158.
[11] Camici P, Araujo LI, Spinks T, et al. Increased uptake of 18F-fluorodeoxyglucose in postischemic myocardium of patients with exercise-induced angina. Circulation 1986;74:81–88.
[12] Weiss JN, Lamp ST. Cardiac ATP-sensitive K^+ channels. Evidence for preferential regulation by glycolysis. J Gen Physiol 1989;94:911–935.
[13] Balaban RS, Bader JP. Studies on the relationship between glycolysis and $(Na^+ + K^+)$-ATPase in cultured cells. Biochim Biophys Acta 1984;804:419–426.
[14] Taegtmeyer H. Energy metabolism of the heart: from basic concepts to clinical applications. Curr Probl Cardiol 1994;19:59–113.
[15] Gould GW, Bell GI. Facilitative glucose transporters: an expanding family. Trends Biochem Sci 1990;15:18–23.
[16] Young LH, Renfu Y, Russell R, et al. Low-flow ischemia leads to translocation of canine heart GLUT-4 and GLUT-1 glucose transporters to the sarcolemma in vivo. Circulation 1997;95:415–422.
[17] Slot JW, Geuze HJ, Gigengack S, James DE, Lienhard GE. Translocation of the glucose transporter GLUT4 in cardiac myocytes of the rat. Proc Natl Acad Sci USA 1991;88:7815–7819.
[18] Barnard RJ, Youngren JF. Regulation of glucose transport in skeletal muscle. FASEB J 1992;6:3238–3244.
[19] Garvey WT, Maianu L, Hueckstead TP, et al. Pretranslational suppression of a glucose transporter protein causes insulin resistance in adipocytes from patients with non-insulin-dependent diabetes mellitus and obesity. J Clin Invest 1991;87:1072–1081.
[20] Sinha MK, Raineri Maldonado C, Buchanan C, et al. Adipose tissue glucose transporters in NIDDM. Decreased levels of muscle/fat isoform. Diabetes 1991;40:472–477.
[21] Vogt B, Muhlbacher C, Carrascosa J, et al. Subcellular distribution of GLUT 4 in the skeletal muscle of lean type 2 (non-insulin-dependent) diabetic patients in the basal state. Diabetologia 1992;35:456–463.
[22] Paternostro G, Clarke K, Heath J, Seymour AM, Radda GK. Decreased GLUT-4 mRNA content and insulin-sensitive deoxyglucose uptake show insulin resistance in the hypertensive rat heart. Cardiovasc Res 1995;30:205–211.
[23] Weinberg EO, Thienelt CD, Lorell BH. Pretranslational regulation of glucose transporter isoform expression in hearts with pressure-overload left ventricular hypertrophy. Circulation 1995;92:I-385.
[24] DeFronzo RA, Tobin JD, Andres R. Glucose clamp technique: a method for quantifying insulin secretion and resistance. Am J Physiol 1979;237:E214–E223.
[25] Lentner C. Geigy scientific tables. Vol. 5. Basel: Ciba-Geigy, 1990.
[26] Araujo LI, Lammertsma AA, Rhodes CG, et al. Noninvasive quantification of regional myocardial blood flow in coronary artery disease with oxygen-15-labeled carbon dioxide inhalation and positron emission tomography. Circulation 1991;83:875–885.
[27] Patlak CS, Blasberg.RG, Fenstermacher JD. Graphical evaluation of blood-to-brain transfer constants from multiple-time uptake data. J Cereb Blood Flow Metab 1983;3:1–7.
[28] Lowry OH, Rosebrough NJ, Farr AL, Randall RJ. Protein measurement with the Folin phenol reagent. J Biol Chem 1951;193:265–275.
[29] Sambrook J, Fritsch EF, Maniatis T. Molecular cloning: a laboratory manual. New York: Cold Spring Harbor Laboratory Press, 1989.
[30] Brant AM, McCoid S, Thomas HM, et al. Analysis of the glucose transporter content of islet cell lines: implications for glucose-stimulated insulin release. Cell Signal 1992;4:641–650.
[31] Piper RC, Hess LJ, James DE. Differential sorting of two glucose transporters expressed in insulin-sensitive cells. Am J Physiol 1991;260:C570–C580.
[32] Armitage P, Berry G. Statistical methods in medical research. Oxford: Blackwell Scientific, 1994.
[33] Katz EB, Stenbit AE, Hatton K, DePinho R, Charron MJ. Cardiac and adipose tissue abnormalities but not diabetes in mice deficient in GLUT4. Nature 1995;377:151–155.
[34] Sun D, Nguyen N, DeGrado TR, Schwaiger M, Brosius FCr . Ischemia induces translocation of the insulin-responsive glucose transporter GLUT4 to the plasma membrane of cardiac myocytes. Circulation 1994;89:793–798.
[35] Roberts R. Molecular basis of cardiology. Cambridge, MA: Blackwell Scientific, 1993.
[36] Wang C, Hu SM. Developmental regulation in the expression of rat heart glucose transporters. Biochem Biophys Res Commun 1991;177:1095–1100.
[37] Santalucia T, Camps M, Castello A, et al. Developmental regulation of GLUT-1 (erythroid/Hep G2) and GLUT-4 (muscle/fat) glucose transporter expression in rat heart, skeletal muscle, and brown adipose tissue. Endocrinology 1992;130:837–846.
[38] Izumo S, Lompre AM, Matsuoka R, et al. Myosin heavy chain messenger RNA and protein isoform transitions during cardiac hypertrophy. Interaction between hemodynamic and thyroid hormone-induced signals. J Clin Invest 1987;79:970–977.
[39] Charlemagne D, Orlowski J, Oliviero P, et al. Alteration of Na,K-ATPase subunit mRNA and protein levels in hypertrophied rat heart. J Biol Chem 1994;269:1541–1547.
[40] Ingwall JS, Kramer MF, Fifer MA, et al. The creatine kinase system in normal and diseased human myocardium. N Engl J Med 1985;313:1050–1054.
[41] Baron AD, Steinberg H, Brechtel G, Johnson A. Skeletal muscle blood flow independently modulates insulin-mediated glucose uptake. Am J Physiol 1994;266:E248–E253.

[42] Laakso M, Edelman SV, Brechtel G, Baron AD. Decreased effect of insulin to stimulate skeletal muscle blood flow in obese man. A novel mechanism for insulin resistance. J Clin Invest 1990;85:1844–1852.
[43] Thomassen A, Nielsen TT, Bagger JP, Henningsen P. Cardiac metabolic and hemodynamic effects of insulin in patients with coronary artery disease. Diabetes 1989;38:1175–1180.
[44] Barrett EJ, Schwartz RG, Francis CK, Zaret BL. Regulation by insulin of myocardial glucose and fatty acid metabolism in the conscious dog. J Clin Invest 1984;74:1073–1079.
[45] Taegtmeyer H, Overturf ML. Effects of moderate hypertension on cardiac function and metabolism in the rabbit. Hypertension 1988;11:416–4126.
[46] Zhang J, Duncker DJ, Xu Y, et al. Glucose uptake in the severely hypertrophied left ventricle. Circulation 1993;88:I-378.
[47] Paolisso G, Gambardella A, Galzerano D, et al. Total-body and myocardial substrate oxidation in congestive heart failure. Metabolism 1994;43:174–179.
[48] Nuutila P, Koivisto VA, Knuuti J, et al. Glucose-free fatty acid cycle operates in human heart and skeletal muscle in vivo. J Clin Invest 1992;89:1767–1774.
[49] Randle PJ, Garland PB, Hales CN, Newsholme EA. The glucose fatty-acid cycle: its role in insulin sensitivity and metabolic disturbances of diabetes mellitus. Lancet 1963;1:785–789.
[50] Maki M, Luotolahti M, Nuutila P, et al. Glucose uptake in the chronically dysfunctional but viable myocardium. Circulation 1996;93:1658–1666.
[51] Morgan HE, Randle PJ, Regen DM. Regulation of glucose uptake by muscle. 3. The effects of insulin, anoxia, salicylate and 2,4-dinitrophenol on membrane transport and intracellular phosphorylation of glucose in the isolated rat heart. Biochem J 1959;73:573–579.
[52] Neely JR, Denton RM, England PJ, Randle PJ. The effects of increased heart work on the tricarboxylate cycle and its interactions with glycolysis in the perfused rat heart. Biochem J 1972;128:147–159.
[53] Sugden PH, Smith DM. The effects of insulin on glucose uptake and lactate release in perfused working rat heart preparations. Biochem J 1982;206:473–479.
[54] Nuutila P, Knuuti MJ, Raitakari M, et al. Effect of antilipolysis on heart and skeletal muscle glucose uptake in overnight fasted humans. Am J Physiol 1994;267:E941–E946.
[55] Hariharan R, Bray M, Ganim R, et al. Fundamental limitations of [^{18}F]2-deoxy-2-fluoro-D-glucose for assessing myocardial glucose uptake. Circulation 1995;91:2435–2444.
[56] Pollare T, Lithell H, Berne C. A comparison of the effects of hydrochlorothiazide and captopril on glucose and lipid metabolism in patients with hypertension [see comments]. N Engl J Med 1989;321:868–873.
[57] Beltrami CA, Finato N, Rocco M, et al. The cellular basis of dilated cardiomyopathy in humans. J Mol Cell Cardiol 1995;27:291–305.
[58] Beltrami CA, Finato N, Rocco M, et al. Structural basis of end-stage failure in ischemic cardiomyopathy in humans. Circulation 1994;89:151–163.
[59] Saba Z, Nassar R, Ungerleider RM, Oakeley AE, Anderson PA. Cardiac troponin T isoform expression correlates with pathophysiological descriptors in patients who underwent corrective surgery for congenital heart disease. Circulation 1996;94:472–476.
[60] Morano I, Hadicke K, Grom S, et al. Titin, myosin light chains and C-protein in the developing and failing human heart. J Mol Cell Cardiol 1994;26:361–368.
[61] Reinecke H, Studer R, Vetter R, Holtz J, Drexler H. Cardiac Na/Ca exchange activity in patients with end stage heart failure. Cardiovasc Res 1996;31:48–54.
[62] Studer R, Reinecke H, Bilger J, et al. Gene expression of the cardiac Na–Ca exchanger in end-stage heart failure. Circ Res 1994;75:443–453.
[63] Schwaiger M, Sun DQ, Deeb M, et al. Expression of myocardial glucose transporter (GLUT) mRNAs in patients with advanced coronary artery disease (CAD). Circulation 1994;90:I-113.
[64] Sivitz WI, Lee EC. Assessment of glucose transporter gene expression using the polymerase chain reaction. Endocrinology 1991;128:2387–2394.
[65] DeFronzo RA. Glucose intolerance and aging: evidence for tissue insensitivity to insulin. Diabetes 1979;28:1095–1101.
[66] Schelbert HR. Principles of positron emission tomography. In: Marcus ML, Schelbert HR, Skorton DJ, Wolf GL, editors. Cardiac imaging. Philadelphia: WB Saunders, 1991:1140–1168.
[67] Huang SC, Williams BA, Barrio JR, et al. Measurement of glucose and 2-deoxy-2-[^{18}F]fluoro-D-glucose transport and phosphorylation rates in myocardium using dual-tracer kinetic experiments. FEBS Lett 1987;216:128–132.
[68] Krivokapich J, Huang SC, Selin CE, Phelps ME. Fluorodeoxyglucose rate constants, lumped constant, and glucose metabolic rate in rabbit heart. Am J Physiol 1987;252:H777–H787.
[69] Marshall RC, Huang SC, Nash WW, Phelps ME. Assessment of the [^{18}F]fluorodeoxyglucose kinetic model in calculations of myocardial glucose metabolism during ischemia. J Nucl Med 1983;24:1060–1064.
[70] Russell RR, Mrus JM, Mommessin JI, Taegtmeyer H. Compartmentation of hexokinase in rat heart. A critical factor for tracer kinetic analysis of myocardial glucose metabolism. J Clin Invest 1992;90:1972–1977.

Exhibit E

Matsushima, *et al.* (2006)
"Overexpression of Mitochondrial Peroxiredoxin-3 Prevents Left Ventricular Remodeling and Failure after Myocardial Infraction in Mice."
Circulation 113: 1779-1786

Overexpression of Mitochondrial Peroxiredoxin-3 Prevents Left Ventricular Remodeling and Failure After Myocardial Infarction in Mice

Shouji Matsushima, MD; Tomomi Ide, MD, PhD; Mayumi Yamato, PhD; Hidenori Matsusaka, MD; Fumiyuki Hattori, PhD; Masaki Ikeuchi, MD; Toru Kubota, MD, PhD; Kenji Sunagawa, MD, PhD; Yasuhiro Hasegawa, PhD; Tatsuya Kurihara, PhD; Shinzo Oikawa, PhD; Shintaro Kinugawa, MD, PhD; Hiroyuki Tsutsui, MD, PhD

Background—Mitochondrial oxidative stress and damage play major roles in the development and progression of left ventricular (LV) remodeling and failure after myocardial infarction (MI). We hypothesized that overexpression of the mitochondrial antioxidant, peroxiredoxin-3 (Prx-3), could attenuate this deleterious process.

Methods and Results—We created MI in 12- to 16-week-old, male Prx-3–transgenic mice (TG+MI, n=37) and nontransgenic wild-type mice (WT+MI, n=39) by ligating the left coronary artery. Prx-3 protein levels were 1.8 times higher in the hearts from TG than WT mice, with no significant changes in other antioxidant enzymes. At 4 weeks after MI, LV thiobarbituric acid–reactive substances in the mitochondria were significantly lower in TG+MI than in WT+MI mice (mean±SEM, 1.5±0.2 vs 2.2±0.2 nmol/mg protein; n=8 each, $P<0.05$). LV cavity dilatation and dysfunction were attenuated in TG+MI compared with WT+MI mice, with no significant differences in infarct size (56±1% vs 55±1%; n=6 each, P=NS) and aortic pressure between groups. Mean LV end-diastolic pressures and lung weights in TG+MI mice were also larger than those in WT+sham-operated mice but smaller than those in WT+MI mice. Improvement in LV function in TG+MI mice was accompanied by a decrease in myocyte hypertrophy, interstitial fibrosis, and apoptosis in the noninfarcted LV. Mitochondrial DNA copy number and complex enzyme activities were significantly decreased in WT+MI mice, and this decrease was also ameliorated in TG+MI mice.

Conclusions—Overexpression of Prx-3 inhibited LV remodeling and failure after MI. Therapies designed to interfere with mitochondrial oxidative stress including the antioxidant Prx-3 might be beneficial in preventing cardiac failure. (***Circulation.* 2006;113:1779-1786.**)

Key Words: antioxidants ■ free radicals ■ heart failure ■ myocardial infarction ■ remodeling

Experimental and clinical studies have demonstrated excessive generation of reactive oxygen species (ROS) in failing hearts.[1,2] Among the potential sources of ROS within the heart, mitochondrial electron transport produces superoxide anion ($\cdot O_2^-$) in this disease state.[3] Furthermore, increased ROS leads to mitochondrial DNA (mtDNA) damage and dysfunction.[4,5] Therefore, the intimate link between mitochondrial oxidative stress, mtDNA decline, and mitochondrial dysfunction plays an important role in the development and progression of left ventricular (LV) remodeling and failure that occur after myocardial infarction (MI).

Clinical Perspective p 1786

Peroxiredoxin-3 (Prx-3) is a mitochondrial antioxidant protein and member of the Prx family that can scavenge H_2O_2 in cooperation with thiol and peroxynitrite.[6] In mammals, 6 distinct Prx family members have been identified (Prx-1 through -6). Among the Prxs, Prx-3 is unique because it is localized specifically within the mitochondria.[7] Furthermore, in vivo transfer of the *Prx-3* gene protected neurons against cell death induced by oxidative stress.[8] These beneficial characteristics make Prx-3 an important candidate for therapy against LV failure after MI, in which ROS production has been demonstrated to be increased within the mitochondria.[1,4] Although several previous reports showed the beneficial effects of antioxidants on heart failure,[9,10] no study has ever been performed to specifically examine the protective role of Prx-3. To address these questions, we created transgenic (TG) mice containing the rat *Prx-3* gene. Rat Prx-3–TG mice and their wild-type (WT) littermates were randomized to receive

Received August 10, 2005; revision received January 26, 2006; accepted February 2, 2006.

From the Department of Cardiovascular Medicine, Graduate School of Medical Sciences (S.M., T.I., H.M., M.I., T.K., K.S.), and the Department of Redox Medicinal Science, Graduate School of Pharmaceutical Sciences (M.Y.), Kyushu University, Fukuoka; Biomedical Research Laboratories (F.H., Y.H., T.K., S.O.), Daiichi Suntory Pharma Co, Ltd, Osaka; and the Department of Cardiovascular Medicine (S.K., H.T.), Hokkaido University Graduate School of Medicine, Sapporo, Japan.

Correspondence to Hiroyuki Tsutsui, MD, PhD, Department of Cardiovascular Medicine, Hokkaido University Graduate School of Medicine, Kita-15, Nishi-7, Kita-ku, Sapporo 060-8638, Japan. E-mail htsutsui@med.hokudai.ac.jp

Circulation is available at http://www.circulationaha.org

DOI: 10.1161/CIRCULATIONAHA.105.582239

either a large transmural MI induced by coronary artery ligation or sham operation.

Methods

Generation of TG Mice

The rat Prx-3 cDNA fragment including the entire open reading frame from nucleotide 5 to 802 was amplified by polymerase chain reaction (PCR) and cloned into pCRII (Invitrogen, Carlsbad, Calif). An expression vector for Prx-3 was constructed with pQBI25 (TaKaRa), and the gene for green fluorescent protein was removed at the site of *Nhe*I-*Bam*HI. A cytomegalovirus promoter–driven expression cassette containing rat Prx-3 cDNA in the sense orientation was purified by ultracentrifugation with CsCl. The pronuclei of fertilized eggs from hyperovulated C57BL/6J mice were randomly microinjected with this DNA construct. Tail clips and a PCR protocol to confirm the genotype were performed by one group of investigators. Homozygous TG mice and C57BL/6J WT mice were used at 12 to 16 weeks of age. The study was approved by our institutional animal research committee and conformed to the animal care guidelines of the American Physiological Society.

Creation of MI

We created MI in 12- to 16-week-old, male TG mice (TG+MI) and nontransgenic WT littermates (WT+MI) by ligating the left coronary artery. Sham operation without coronary artery ligation was also performed in WT (WT+sham) and TG (TG+sham) mice. This assignment procedure was performed with the use of numeric codes to identify the animals.

Prx-3 Protein

Prx-3 protein levels were analyzed in cardiac tissue homogenates by Western blot analysis with a monoclonal antibody against rat Prx-3. Our preliminary studies revealed that this antibody against rat Prx-3 cross-reacted with mouse Prx-3 as a single band of 25 kDa. In brief, the LV tissues were homogenized with lysis buffer (20 mmol/L Tris-HCl, 1 mmol/L EDTA, 1 mmol/L EGTA, and 1 mmol/L phenylmethylsulfonylfluoride; pH 7.4). After centrifugation, equal amounts of protein (5 μg protein/lane), estimated by the Bradford method with a protein assay (Bio-Rad, Hercules, Calif), were electrophoresed on a 15% sodium dodecyl sulfate–polyacrylamide gel and then electrophoretically transferred to a nitrocellulose membrane (Millipore, Billerica, Mass). After being blocked with 5% nonfat milk in phosphate-buffered saline (PBS) containing 0.05% Tween 20 at 4°C for 1 hour, the membrane was incubated with the first antibody and then with the peroxidase-linked second antibody (Amersham Pharmacia, Uppsala, Sweden). Chemiluminescence was detected with an enhanced chemiluminescence Western blot detection kit (Amersham Pharmacia) according to the manufacturer's recommendation.

To further assess the subcellular localization of Prx-3 protein, mitochondrial and cytoplasmic fractions were prepared from LVs and subjected to Western blot analysis. In brief, the LV tissues were homogenized at 4°C for 1 minute in 6 volumes of buffer consisting of 10 mmol/L HEPES-NaOH (pH 7.4), 1 mmol/L disodium EDTA, and 250 mmol/L sucrose. The homogenate was centrifuged at 4°C and 3000*g* for 10 minutes to remove any nuclear and myofibrillar debris, and the resultant supernatant was centrifuged at 10 000*g* for 10 minutes to separate any cardiac subcellular fractions. The supernatant was used for the cytoplasmic fraction assay. To isolate the mitochondrial fraction, the pellet was resuspended at 4°C in a buffer consisting of 10 mmol/L HEPES-NaOH (pH 7.4), 1 mmol/L sodium EDTA, and 250 mmol/L sucrose and was washed 3 times with the same buffer. Murine antibodies directed toward glyceraldehyde 3-phosphate dehydrogenase (GAPDH) and cytochrome oxidase (COX) subunit I were also used to verify the integrity of these subcellular fractions.

Immunohistochemistry

Frozen sections of cardiac tissues were incubated in the presence of 100 nmol/L MitoTracker Red CMXRos (Molecular Probes, Eugene, Ore) at 37°C for 20 minutes. We did not repeat the freeze/thaw procedure to avoid the loss of mitochondrial integrity. After being washed with PBS (10 mmol/L sodium phosphate, pH 7.4, and 150 mmol/L NaCl), the sections were fixed with 3.7% formaldehyde for 5 minutes. After being washed, the fixed sections were incubated with 100-fold–diluted anti-rat Prx-3 antibody (10 μg/mL) in PBS at 4°C overnight. Fluorescence images were taken with a confocal laser scanning microscope (Bio-Rad MRC 1024) with laser beams of 488 and 568 nm for excitation.

Myocardial Antioxidant Enzyme Activities and Lipid Peroxidation

For the subsequent biochemical studies, the myocardial tissues with MI were carefully dissected into 3 parts: one consisting of the infarcted LV, one consisting of the border zone LV with the peri-infarct rim (a 1-mm rim of normal-appearing tissue), and one consisting of the remaining noninfarcted (remote) LV. The antioxidant enzymatic activities of superoxide dismutase (SOD), catalase, and glutathione peroxidase (GSHPx) were measured in the noninfarcted LV.[11] The formation of lipid peroxides was measured in the mitochondrial fraction isolated from the LV myocardium with use of a biochemical assay with thiobarbituric acid–reactive substances (TBARS).[4]

Survival

A survival analysis was performed in WT+sham (n=15), TG+sham (n=14), WT+MI (n=39), and TG+MI (n=37) mice. During the study period of 4 weeks, the cages were inspected daily for deceased animals. All deceased mice were examined for the presence of MI as well as pleural effusion and cardiac rupture.

Echocardiographic and Hemodynamic Measurements

At 4 weeks after surgery, echocardiographic studies were performed under light anesthesia with tribromoethanol/amylene hydrate (2.5% wt/vol, 8 μL/g IP) and spontaneous respiration. Two-dimensional, targeted M-mode tracings were recorded at a paper speed of 50 mm/s. Under the same anesthesia with Avertin, a 1.4F micromanometer-tipped catheter (Millar Instruments, Houston, Tex) was inserted into the right carotid artery and then advanced into the LV to measure LV pressures. One subset of investigators who were not informed of the experimental group assignments performed the in vivo LV function studies.

Infarct Size

To measure infarct size 28 days after MI, the heart was excised and the LVs were cut from apex to base into 3 transverse sections. Five-micron sections were cut and stained with Masson's trichrome. Infarct length was measured along the endocardial and epicardial surfaces in each of the cardiac sections, and the values from all specimens were summed. Infarct size (as a percentage) was calculated as total infarct circumference divided by total cardiac circumference.[12]

In addition, to measure infarct size after 24 hours (when most animals were still alive), a separate group of animals including WT+MI (n=5) and TG+MI (n=5) mice was created by ligating the left coronary artery according to the same methods described earlier. After 24 hours of coronary artery ligation, Evans blue dye (1%) was perfused into the aorta and coronary arteries, and tissue sections were weighed and then incubated with a 1.5% triphenyltetrazolium chloride solution. The infarct area (pale), the area at risk (not blue), and the total LV area from each section were measured.[13] In our preliminary study, we confirmed excellent reliability of infarct size measurements, in which a morphometric method similar to that performed in this study was used. The intraobserver and interob-

server variabilities between 2 measurements divided by these means, expressed as a percentage, were each <5%.

Myocardial Histopathology and Apoptosis

Myocyte cross-sectional area and collagen volume fraction were determined by quantitative morphometry of tissue sections from the mid-LV. To detect apoptosis, tissue sections from the mid-LV were stained with terminal deoxynucleotidyl transferase–mediated dUTP nick end-labeling (TUNEL) staining. The number of TUNEL-positive cardiac myocyte nuclei was counted, and the data were normalized per 10^5 total nuclei identified by hematoxylin-positive staining in the same sections. The proportion of apoptotic cells was counted in the noninfarcted LV. We further examined whether apoptosis was present by the more sensitive ligation-mediated PCR fragmentation assays (Maxim Biotech, Inc, Rockville, Md).

mtDNA Copy Number

DNA was extracted from cardiac tissues, and a Southern blot analysis was performed to measure the mtDNA copy number, as described earlier.[4] Primers for the mtDNA probe corresponded to nucleotides 2424 to 3605 of the mouse mitochondrial genome, and those for the nuclear-encoded mouse 18S rRNA probe corresponded to nucleotides 435 to 1951 of the human 18S rRNA genome. The mtDNA levels were normalized to the abundance of the 18S rRNA gene run on the same gel.

Mitochondrial Complex Enzyme Activity

The specific activity of mitochondrial electron transport chain complex I (rotenone-sensitive NADH-ubiquinone oxidoreductase), complex II (succinate-ubiquinone oxidoreductase), complex III (ubiquinol–cytochrome *c* oxidoreductase), and complex IV (cytochrome *c* oxidase) was measured in myocardial tissues according to methods described previously.[4] All enzymatic activities were expressed as nanomoles per minute per milligram protein.

Plasma TBARS

The formation of TBARS in peripheral blood samples from WT+MI and TG+MI mice was measured by a fluorometric assay, as described previously.[14] In brief, 100 μL of whole blood was mixed with 1 mL of saline and centrifuged at 3000*g* for 15 minutes. The supernatant was mixed with $\frac{1}{12}$N H_2SO_4 and 10% phosphotungstic acid, and the mixture was centrifuged. The sediment was suspended in distilled water, 0.3% thiobarbituric acid, and 0.1% butylated hydroxytoluene. The reaction mixture was then heated at 100°C for 60 minutes in an oil bath. After being cooled with tap water, the mixture was extracted with *n*-butanol and centrifuged at 1600*g* for 15 minutes. The fluorescence intensity of the organic phase was measured by spectrofluorometry with a wavelength of 510-nm excitation and 550-nm emission. Malondialdehyde standards (Sigma-Aldrich, St. Louis, Mo) were included with each assay batch, and plasma TBARS were expressed as micromoles per gram of plasma protein in reference to these standards.

Statistical Analysis

Data are expressed as mean±SEM. Survival analysis was performed by the Kaplan-Meier method, and between-group differences in survival were tested by the log-rank test. A between-group comparison of means was performed by 1-way ANOVA, followed by *t* tests. The Bonferroni correction was applied for multiple comparisons of means. $P<0.05$ was considered statistically significant.

The authors had full access to the data and take full responsibility for their integrity. All authors have read and agreed to the manuscript as written.

Results

We investigated 4 groups of mice, WT+sham (n=15), TG+sham (n=14), WT+MI (n=39), and TG+MI (n=37), in the present study. A survival analysis was performed for all of these mice. Subsequent echocardiographic and hemodynamic measurements were performed in the 4-week survivors: 15 WT+sham, 14 TG+sham, 25 WT+MI, and 31 TG+MI mice. These measurements could not be accomplished in 4 WT+MI and 5 TG+MI mice owing to technical difficulties. Survivor mice were further divided into 2 groups: those studied for subsequent histological analysis, including infarct size, myocyte size, and collagen volume fraction measurements as well as TUNEL staining (5 WT+sham, 5 TG+sham, 8 WT+MI, and 8 TG+MI), and those for the biochemical assay, including antioxidant enzyme activity, Prx-3 protein levels, mitochondrial lipid peroxidation, mtDNA copy number, and mitochondrial complex enzyme activities (8 WT+sham, 8 TG+sham, 8 WT+MI, and 8 TG+MI). Infarct size was not measured in the mice that died.

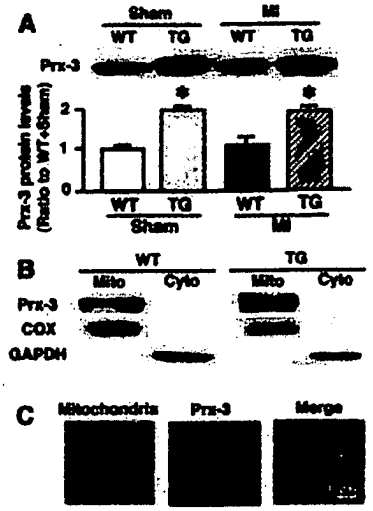

Figure 1. A, Representative Western blot analysis of Prx-3 protein levels (upper panels) and summary data (lower panels) in hearts from WT+sham, TG+sham, WT+MI, and TG+MI mice (n=6 each). Total protein extracts from the hearts were probed with a monoclonal antibody against rat Prx-3. The antibody recognized both rat and mouse Prx-3 as a single band of 25k Da. Data were obtained by densitometric quantification of the Western blots. Values are expressed as the ratio to the WT+sham value and mean±SEM. *$P<0.05$ for the difference from the ratio to WT+sham values. B, Localization of Prx-3 to mitochondria (mito). Western blot analysis of mitochondrial and cytoplasmic (cyto) fractions that were probed with antibodies directed toward Prx-3 as well as specific mitochondrial and cytoplasmic markers: GAPDH was detected in the cytoplasmic but not the mitochondrial fraction, and COX subunit I was detected in the mitochondrial but not the cytoplasmic fraction. Importantly, Prx-3 proteins were detected only in the mitochondrial fraction but not in the cytoplasmic fraction. C, Myocardial tissue sections from TG mice were doubly stained with MitoTracker dye (red) and a rat Prx-3–specific antibody (green). Immunoreactivity for Prx-3 was observed in the cytoplasm of cardiac myocytes. The merged images show that Prx-3 colocalized with the mitochondria (yellow). Scale bar=10 μm.

Myocardial Antioxidants and TBARS

First, baseline differences in Prx-3 proteins as well as other antioxidant enzyme activities between WT and TG mice were determined. In TG+sham, there was a significant increase in Prx-3 protein levels in the LV compared with that of WT+sham (Figure 1A). Importantly, the antioxidants, in-

TABLE 1. Characteristics of Animal Models

	WT+Sham	TG+Sham	WT+MI	TG+MI
Antioxidant enzymes				
n	7	7	7	7
SOD, U/mg protein	26.4±1.1	27.8±1.4	25.1±1.7	23.9±1.2
GSHPx, nmol/min per mg protein	74.1±3.2	77.7±6.7	87.8±4.8	86.1±4.2
Catalase, nmol/mg protein	79.9±6.4	85.0±6.2	87.1±3.5	81.4±5.8
Echocardiographic data				
n	15	14	21	26
Heart rate, bpm	481±11	451±8	463±13	458±8
LVEDD, mm	3.47±0.05	3.37±0.08	5.51±0.13†	4.9±0.10†§
LVESD, mm	2.22±0.05	2.12±0.10	4.78±0.13†	4.08±0.10†§
Fractional shortening, %	35.3±0.8	37.0±1.1	13.1±0.6†	16.9±0.6†§
Hemodynamic data				
n	15	14	21	26
Heart rate, bpm	447±14	455±14	453±9	466±7
Mean aortic pressure, mm Hg	83±3	78±2	76±2	77±3
LVEDP, mm Hg	2.7±0.5	2.5±0.3	11.4±1.5†	7.6±1.0*‡
Organ weight data				
n	15	14	21	26
Body wt, g	26.9±0.5	27.0±0.8	27.0±0.3	26.4±0.4
LV wt/body wt, mg/g	3.2±0.1	3.0±0.1	4.6±0.3†	4.4±0.1†
Lung wt/body wt, mg/g	5.0±0.1	5.2±0.1	7.6±0.5†	6.4±0.3†‡
Pleural effusion, %	0	0	43	15‡

EDD indicates end-diastolic diameter; ESD, end-systolic diameter; and wt, weight. Values are mean±SEM.

*$P<0.05$, †$P<0.01$ vs WT+Sham. ‡$P<0.05$, §$P<0.01$ vs WT+MI.

cluding SOD, GSHPx, and catalase activities, were not altered in the TG hearts (Table 1), indicating no effects of Prx-3 overexpression on other antioxidant enzymes. Second, the changes in antioxidants after MI were assessed. Prx-3 protein levels were significantly higher in TG+MI than in WT+MI (Figure 1A) mice. The activities of other antioxidant enzymes were not altered in WT+MI or TG+MI compared with WT+sham animals (Table 1).

The cytoplasmic marker GAPDH was detected exclusively in the cytoplasmic but not in the mitochondrial fraction, whereas COX subunit I was detected preferentially in the mitochondrial but not in the cytoplasmic fraction. This substantiates the integrity of our cellular fractions. Importantly, Prx-3 was detected only in the mitochondrial fraction but not in the cytoplasmic fraction, further confirming that Prx-3 was localized exclusively in the mitochondria (Figure 1B). In addition, immunohistochemical studies showed a homogeneous Prx-3 distribution in cardiac myocytes that colocalized with the mouse mitochondria (Figure 1C). Prx-3 staining showed a relatively spotty pattern. These results further confirm that the rat Prx-3 transgene is not expressed in the cytoplasm within the mouse heart. Mitochondrial TBARS measured in the noninfarcted LV were significantly greater in WT+MI compared with sham animals and were significantly lower in the TG+MI group (Figure 2).

Survival

There were no deaths in the sham-operated groups. Early operative mortality (within 6 hours) was comparable between WT+MI and TG+MI animals (15% versus 7%; P=NS). The survival rate up to 4 weeks tended to be higher in TG+MI compared with WT+MI mice, but this difference did not reach statistical significance (P=0.06 by log-rank test; Figure 3A). Death was suspected to be attributable to heart failure and/or arrhythmia. Five WT+MI (15%) and 2 TG+MI (5%) mice died of LV rupture (P=NS).

Infarct Size

Infarct size as determined by morphometric analysis 28 days after MI was comparable (55±1% versus 56±1%; P=0.83) between WT+MI (n=6) and TG+MI (n=6) groups. To further confirm that overexpression of Prx-3 did not alter infarct size, both the area at risk and infarct area were

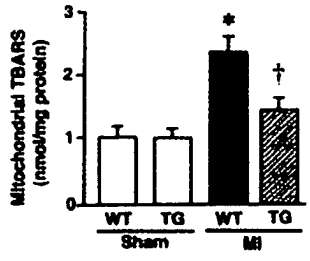

Figure 2. Mitochondrial TBARS in 4 experimental groups of animals (n=8 each). Values are mean±SEM. *$P<0.05$ for difference from the WT+sham value. †$P<0.05$ for difference from the WT+MI value.

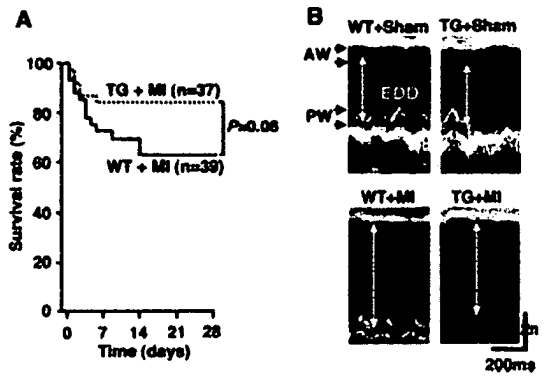

Figure 3. A, Kaplan-Meier survival analysis. Percentages of surviving WT+MI (n=39) and TG+MI (n=37) mice were plotted. Between-group difference was tested by the log-rank test. B, M-mode echocardiograms obtained from WT+sham, TG+sham, WT+MI, and TG+MI mice. AW indicates anterior wall; PW, posterior wall; and EDD, end-diastolic diameter.

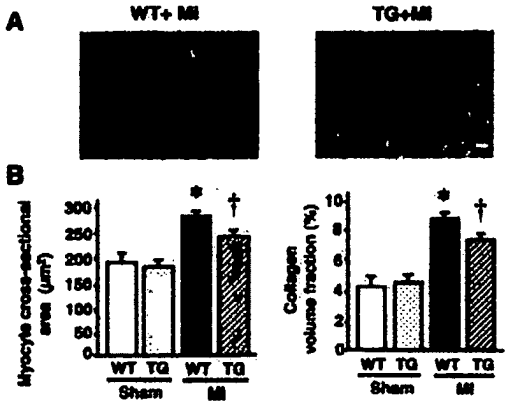

Figure 4. A, Photomicrographs of Masson trichrome-stained LV cross sections obtained from WT+MI and TG+MI mice. Scale bar=10 μm. B, Myocyte cross-sectional area and collagen volume fraction in WT+sham (n=5), TG+sham (n=5), WT+MI (n=8), and TG+MI (n=8) mice. Values are mean±SEM. *$P<0.05$ for difference from the WT+sham value. †$P<0.05$ for difference from the WT+MI value.

measured in mice 24 hours after coronary artery ligation. Percentages of the LV at risk (risk area/LV, 51±3% versus 52±2%; $P=0.89$) and infarct size (infarct/risk area, 79±1% versus 78±1%; $P=0.13$) were also comparable between WT+MI (n=5) and TG+MI (n=5) animals.

Echocardiography and Hemodynamics

The echocardiographic and hemodynamic data of surviving mice at 28 days are shown in Figure 3B and Table 1. LV diameters were significantly larger in WT+MI mice with respect to WT+sham animals. TG+MI mice displayed less LV cavity dilatation and greater fractional shortening than did WT+MI mice. There was no significant difference in heart rate or aortic blood pressure among the 4 groups of mice. LV end-diastolic pressure (LVEDP) was higher in WT+MI than in WT+sham animals, but this increase was significantly attenuated in TG+MI mice.

Organ Weights and Histomorphometry

Coincident with an increased LVEDP, lung weight/body weight was larger in WT+MI mice, and this increase was attenuated in TG+MI mice (Table 1). The prevalence of pleural effusion was also lower in TG+MI than in WT+MI groups. Histomorphometric analysis of noninfarcted LV sections showed that myocyte cross-sectional area was greater in WT+MI mice but was significantly attenuated in TG+MI mice (Figure 4). Collagen volume fraction was greater in WT+MI mice, but this change was inhibited in TG+MI mice (Figure 4).

Myocardial Apoptosis

There were rare TUNEL-positive nuclei in sham-operated mice. The number of TUNEL-positive myocytes in the noninfarcted LV was larger in WT+MI mice but was significantly smaller in TG+MI animals (Figure 5A). In addition, the intensity of the DNA ladder indicated that apoptosis in TG+MI animals was decreased compared with that in WT+MI mice (Figure 5B).

mtDNA and Mitochondrial Complex Enzymes Activity

Consistent with our previous studies,[4] mtDNA copy number in the noninfarcted LV from WT+MI animals showed a 36% decrease ($P<0.05$) compared with that in sham-operated mice, which was significantly prevented and was preserved at normal levels in TG+MI animals (Figure 6).

To determine the effects of mtDNA alterations on mitochondrial function, we next measured the mitochondrial electron transport chain complex enzyme activities. The enzymatic activities of complexes I, III, and IV were significantly lower in the noninfarcted LV from WT+MI than in those from WT+sham animals (Table 2). Most important, no such decrease was observed in TG+MI mice. The enzymatic activity of complex II, exclusively encoded by nuclear DNA, was not altered in either group. These results indicate that mtDNA copy number and mitochondrial complex enzymatic activities are downregulated in the post-MI heart and that Prx-3 gene overexpression efficiently counteracts these mitochondrial deficiencies.

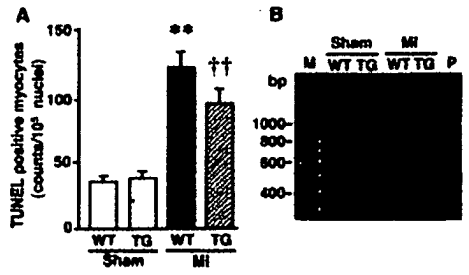

Figure 5. A, Numbers of TUNEL-positive myocytes in the noninfarcted LV from WT+sham, TG+sham, WT+MI, and TG+MI mice (n=5 each). Values are mean±SEM. **$P<0.01$ for the difference from the WT+sham value. ††$P<0.01$ for the difference from the WT+MI value. B, DNA ladder indicative of apoptosis in the genomic DNA from the LV. M indicates marker; P, positive control.

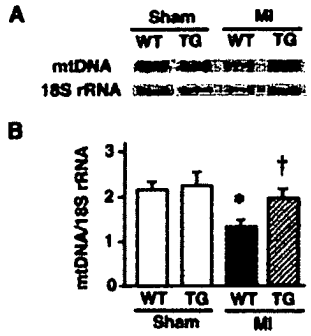

Figure 6. A, Southern blot analysis of mtDNA copy number in total DNA extracts from the hearts from WT+sham, TG+sham, WT+MI, and TG+MI mice. Top bands show signals from the mtDNA fragments, and bottom bands show signals from the nuclear DNA fragments containing the 18S rRNA gene. B, Summary data for a Southern blot analysis of mtDNA copy number in 4 groups of animals (n=8 each). Data were obtained by densitometric quantification of the Southern blots, such as shown in A. Values are expressed as the ratio to WT+sham values and mean±SEM. *$P<0.05$ for the difference from the WT+sham value. †$P<0.05$ for the difference from the WT+MI value.

Plasma TBARS

Plasma TBARS were comparable between WT+MI and TG+MI mice (0.46±0.04 versus 0.54±0.05 μmol/g protein; P=NS).

Discussion

The present study provides the first direct evidence that overexpression of mitochondrial antioxidant Prx-3 protects the heart against post-MI remodeling and failure in mice. It reduced LV cavity dilatation and dysfunction, as well as myocyte hypertrophy, interstitial fibrosis, and apoptosis of the noninfarcted myocardium. These beneficial effects of *Prx-3* gene overexpression were associated with an attenuation of mitochondrial oxidative stress, mtDNA decline, and dysfunction. They were not due to its MI size-sparing effect but occurred secondary to more adaptive remodeling.

Mitochondria are the predominant source of ROS in the failing myocardium.[1] Most of the $\cdot O_2^-$ generated by the mitochondria is vectorially released into the mitochondrial matrix. $\cdot O_2^-$ impairs mitochondrial function by oxidizing the Fe-S centers of complex enzymes. In addition, $\cdot O_2^-$ is converted to peroxynitrite, an extremely powerful oxidant, as a result of its reaction with NO produced by mitochondrial NO synthase. $\cdot O_2^-$ is also converted to H_2O_2 by a specific intramitochondrial Mn-SOD. Although Mn-SOD relieves mitochondrial oxidative stress caused by $\cdot O_2^-$, it generates H_2O_2 and therefore, further enhances a different type of oxidative stress. H_2O_2 can damage cellular macromolecules such as proteins, lipids, and nucleic acids, especially after its conversion to ·OH. Moreover, these increased ROS in the mitochondria were associated with a decreased mtDNA copy number and reduced oxidative capacity owing to low complex enzyme activities.[4] Therefore, chronic increases in mitochondrial ROS production cause mtDNA damage and dysfunction, which thus, can lead to a catastrophic cycle of further oxidative stress and ultimate cellular injury.[5] This deleterious process may play an important role in the development and progression of myocardial remodeling and failure.[4] Based on these results, mitochondrial antioxidants are expected to be the first line-of-defense mechanism against ROS generation in the mitochondria and ROS-mediated mitochondrial injury and thus, may protect the heart from adverse remodeling and failure.

Prx-3, which was formerly known as SP-22, or MER5, is currently identified as a mitochondrial member of the novel antioxidant proteins designated as Prxs.[15] Among 6 known mammalian Prxs, Prx-1 to -4 require the small redox protein thioredoxin (Trx) as an electron donor to remove H_2O_2, whereas Prx-5 and -6 can use other cellular reductants, such as GSH, as their electron donor.[16] Prx-1, -2, and -6 are found in the cytoplasm and nucleus,[7] whereas Prx-3 contains a mitochondrial localization sequence, is found exclusively in the mitochondria, and uses mitochondrial Trx-2 as the electron donor for its peroxidase activity.[17] It functions not only by removing H_2O_2 formed after the SOD-catalyzed dismutation reaction but also by detoxifying peroxynitrite.[6] Therefore, the great efficiency of Prx-3 as an antioxidant shown in the present study may be attributable to the fact that it is located in the mitochondria and can utilize lipid peroxides as well as H_2O_2 for substrates. In fact, overexpression of Prx-3 has been shown to protect thymoma cells from apoptosis induced by hypoxia, a bolus of peroxide, or an anticancer drug.[18] Moreover, Prx-3 overexpression has been reported to protect rat hippocampal neurons from excitotoxic injury.[8] Prx-5 is also associated with the mitochondria in addition to the peroxisomes and nucleus. Recently, increased expression of Prx-5 was found to have protected Chinese hamster ovary cells from mtDNA damage induced by oxidative stress.[19] Therefore, Prx-5 may also exert beneficial effects against mitochondrial oxidative stress in post-MI hearts.

GSHPx also catalyzes the reduction of H_2O_2. In fact, our previous studies demonstrated that overexpression of GSHPx

TABLE 2. Mitochondrial Complex Enzyme Activities

	WT+Sham	TG+Sham	WT+MI	TG+MI
n	7	7	7	7
Complex I, nmol/min per mg protein	282±26	265±38	159±25*	287±16†
Complex II, nmol/min per mg protein	770±70	718±93	711±85	726±128
Complex III, nmol/min per mg protein	505±11	470±31	367±20*	451±21†
Complex IV, nmol/min per mg protein	1223±37	1175±34	744±68*	939±54†

Values are mean±SEM.
*$P<0.05$ vs WT+sham; †$P<0.05$ vs WT+MI.

inhibited LV remodeling and failure after MI.[13] However, GSHPx is located predominantly in the cytosol, and only a small proportion (≈10%) is present in the mitochondria.[20] Therefore, it remains unclear whether the beneficial effects of GSHPx overexpression on post-MI hearts were attributable to an increase of this enzyme in the cytosol, the mitochondria, or both. The specific localization of Prx-3 in the mitochondria suggests that mitochondrial oxidative stress plays an important role in the development and progression of heart failure, and antioxidants localized specifically within the mitochondria provide a primary line of defense against this disease process.

A growing body of evidence suggests that ROS play a major role in the pathogenesis of cardiac failure. Furthermore, antioxidants have been shown to exert protective and beneficial effects against heart failure.[21,22] A previous study from our laboratory demonstrated that dimethylthiourea improved survival and prevented LV remodeling and failure after MI.[10] However, the most effective way to evaluate the contribution of any specific antioxidant and obtain direct evidence of an adverse role for ROS in heart failure is through gene manipulation. Therefore, the present study not only extends the previous observation that used antioxidants but also reveals the major role of mitochondrial oxidative stress in the pathophysiology of post-MI remodeling and failure.

The beneficial effects of Prx-3 overexpression shown in the present study were not due to its MI size-sparing effect, because there was no statistically significant difference in infarct size between WT+MI and TG+MI mice. Furthermore, its effects were not attributable to hemodynamics because blood pressures and heart rates were not altered (Table 1). Importantly, it is also unlikely that these effects were caused by the altered expression of antioxidant enzymes other than Prx-3 (Table 1). Moreover, the beneficial effects of Prx-3 overexpression were not due to systemic induction of antioxidant defenses. This possibility is less likely because plasma TBARS were comparable between WT+MI and TG+MI mice. Nevertheless, we cannot completely exclude the possibility that the systemic effects of Prx-3 induction might also have contributed to this phenotype because this TG is not heart-specific.

There may be several factors contributing to the protective effects conferred by Prx-3 overexpression on post-MI remodeling and failure. First, recent studies have demonstrated that a Trx-related antioxidant system is closely associated with the regulation of apoptosis, probably through quenching of ROS and redox control of the mitochondrial permeability transition pores that release cytochrome *c*.[23] A subtle increase in ROS caused by partial inhibition of SOD results in apoptosis in isolated cardiac myocytes.[24] Previous studies have demonstrated that apoptosis appears not only in infarcted but also in noninfarcted myocardium after MI.[25] Specifically, apoptosis occurs in the noninfarcted LV late after MI. This is an intriguing observation, in light of the remodeling process known to occur within the noninfarcted area, which is characterized by the loss of myocytes and hypertrophy. In fact, recent studies have suggested cardiac myocyte apoptosis contributes to LV remodeling after MI.[26,27] Importantly, increased oxidative stress occurs concomitantly with increased cardiac myocyte apoptosis within the noninfarcted area. This is a provoking observation, because oxidative stress is a powerful inducer of apoptotic cell death.[28] The present study suggests that the coexistence of oxidative stress and myocyte apoptosis in the noninfarcted LV after MI is causally related. Oxidative stress may mediate myocyte apoptosis, which may lead to myocardial remodeling and failure. Therefore, the decreased mitochondrial oxidative stress due to Prx-3 overexpression could contribute to the amelioration of apoptosis (Figure 5) and eventual post-MI cardiac failure. Second, Prx-3 overexpression prevented the decrease in mtDNA copy number (Figure 6) as well as mitochondrial complex enzyme activities (Table 2). Our previous studies have demonstrated an intimate link between mtDNA damage, increased lipid peroxidation, and a decrease in mitochondrial function, which might play a major role in the development and progression of cardiac failure.[4]

There are several issues to be acknowledged as limitations of this study. First, the differences between WT+MI and TG+MI groups in their echocardiographic measurements are not remarkable, even though they are statistically significant (Table 1). However, our previous study showed that the intraobserver and interobserver variabilities in our echocardiographic measurements for LV dimensions were small, and measurements made in the same animals on separate days were highly reproducible.[12] Therefore, these values are considered to be valid. Second, longer-term follow-up data are not available for the animals in the current study. We therefore could not determine whether the differences between WT+MI and TG+MI groups seen in the present study were more or less significant at later time points, when additional LV remodeling would have been expected to occur.

In conclusion, Prx-3 overexpression inhibited the development of LV remodeling and failure after MI, which was associated with an attenuation of myocyte hypertrophy, apoptosis, and interstitial fibrosis. It also ameliorated mitochondrial oxidative stress as well as mtDNA decline and mitochondrial dysfunction in post-MI hearts. Therapies designed to interfere with mitochondrial oxidative stress could be beneficial to prevent heart failure after MI.

Acknowledgments

This study was supported in part by grants from the Ministry of Education, Science and Culture (No. 12670676, 14370230, 17390223). A portion of this study was conducted at Kyushu University Station for Collaborative Research I and II.

Disclosures

None.

References

1. Ide T, Tsutsui H, Kinugawa S, Suematsu N, Hayashidani S, Ichikawa K, Utsumi H, Machida Y, Egashira K, Takeshita A. Direct evidence for increased hydroxyl radicals originating from superoxide in the failing myocardium. *Circ Res*. 2000;86:152–157.
2. Mallat Z, Philip I, Lebret M, Chatel D, Maclouf J, Tedgui A. Elevated levels of 8-iso-prostaglandin F2α in pericardial fluid of patients with heart failure: a potential role for in vivo oxidant stress in ventricular dilatation and progression to heart failure. *Circulation*. 1998;97:1536–1539.

3. Ide T, Tsutsui H, Kinugawa S, Utsumi H, Kang D, Hattori N, Uchida K, Arimura K, Egashira K, Takeshita A. Mitochondrial electron transport complex I is a potential source of oxygen free radicals in the failing myocardium. *Circ Res*. 1999;85:357–363.
4. Ide T, Tsutsui H, Hayashidani S, Kang D, Suematsu N, Nakamura K, Utsumi H, Hamasaki N, Takeshita A. Mitochondrial DNA damage and dysfunction associated with oxidative stress in failing hearts after myocardial infarction. *Circ Res*. 2001;88:529–535.
5. Suematsu N, Tsutsui H, Wen J, Kang D, Ikeuchi M, Ide T, Hayashidani S, Shiomi T, Kubota T, Hamasaki N, Takeshita A. Oxidative stress mediates tumor necrosis factor-α–induced mitochondrial DNA damage and dysfunction in cardiac myocytes. *Circulation*. 2003;107:1418–1423.
6. Bryk R, Griffin P, Nathan C. Peroxynitrite reductase activity of bacterial peroxiredoxins. *Nature*. 2000;407:211–215.
7. Kang SW, Chae HZ, Seo MS, Kim K, Baines IC, Rhee SG. Mammalian peroxiredoxin isoforms can reduce hydrogen peroxide generated in response to growth factors and tumor necrosis factor-α. *J Biol Chem*. 1998;273:6297–6302.
8. Hattori F, Murayama N, Noshita T, Oikawa S. Mitochondrial peroxiredoxin-3 protects hippocampal neurons from excitotoxic injury in vivo. *J Neurochem*. 2003;86:860–868.
9. Sia YT, Lapointe N, Parker TG, Tsoporis JN, Deschepper CF, Calderone A, Pourdjabbar A, Jasmin JF, Sarrazin JF, Liu P, Adam A, Butany J, Rouleau JL. Beneficial effects of long-term use of the antioxidant probucol in heart failure in the rat. *Circulation*. 2002;105:2549–2555.
10. Kinugawa S, Tsutsui H, Hayashidani S, Ide T, Suematsu N, Satoh S, Utsumi H, Takeshita A. Treatment with dimethylthiourea prevents left ventricular remodeling and failure after experimental myocardial infarction in mice: role of oxidative stress. *Circ Res*. 2000;87:392–398.
11. Ho YS, Magnenat JL, Bronson RT, Cao J, Gargano M, Sugawara M, Funk CD. Mice deficient in cellular glutathione peroxidase develop normally and show no increased sensitivity to hyperoxia. *J Biol Chem*. 1997;272:16644–16651.
12. Shiomi T, Tsutsui H, Hayashidani S, Suematsu N, Ikeuchi M, Wen J, Ishibashi M, Kubota T, Egashira K, Takeshita A. Pioglitazone, a peroxisome proliferator–activated receptor-γ agonist, attenuates left ventricular remodeling and failure after experimental myocardial infarction. *Circulation*. 2002;106:3126–3132.
13. Shiomi T, Tsutsui H, Matsusaka H, Murakami K, Hayashidani S, Ikeuchi M, Wen J, Kubota T, Utsumi H, Takeshita A. Overexpression of glutathione peroxidase prevents left ventricular remodeling and failure after myocardial infarction in mice. *Circulation*. 2004;109:544–549.
14. Ide T, Tsutsui H, Ohashi N, Hayashidani S, Suematsu N, Tsuchihashi M, Tamai H, Takeshita A. Greater oxidative stress in healthy young men compared with premenopausal women. *Arterioscler Thromb Vasc Biol*. 2002;22:438–442.
15. Wood ZA, Schroder E, Robin Harris J, Poole LB. Structure, mechanism and regulation of peroxiredoxins. *Trends Biochem Sci*. 2003;28:32–40.
16. Fisher AB, Dodia C, Manevich Y, Chen JW, Feinstein SI. Phospholipid hydroperoxides are substrates for non-selenium glutathione peroxidase. *J Biol Chem*. 1999;274:21326–21334.
17. Watabe S, Hiroi T, Yamamoto Y, Fujioka Y, Hasegawa H, Yago N, Takahashi SY. SP-22 is a thioredoxin-dependent peroxide reductase in mitochondria. *Eur J Biochem*. 1997;249:52–60.
18. Nonn L, Berggren M, Powis G. Increased expression of mitochondrial peroxiredoxin-3 (thioredoxin peroxidase-2) protects cancer cells against hypoxia and drug-induced hydrogen peroxide–dependent apoptosis. *Mol Cancer Res*. 2003;1:682–689.
19. Banmeyer I, Marchand C, Clippe A, Knoops B. Human mitochondrial peroxiredoxin 5 protects from mitochondrial DNA damages induced by hydrogen peroxide. *FEBS Lett*. 2005;579:2327–2333.
20. Chang TS, Cho CS, Park S, Yu S, Kang SW, Rhee SG. Peroxiredoxin III, a mitochondrion-specific peroxidase, regulates apoptotic signaling by mitochondria. *J Biol Chem*. 2004;279:41975–41984.
21. Dhalla AK, Hill MF, Singal PK. Role of oxidative stress in transition of hypertrophy to heart failure. *J Am Coll Cardiol*. 1996;28:506–514.
22. Nakamura R, Egashira K, Machida Y, Hayashidani S, Takeya M, Utsumi H, Tsutsui H, Takeshita A. Probucol attenuates left ventricular dysfunction and remodeling in tachycardia-induced heart failure: roles of oxidative stress and inflammation. *Circulation*. 2002;106:362–367.
23. Petronilli V, Costantini P, Scorrano L, Colonna R, Passamonti S, Bernardi P. The voltage sensor of the mitochondrial permeability transition pore is tuned by the oxidation-reduction state of vicinal thiols: increase of the gating potential by oxidants and its reversal by reducing agents. *J Biol Chem*. 1994;269:16638–16642.
24. Siwik DA, Tzortzis JD, Pimental DR, Chang DL, Pagano PJ, Singh K, Sawyer DB, Colucci WS. Inhibition of copper-zinc superoxide dismutase induces cell growth, hypertrophic phenotype, and apoptosis in neonatal rat cardiac myocytes in vitro. *Circ Res*. 1999;85:147–153.
25. Palojoki E, Saraste A, Eriksson A, Pulkki K, Kallajoki M, Voipio-Pulkki LM, Tikkanen I. Cardiomyocyte apoptosis and ventricular remodeling after myocardial infarction in rats. *Am J Physiol Heart Circ Physiol*. 2001;280:H2726–H2731.
26. Sam F, Sawyer DB, Chang DL, Eberli FR, Ngoy S, Jain M, Amin J, Apstein CS, Colucci WS. Progressive left ventricular remodeling and apoptosis late after myocardial infarction in mouse heart. *Am J Physiol Heart Circ Physiol*. 2000;279:H422–H428.
27. Oskarsson HJ, Coppey L, Weiss RM, Li WG. Antioxidants attenuate myocyte apoptosis in the remote non-infarcted myocardium following large myocardial infarction. *Cardiovasc Res*. 2000;45:679–687.
28. von Harsdorf R, Li PF, Dietz R. Signaling pathways in reactive oxygen species–induced cardiomyocyte apoptosis. *Circulation*. 1999;99:2934–2941.

CLINICAL PERSPECTIVE

A growing body of evidence suggests that oxidative stress, an excess generation of reactive oxygen species (ROS), plays a major role in the pathogenesis of heart failure. Furthermore, antioxidants have been shown to exert protective and beneficial effects against this process. Recent studies have suggested that mitochondria are the predominant source of ROS in the failing heart, and mitochondrial antioxidants are expected to be the first line of defense against mitochondrial oxidative stress–mediated myocardial injury. The present study demonstrated that overexpression of peroxiredoxin-3 (Prx-3) inhibited cardiac remodeling and failure after myocardial infarction (MI) created by ligation of the left coronary artery in mice. Prx-3 contains a mitochondrial localization sequence, is found exclusively in the mitochondria, and uses mitochondrial thioredoxin (Trx)-2 as the electron donor for its peroxidase activity. It functions not only by removing H_2O_2 formed after the superoxide dismutase (SOD)–catalyzed dismutation reaction but also by detoxifying peroxynitrite. Therefore, the great efficiency of Prx-3 as an antioxidant shown in the present study may be attributable to the fact that it is located in the mitochondria and can utilize lipid peroxides as well as H_2O_2 for substrates. The present study not only extends previous investigations that used antioxidants but also reveals a major role for mitochondrial oxidative stress in the pathophysiology of postinfarct heart failure. Therapies designed to interfere with mitochondrial oxidative stress by using antioxidant Prx-3 might also beneficial in preventing clinical heart failure.

Circulation
JOURNAL OF THE AMERICAN HEART ASSOCIATION

American Heart Association®
Learn and Live℠

Overexpression of Mitochondrial Peroxiredoxin-3 Prevents Left Ventricular Remodeling and Failure After Myocardial Infarction in Mice

Shouji Matsushima, Tomomi Ide, Mayumi Yamato, Hidenori Matsusaka, Fumiyuki Hattori, Masaki Ikeuchi, Toru Kubota, Kenji Sunagawa, Yasuhiro Hasegawa, Tatsuya Kurihara, Shinzo Oikawa, Shintaro Kinugawa and Hiroyuki Tsutsui

Circulation 2006;113;1779-1786; originally published online Apr 3, 2006;
DOI: 10.1161/CIRCULATIONAHA.105.582239
Circulation is published by the American Heart Association. 7272 Greenville Avenue, Dallas, TX 72514
 Print ISSN: 0009-7322. Online ISSN: 1524-4539